13. BROKEN RIDGE SUMMARY[1]

Shipboard Scientific Party[2]

Ocean Drilling Program (ODP) Leg 121 drilling on Broken Ridge was primarily intended to improve our understanding of the rifting process, particularly two important aspects:

1. Is extension initiated by heat introduced into the lithosphere by mantle convection (i.e., "active" rifting) or is extension driven by far-field horizontal stress that originates from forces acting at plate boundaries (i.e., "passive" rifting)?
2. What is the mechanism for the uplift of rift flanks?

The stratigraphic section on Broken Ridge was drilled at Sites 752 through 755 (see the site chapters, this volume) in an attempt to answer these two questions. Drilling provided critical information on the following:

1. Age, lithology, and depositional depth of the sediments in the northward-dipping sequences below the erosional unconformity.
2. Age, lithology, and depositional depth of the sediments in the subhorizontally layered capping sequence.
3. What parts of the total sedimentary section are pre- and post-rift.
4. The age and duration of the rifting event.
5. The vertical motion of Broken Ridge in response to rifting.

The drilling results also provided many new insights into problems concerning sedimentation processes, austral mid- to high-latitude biostratigraphy, and the magnetic, geochemical, and physical properties of sediments. These unanticipated drilling results, as well as those bearing on the main, rifting-related objectives, are discussed in this chapter in six sections on the sedimentary record of Broken Ridge, tephra, biostratigraphy, paleomagnetics, geochemistry, and physical properties and geophysical well logging. The main points from these studies are summarized in the "Conclusions" section of this chapter. The Cretaceous/Tertiary boundary, which was recovered in Hole 752B, is discussed in the "Cretaceous/Tertiary Boundary Summary" chapter (this volume).

SEDIMENTARY RECORD OF BROKEN RIDGE (THE BROKEN RIDGE BLUES)

Drilling on Broken Ridge (Fig. 1) was designed to test concepts of lithospheric flexure in response to rifting as developed from analysis of the seismic stratigraphy by studying the sediments and fauna that record changing seafloor depths. From considerations of the ODP Leg 121 preliminary results, regional tectonics, dating of dredged basalts, and by analogy with Kerguelen Plateau drill hole basement ages (ODP Legs 119 and 120), Broken Ridge appears to have formed during the mid-Cretaceous, probably during Albian and perhaps Cenomanian time. Ensuing subsidence allowed deposition of a shallow depth (outer shelf to upper slope equivalent), high- to middle-latitude carbonate sequence. Older parts of this sequence contain a remarkable amount of basaltic volcanic ash. Fifty or sixty million years after it was formed, Broken Ridge was uplifted by flexure that occurred in response to intraplateau rifting followed by the onset of seafloor spreading along the Southeast Indian Ridge at anomaly 18 time, about 42 Ma. Presently low heatflow values imply that the thermal subsidence curve for Broken Ridge was not reset during the late Eocene events, so mostly mechanically-induced subsidence has occurred since then, with minimal subsidence related to lithospheric cooling.

Broken Ridge has always been above the shallow (about 2.5 km deep) Late Cretaceous and Paleogene carbonate compensation depth (CCD), thus permitting deposition of a complete and expanded fossiliferous sedimentary section during those times. A pronounced angular unconformity (Fig. 2) crosses the ridge, separating the underlying, northerly-dipping Cretaceous and lower Paleogene carbonates from the overlying upper Paleogene and Neogene oozes and denoting the Eocene uplift and ensuing erosion. A middle to upper Oligocene disconformity recognized within the ooze section at Sites 752 and 754 may correspond to the relatively large late Oligocene eustatic sea-level drop (Haq et al., 1987).

About half of the Leg 121 drilling time on the *JOIDES Resolution* was devoted to completing a series of four drill sites (752–755) along a 25-km north-south profile extending across the level shallow platform of Broken Ridge (Figs. 2 and 3). The goals of the drilling were to establish, as closely as possible, the age of uplift and erosion of the ridge and to determine the water depth record in an effort to decipher the response of the lithosphere to the Eocene rifting episode. The total thickness of section encountered during drilling on Broken Ridge was about 1465 m, of which 815 m was cored and 650 m occurs between the offset drill holes (Fig. 4).

Sedimentary Section at Broken Ridge

Pelagic Cap

The shallow plateau region of Broken Ridge is underlain by a nannofossil ooze with foraminifers, which comprises Unit I of each site (Fig. 4). The ooze reaches a maximum thickness of about 150 m at Site 754 and thins to the north, where it is barely 40 m thick at Site 753, and to the south, where it is about 65 m thick at Site 755. Farther south, the 3.5-kHz reflection profile indicates that the ooze layer becomes indistinguishably thin as it onlaps the high southern crest of Broken Ridge. The ooze is essentially a pure carbonate, stark white throughout much of the section and becoming pale brown with depth. The foraminifer content varies up to about 30%, but is generally quite low, in the range of 5% to 15%. A layer of sand with limestone and chert pebbles divides the ooze section into upper and lower parts. Shell fragments and whole valves of oysterlike pelecypods occur near the bottom of the upper ooze unit.

The lower part of the ooze sequence, below the upper pebble layer, is well recovered from Core 121-752A-11H and poorly recovered from Cores 121-754A-14X and 121-754B-2R. The lower

[1] Peirce, J., Weissel, J., et al., 1989. *Proc. ODP, Init. Repts.*, 121: College Station, TX (Ocean Drilling Program).

[2] Shipboard Scientific Party is as given in the list of Participants preceding the contents.

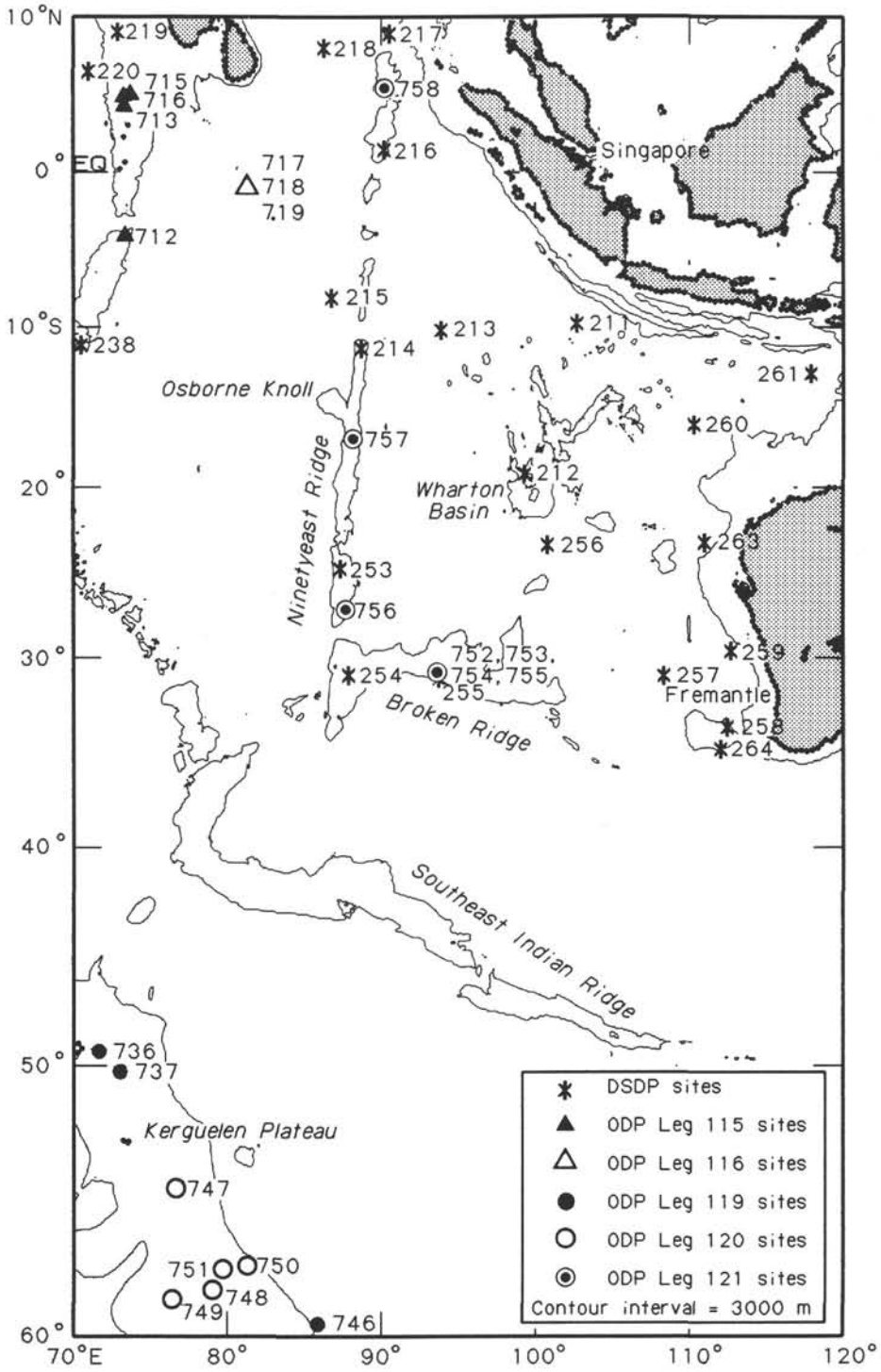

Figure 1. Map of the eastern Indian Ocean showing the operational area of Leg 121 and DSDP and ODP drill sites.

ooze is a rich brown color and contains numerous large foraminifers, 1% or 2% sand-sized iron-stained quartz grains, and abundant fossil material reworked from the underlying Paleogene and Cretaceous sediments. This interval of ooze is of late Eocene age, 38 to 40 Ma; the oozes above the upper pebble layer range in age from Pleistocene to late Oligocene, 0 to 30 Ma.

The Deep Sea Drilling Project (DSDP) Leg 26 scientists who visited Broken Ridge in 1972 (Davies, Luyendyk, et al., 1974) identified the upper part of this unit as a winnowed pelagic ooze, deposited under the influence of the Southern Hemisphere drift currents. The winnowing process obliterates some paleoceanographic information preserved by more normal marine carbonate sequences, particularly any primary flux information, so it is essential to determine the extent of any winnowing. To this end we conducted grain-size analyses of the bulk sediment of this unit at quasiregular intervals using cores recovered with

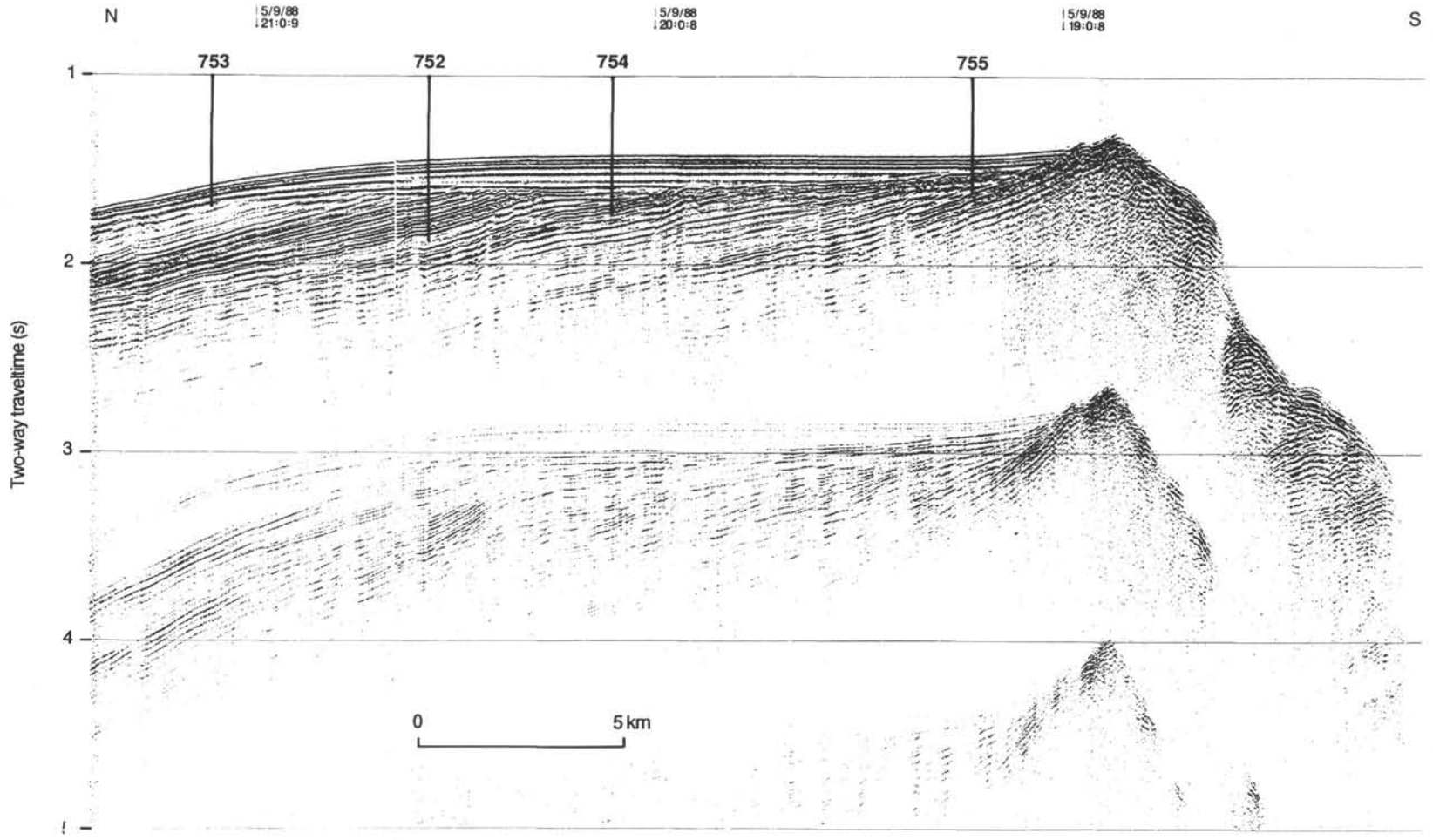

Figure 2. Seismic-reflection profile across the crest of Broken Ridge in the vicinity of the Leg 121 drill sites.

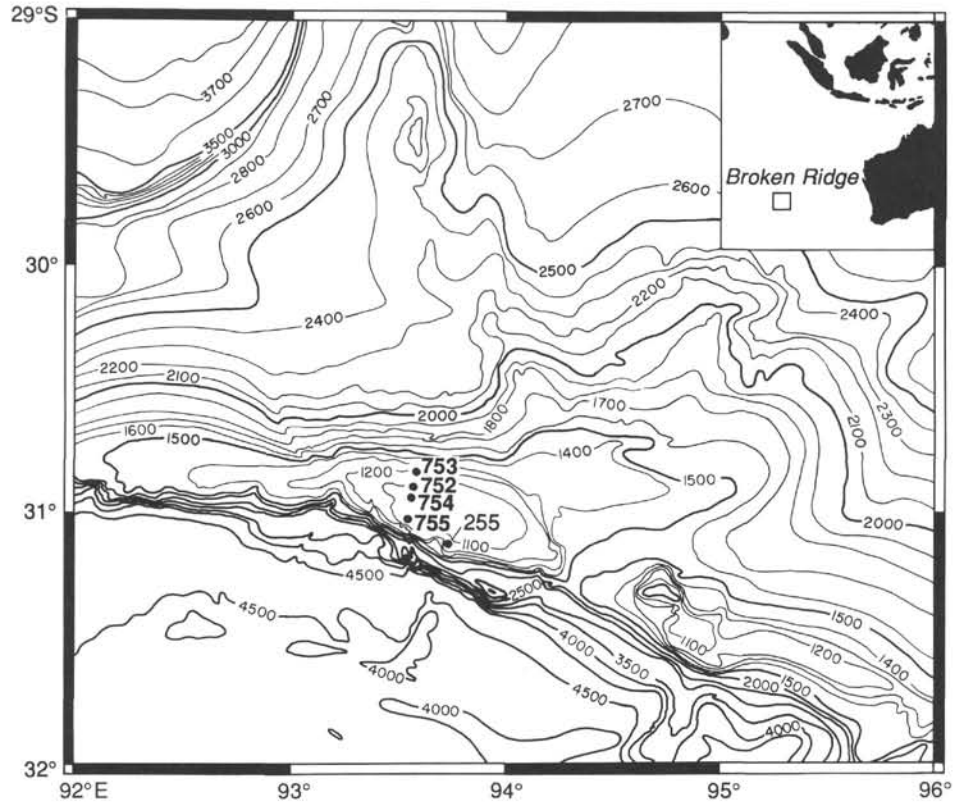

Figure 3. Bathymetric map of Broken Ridge showing the four Leg 121 drill sites. Contour interval = 100 m (corrected).

the advanced piston corer (APC) from Sites 752, 753, and 754. Other studies show that the grain size of purely pelagic sediment contains paleocurrent information (Rea and Janecek, 1986; Ledbetter, 1986). Our results (Fig. 5) show large changes in the grain size of the bulk sediment, from 5.4 to 3.3 ϕ (24 to 100 μm), which are systematic and coherent among the three drill sites studied.

Shallow-Water Deposits at the Eocene Angular Unconformity

Lying on the upper Eocene erosion surface beneath the ooze unit are largely unrecovered deposits that indicate the presence of shallow marine (beach) conditions. This layer is similar in lithology to the upper gravel layer with quartz sand, chert and limestone pebbles, and shell hash mixed with Cretaceous through Eocene reworked carbonate material (Fig. 6). The two pebble layers coalesce to the north, where they form one layer in Hole 753A, which is also characterized by greenish gray limestone pebbles. At southern Site 755 the material lying on the Eocene erosion surface is a foraminifer sandstone, and the underlying Santonian limestones have been oxidized to a depth of 1.5 m (Fig. 6). This lower sand and gravel horizon may be as much as 25 m thick at Site 754, but very little was recovered.

Lower Paleogene and Cretaceous Carbonates and Cherts

The youngest sediments below the angular unconformity were recovered at Site 753, the northernmost of the four Broken Ridge drill sites. The recovered sediments consist of 20 m of light-colored to white nannofossil chalks that commonly contain foraminifers (Unit II of Hole 753A; Fig. 4). These light-colored chalks are characterized by millimeter-scale green laminae in 1- or 2-cm-thick bundles. The lower chalks are a bit darker and contain ash layers. Traces of quartz occur throughout. At Site 753, the chalk sequence is middle to late Eocene in age, about 45 Ma.

Interpretation of the seismic-reflection profiles suggests that about 190 m of Eocene chalks remains undrilled between the bottom of Hole 753A and the uppermost subunconformity chalks of the next southerly Site 752. *JOIDES Resolution* cored a 323-m-thick sequence of lower Eocene to middle or upper Maestrichtian nannofossil calcareous chalks at Site 752 (Fig. 4). The chalks can be subdivided into a 97-m-thick upper chalk (Subunit IIA), a middle opal-rich 79-m-thick section (Subunit IIB), and a lower 147-m-thick interval of more indurated chalk (Subunit IIC). The upper sequence is strongly bioturbated and contains a few ash layers; the color darkens downhole toward a grayish green with increasing ash content. Ash layers increase in abundance in the siliceous unit, and gray-green laminae similar to those above become more common. These laminae also occur in bundles and commonly exhibit sharp and scoured basal contacts, cross laminae, and gradational coloration suggestive of graded bedding. Chert and porcellanite become more common in this silica-rich unit. The lower indurated chalk also contains the gray-green laminae, some of which now appear to be secondary because they continue through the mottles, along with somewhat more abundant ash layers, porcellanite and gray chert, and scattered occurrences of pyrite.

The Cretaceous/Tertiary boundary occurs within the lower indurated chalk unit of Hole 752B at about 358 m below seafloor (mbsf). The boundary lies within a 60-cm-long ash-chert-chalk sequence (Fig. 7) that directly underlies a 5.5- to 6.5-m-thick ash layer. Details of the magnetic susceptibility data for this sequence (see "Paleomagnetics" section of this chapter and the "Cretaceous/Tertiary Boundary Summary" chapter) suggest that the thick ash may be the result of multiple lesser ash falls rather than one large one.

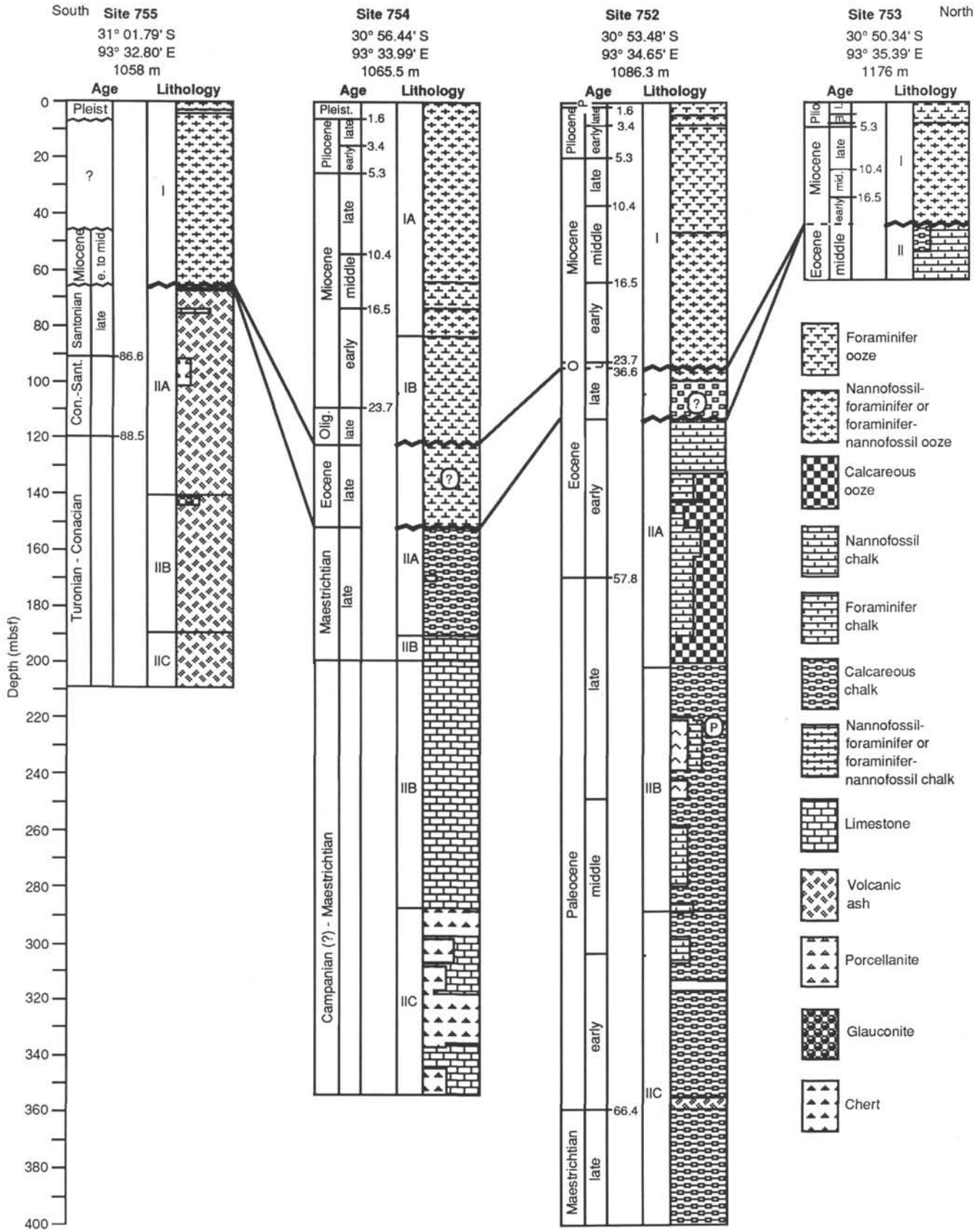

Figure 4. Composite lithologic summary diagram of representative holes from each of the Broken Ridge sites.

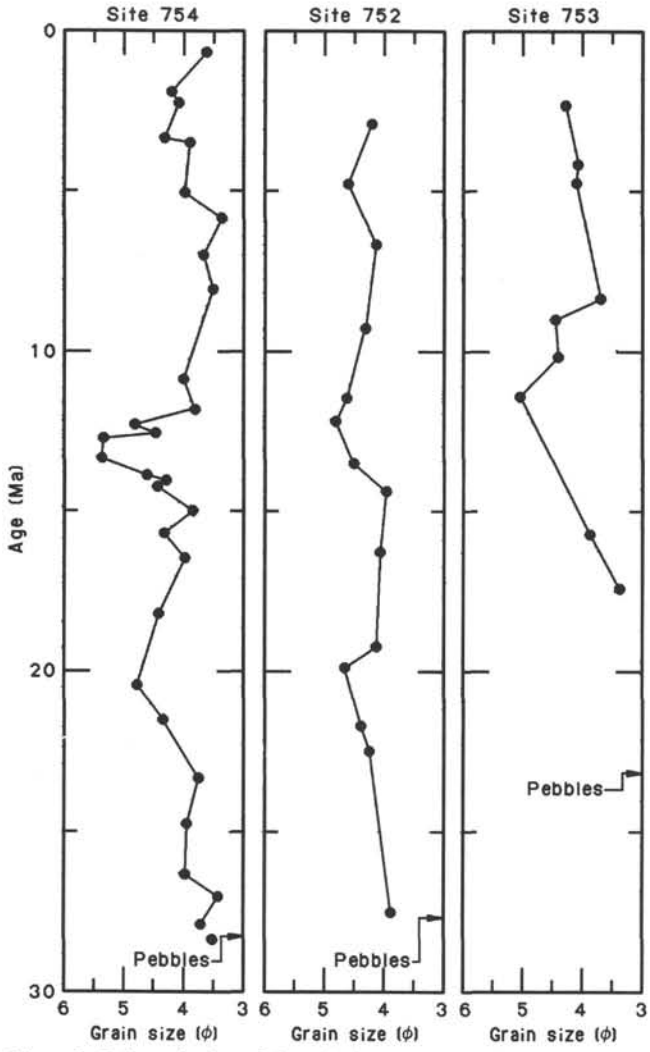

Figure 5. Bulk grain size of the pelagic ooze on Broken Ridge.

Seismic, paleomagnetic, and biostratigraphic data indicate that the lowermost indurated chalks of Hole 752B overlap by approximately 20 m with the sediment of identical lithology and late Maestrichtian age below the angular unconformity in Holes 754A and 754B. These two sites thus provide the longest continuous section on Broken Ridge, a total of 507 m.

The Maestrichtian chalks, limestones, cherts, and ashes of Site 754 form a 204-m-thick sequence that can be divided into three intervals. The upper interval represented is 39 m of greenish gray calcareous chalk containing the previously described greenish gray laminae, chert, common pyrite, and an increasing number of ash layers (Subunit IIA). The ash layers commonly contain 10% to 50% volcanic glass and locally exhibit sharp basal contacts and gradational upper contacts. *Inoceramus* fragments also occur in this interval.

The middle interval consists of 97 m of strongly mottled greenish gray limestone (Subunit IIB). As induration increases, incipient stylolite seams become apparent and the parallel laminae become slightly wavy. Microfaults, which are sporadic upsection, become more abundant. Pyrite blebs and *Inoceramus* fragments occur throughout the unit. Volcanic ash layers are common throughout the interval. Below the mottled limestone lies 68 m of alternating gray to olive limestone and black chert (Subunit IIB). The limestone is weakly laminated and mottled and contains *Inoceramus* fragments. Dolomite in the form of

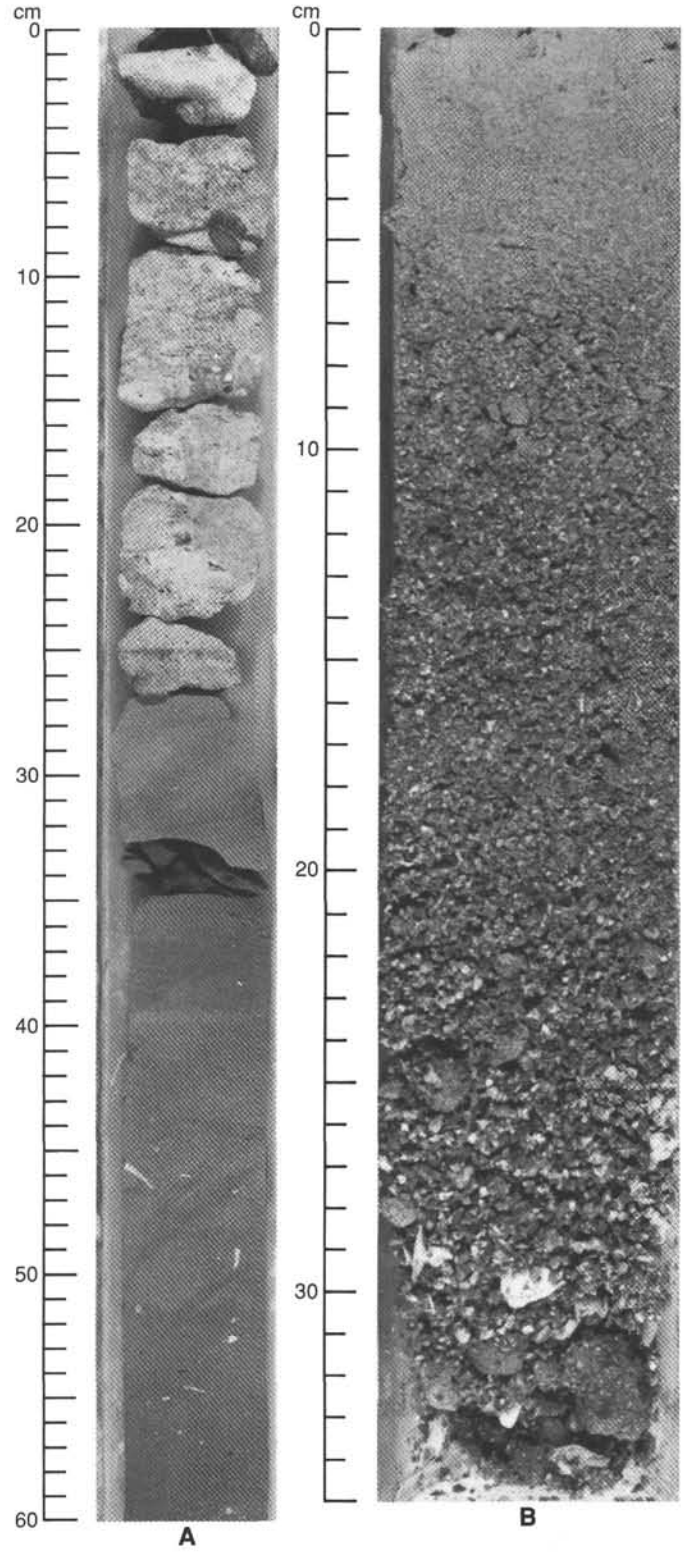

Figure 6. Two instances of the pebble layer on the Eocene angular unconformity. **A.** Miocene foraminifer limestone overlying weathered Santonian limestone (Section 121-755A-5R-1, 0–60 cm). **B.** Sand and gravels (size sorting from drilling disturbance) overlying Maestrichtian limestone (Section 121-754B-2R-1, 0–35 cm).

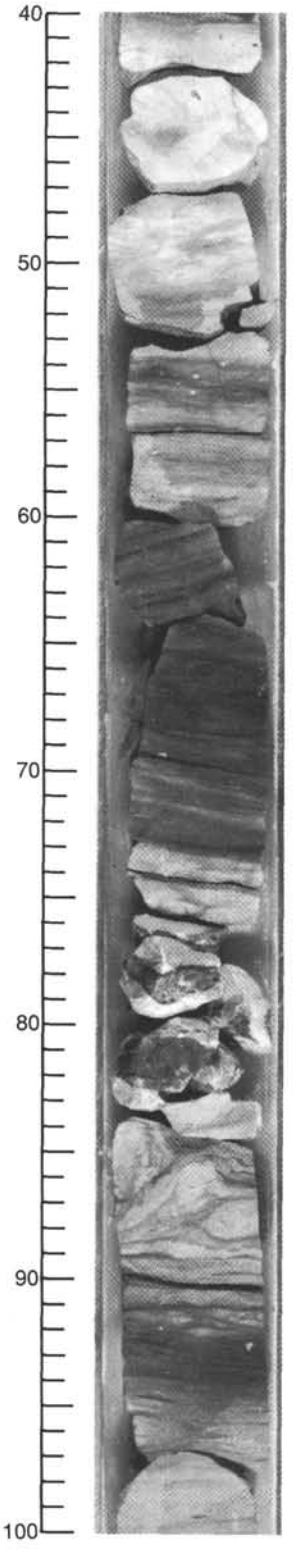

Figure 7. The Cretaceous/Tertiary boundary at about 358 mbsf (Section 121-752B-11R-3, 40–100 cm).

millimeter-sized rhombs replaces about one-third of the olive limestone in Core 121-754B-22R. The cherts contain chalcedony veinlets and sporadic vugs lined with white or black quartz microcrystals.

Santonian to Turonian Ash

The lowest portion of the recovered Broken Ridge sedimentary section occurs in Hole 755A, stratigraphically about 460 m below the bottom of Hole 754B. It consists of a 143-m-thick section of ash with limestone and glauconite of roughly late Santonian to Turonian age (85 to 90 Ma). The sediments are dark greenish gray to black. Glauconite occurs throughout, in a more disseminated form than in the upper part of the hole and in fining-upward units with sharp lower contacts in the lower few cores (Fig. 8). Numerous minor components occur: porcellanite, shell fragments, pyrite (some of which is associated with the calcite veinlets), apatite, and rare gypsum crystals found in vugs. The entire section displays mottles and burrow structures.

Three rounded pebbles of a light gray, pure (99% recrystallized calcite) limestone, 2 to 4 cm in diameter, occur in Cores 121-755A-16R and 121-755A-19R. These pebbles are the only clue to the underlying lithology, which is perhaps the interval of high acoustic velocity that forms the prominent lowermost reflector in the seismic profiles. One pebble has a seismic velocity of 4.0–4.1 km/s and a bulk density of 2.45 g/cm^3, both of which are appropriate values for a lithified limestone and for a bright reflector in seismic profiles.

Comparison with the Section Recovered from Kerguelen Plateau

ODP Legs 119 and 120 spent nearly five months drilling (and in transit) along the Kerguelen Plateau and on the continental margin of Antarctica (Leg 119 Scientific Drilling Party, 1988; Leg 120 Scientific Drilling Party, 1988). The composite section recovered from the central and northern parts of the Kerguelen Plateau, those locations that might reasonably be expected to represent the same general sedimentary environment as the Broken Ridge drill sites, is generally similar to the Broken Ridge composite section. Regional geologic units on Kerguelen Plateau include:

Unit I: Upper Miocene to Quaternary diatom ooze that includes small percentages of foraminifers and nannofossils. Ice-rafted debris occurs in sediments younger than middle Pliocene.

Unit II: Paleocene to middle Miocene nannofossil ooze, commonly with foraminifers. This unit is stark white in the younger parts, but takes on more color, generally light greenish gray, with depth. Faint greenish laminae interpreted as secondary features occur along with minor intervals of chalk, chert, and porcellanite. A middle Eocene hiatus is within this unit.

Unit III: Campanian to Maestrichtian chalk with black chert and green laminae. Glauconite (5% to 58% of the sediment) and glauconite sandstones occur lower in this unit. Indications of shallow-water deposition include a 40-m-thick Maestrichtian series of gravels and breccias, derived from volcanic basement, that interrupts the pelagic limestone sequence.

Unit IV: Santonian through Turonian pelagic limestone and chalk with clayey interlayers, shelly layers, layers with sharp lower contacts, and abundant glauconite.

Unit V: Basalt. Silica-saturated transitional tholeiites (T-MORB) underlie lower Turonian and perhaps Cenomanian(?) limestones.

This composite section of upper oozes, chalks with green laminae and black chert, and glauconitic limestones is basically quite similar to the Broken Ridge section, with three significant differences. The first is the vast quantities of ash recovered in the Broken Ridge sections, roughly two orders of magnitude more ash than occurs in the Kerguelen Plateau sections. This aspect of the Leg 121 recovery requires a large, local source of basaltic tephra. Second, there is a greater extent of lithification or early diagenesis at the Broken Ridge sites than in the Kerguelen

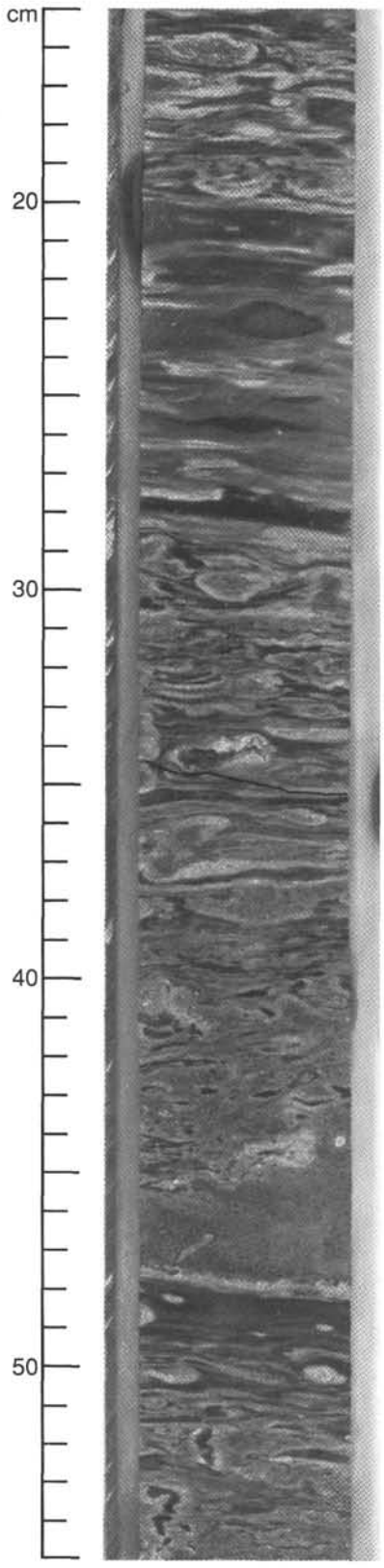

Figure 8. Bioturbated mixture of glauconite and ash and glauconite turbidite in Turonian tuffs (Section 121-755A-18R-1, 15–55 cm). The base of the glauconite turbidite is at 47 cm, and soft-sediment deformation may be at 14–19 and 26–45 cm.

Plateau sediments. This appears to be the result of the greater overburden in the more northerly locations, an inference consistent with the observation of higher sediment mass-accumulation rates on Broken Ridge than on Kerguelen. Finally, the Neogene sequence on Kerguelen Plateau records the great increase in silica productivity that occurred in the Antarctic Circumpolar Ocean during the late Cenozoic, a paleoceanographic event that occurred well to the south of the late Neogene paleoposition of Broken Ridge.

This comparison raises two questions. The first is the nature, origin, distribution, and history of the voluminous ash sequence (see "Tephra" section, this chapter). Just as curious are the extensive and broadly distributed deposits of glauconite. Glauconite sands are usually interpreted as a shallow-water, low to very low deposition rate, (micro)reducing environment sort of deposit, which is typically found on outer continental shelves. Does this description characterize broad regions of the Kerguelen–Broken Ridge Plateau in Turonian to Santonian time?

Rates of Sediment Accumulation

Combining the shipboard biostratigraphic, lithologic, and physical-properties data permits the calculation of rates of sediment deposition (Table 1). The traditional value for deposition rate is the linear sedimentation rate (LSR), commonly measured in meters per million years or centimeters per thousand years. A more useful value to describe sediment deposition is the mass-accumulation rate (MAR). MAR is a quantification of the true mass flux of sedimentary material to the sediment column and is the product of LSR and the dry-bulk density (DBD):

$$\text{MAR (g/cm}^2\text{/1000 yr)} = \text{LSR (cm/1000 yr)} \times \text{DBD (g/cm}^3\text{)}.$$

This value inherently accounts for the variable amounts of pore space in sediments and for changing degrees of compaction and permits quantification of the fluxes of all sedimentary components, thus avoiding the pitfalls of percentage abundance data.

The nannofossil ooze that forms the pelagic cap of Broken Ridge accumulated at rather slow rates for that sort of sediment (Table 1). At Site 752 LSR values average about 0.4 cm/1000 yr and DBD is about 1.0 g/cm^3, so the resulting MAR values are about 0.4 g/cm^2/1000 yr, a value on the low side of normal mid-gyre shallow-water carbonate fluxes. Values at Site 754, where the pelagic cap is slightly thicker, are slightly higher, about 0.5 g/cm^2/1000 yr.

The youngest chalks recovered below the angular unconformity at Site 753, of middle Eocene age, have an LSR of about 1.1 cm/1000 yr and a flux of 1.2 g/cm^2/1000 yr. These values are approximately normal for a low-productivity carbonate depositional environment. Farther downsection the rates are considerably higher. The lower parts of Holes 752A and 752B provide sedimentation rate information for the lower Paleogene and upper Maestrichtian chalks (Table 1). These rates are moderately variable, with LSR values ranging from 2.0 to a high of 11.6 cm/1000 yr in a short-duration zone at the bottom of Hole 752A, with corresponding MAR values of 2.3 to 15.2 g/cm^2/1000 yr. The mass-accumulation rates average about 3.4 g/cm^2/1000 yr through this interval, with relatively low rates of 1.4 to 1.6 g/cm^2/1000 yr at and just above the Cretaceous/Tertiary boundary and a higher rate of 4.9 g/cm^2/100 yr in the zone just below it. Biostratigraphic zonations are not as detailed in the Maestrichtian chalk-limestone-chert sequence in Hole 754B that is the downward continuation of the chalks at Site 752. Those data indicate an LSR of 3.9 cm/1000 yr and a corresponding MAR of 7.6 g/cm^2/1000 yr (Table 1). These values have an estimated accuracy of ±25%. Farther downsection, the Santonian

to Turonian ash, glauconite, and limestone unit has LSR values of 0.7 to 4.9 cm/1000 yr and MAR values of 1.4 to 9.6 g/cm^2/1000 yr (Table 1); these values are probably somewhat less reliable than those for the Maestrichtian limestones above.

The total flux of sediments can be proportioned among the various sedimentary components on the basis of their percent abundance (Table 2 and Fig. 9):

$$MAR_{component} = MAR_{total} \times \%component.$$

The flux of calcium carbonate increases downcore from 0.4 g/cm^2/1000 yr in the pelagic cap to 1.0 g/cm^2/1000 yr in the mid-Eocene chalks, 2.9 g/cm^2/1000 yr in the Paleocene to upper Maestrichtian chalks, to 4.7 g/cm^2/1000 yr in the Maestrichtian limestones. The lowermost unit, dominated by the Santonian to Turonian ash, has a calcium carbonate flux of 0.7 g/cm^2/1000 yr.

The ash flux increases downcore (Table 2 and Fig. 9). Ash enters the pelagic sediments of the upper unit in trace amounts only. Ash MAR at Site 753 is 0.1 g/cm^2/1000 yr in the middle Eocene chalks, 0.6 g/cm^2/1000 yr in the Paleocene to upper Maestrichtian section, 2.5 g/cm^2/1000 yr in the lower Maestrichtian limestones, and 1.1 to 6.5 g/cm^2/1000 yr in the lowest, ash-rich rocks. These accumulation-rate values for volcanic ash are among the largest recorded from within (not immediately overlying basement) oceanic sedimentary sections and denote important volcanic activity on the northernmost portion of the Kerguelen–Broken Ridge Plateau.

Opal is an important sedimentary component in the Paleocene section, where it accumulated at rates of 0.2 to 1.0 g/cm^2/1000 yr. Glauconite is an important component of the lower part of the Santonian to Turonian ash-dominated unit. An estimate for the mass-accumulation rate of glauconite is about 1.9 g/cm^2/1000 yr.

Paleoceanographic Record of Broken Ridge

Plateau Origin and Earliest History

Various indications, including the dating of dredged basalts and the results of Legs 119 and 120, suggest that the main constructional phase of the Kerguelen–Broken Ridge Plateau occurred during the mid-Cretaceous, perhaps during Albian time, and continued on into the Cenomanian. Based on these data we presume an age for the initiation of thermal subsidence of 100 Ma. The mid-Cretaceous is an important time for constructional volcanism through most of the world's ocean basins; other important rises—Ontong-Java, Manihiki, and Hess—are of similar basement age. It is not clear if the Kerguelen–Broken Ridge Plateau ever broached the sea surface in the vicinity of the Leg 121 drill sites before deposition began. The oldest rock unit recovered from Broken Ridge, at Site 755, is a light gray limestone with no admixture of siliciclastic or volcaniclastic components. Presumably it was deposited all across the plateau, in clear water, at some depth shallower than the approximately 2.5-km-deep CCD. The limestone is a completely recrystallized rock and may represent the lithology of the high-velocity acoustic reflector that forms the clear base to the seismic section of Broken Ridge (Fig. 2).

Turonian to Santonian Volcanism

The Upper Cretaceous ash-rich sediments indicate a somewhat unusual depositional environment. The volcanic component that dominates these sediments requires an enormous and local source of basaltic material. None of the surrounding drill sites—Site 255, 21.7 km southeast of Site 755 (but with very poor recovery), and Sites 256, 257, and 258 to the north and east (Fig. 1; Davies, Luyendyk, et al., 1974)—or any of the Legs 119 and 120 sites on Kerguelen Plateau exhibit more than the normal trace amounts of Cretaceous ash. The very high fluxes of volcanogenic material combined with a truly local distribution of the deposit (see "Tephra" section) suggest that the paleoposition of the Broken Ridge transect was within a few tens of kilometers of the volcanic source. The ash was erupted subaerially (Davies, Luyendyk, et al., 1974); therefore, assuming that the plateau lay beneath prevailing westerlies during the Cretaceous, the volcano was to the west. Lacking information concerning the older geologic record, it is not clear whether the volcanism is part of the waning phase, perhaps subaerial, of plateau construction or a distinctly separate and younger event. The lithology of the underlying light gray limestone reflects carbonate deposition for an unknown length of time without significant volcanic input.

Upon reaching the shallow seafloor of the Kerguelen–Broken Ridge Plateau the ash was subjected to the normal oceanic processes of transport, redistribution, and deposition induced by waves, tidal currents, and ocean currents. Finer-grained material, including most biogenic carbonates, would have been winnowed off the shallower part of the plateau and deposited on the upper parts of the "continental" slope by normal proximal hemipelagic processes. Coarser materials remained on the "shelf" and uppermost parts of the slope.

Glauconite is an important component of these sediments and was incorporated into the ashy material at rates of up to 1.9 g/cm^2/1000 yr. This component has a wide regional distribution, occurring in all Kerguelen Plateau cores of equivalent age and at Site 258 on the Naturaliste Plateau to the east (Davies, Luyendyk, et al., 1974). The normal environment of formation of glauconite is a shallow-water, outer shelf, low to very low sedimentation rate locale. The overlying waters are oxidizing, but the sediments may be reducing; microreducing environments, such as within fecal pellets, may be important in the formation of glauconite (Reading, 1978). The coexistence of significant amounts of glauconite, which required a slow sedimentation rate, and ash, which was deposited at very high rates, seems paradoxical.

One possible scenario that would account for these observations is as follows. The part of the seafloor that is now the crest of Broken Ridge must have been situated at the shelf/slope break on the northern rim of the vast Kerguelen–Broken Ridge Plateau. Glauconite formed in suitable locations all across this plateau in low sedimentation rate, low-productivity but carbonate-rich settings. This environment, recorded at several Kerguelen Plateau drill sites, was subjected to a large but local influx of volcanic debris. Much of this material found its way to the north slope of the Kerguelen–Broken Ridge Plateau. Presumably, episodes of greater current activity brought glauconite over the edge of the plateau, where it was disseminated with the hemipelagic ash and or formed discrete downslope density flows, resulting in the glauconite turbidites of Site 755 (Fig. 8). The resulting deposit underwent bioturbation and is low in organic carbon, both of which are indications of oxygenated waters at the seafloor. The water depth then was probably above the oxygen-minimum zone that occurs in conjunction with the main thermocline.

Maestrichtian Carbonate Platform

Volcanic ash is an important component of the Upper Cretaceous sediments. Fifteen million years after the first ashes were deposited, ash fluxes remained high, at about 2.5 g/cm^2/1000 yr (Fig. 9), which is roughly half the average Turonian to Santo-

Table 1. Mass-accumulation rates of sediment on Broken Ridge.

Age (Ma)	ΔT (m.y.)	Depth (mbsf)	ΔZ (m)	Linear sedimentation rate (cm/1000 yr)	Dry-bulk density (g/cm^3)	Mass-accumulation rate (g/cm^2/1000 yr)
Hole 752A						
0.0–1.9	1.9	0.0–4.3	4.3	0.23	0.86	0.20
1.9–3.4	1.5	4.3–10.3	6.0	0.40	1.06	0.42
3.4–5.0	1.6	10.3–19.1	8.8	0.55	1.02	0.56
5.0–6.4	1.4	19.1–25.1	6.0	0.43	0.90	0.39
6.4–14.3	7.9	25.1–58.1	33.0	0.42	0.96	0.40
14.3–17.1	2.8	58.1–73.1	15.0	0.54	0.93	0.50
17.1–23.7	6.6	73.1–91.7	18.6	0.28	[c]1.10	0.31
23.7–28.1	4.4	91.7–93.4	1.7	0.04	[c]1.01	0.04
Unconformity						
37.8		104.3				
Unconformity						
55.3–57.8	2.5	115.6–171.3	55.7	2.23	1.37	3.06
57.8–59.2	1.4	171.3–202.8	31.5	2.25	1.31	2.95
59.2–60.0	0.8	202.8–219.7	16.9	2.11	1.45	3.06
60.0–61.6	1.6	219.7–251.4	31.7	1.98	1.17	2.32
61.6–62.0	0.4	251.4–297.7	46.2	11.55	1.32	15.25
Hole 752B						
63.8–64.8	1.0	318.7–345.1	26.4	2.64	1.96	5.17
64.8–65.9	1.1	345.1–353.9	8.8	0.80	2.05	1.64
65.9–66.4	0.5	353.9–358.5	4.6	0.92	1.55	1.43
66.4–69.0	2.6	358.5–422.3 TD 435.6	63.8	2.45	1.98	4.86
Hole 753A						
0.0–1.9	1.9	0.0–1.0	1.0	0.05	0.99	0.05
1.9–4.5	2.6	1.0–9.5	8.5	0.33	0.99	0.33
4.5–8.2	3.7	9.5–17.0	7.5	0.20	0.94	0.19
8.2–10.0	1.8	17.0–24.4	7.4	0.41	1.02	0.42
10.0–16.2	6.2	24.4–34.4	10.0	0.16	1.08	0.17
16.2–23.6	7.4	34.4–43.6	9.2	0.12	0.83	0.10
Unconformity						
47.0–48.8	1.8	43.6–62.8 TD 62.8	[b]19.2	[b]1.07	[c]1.08	[b]1.16

nian flux value. The source of this activity remained close at hand to the west, because nearby drill sites do not contain any record of this Broken Ridge volcanism.

Carbonate deposition, however, changed markedly in the same time span. Limestones and chalks accumulated at about 4.3 g/cm²/1000 yr during the early Maestrichtian, in comparison with 0.7 g/cm²/1000 yr in the underlying ash-rich material. Flux rates of similar sediments on other oceanic plateaus were generally much lower than this. Carbonates on Ontong-Java, Shatsky, and Manihiki plateaus and the Magellan Rise accumulated through the later Cretaceous at rates of 1 to 2 g/cm²/1000 yr. Only Hess Rise, which was beneath the equatorial high-productivity zone at the time, has similar carbonate mass-accumulation rates of 3.8 g/cm²/1000 yr in the Campanian and Maestrichtian and 7.6 g/cm²/1000 yr during the early Cenomanian and late Albian (Thiede and Rea, 1981; Vallier et al., 1983).

These high carbonate flux rates for the northern edge of Kerguelen–Broken Ridge Plateau require a setting of high biological productivity and, most likely, deposition above the paleolysocline. Shell fragments were often transported into the area of deposition. Chert, the alteration product of biogenic silica, is also an indicator of high biological productivity. The sediments are completely bioturbated, which is an indication of oxygenated, open-water environments.

The important question posed by these deposits concerns the nature of the source of nutrients necessary to sustain millions of years of apparently high biological productivity. Whatever the source, it became effective some time during the eight million years unrepresented in the Leg 121 cores, between about 83 and 75 Ma. The time of about 80 Ma is important around the world as a time of plate boundary rearrangement, changes in the rates and directions of plate motion, and the opening of oceanic gateways (Berggren and Hollister, 1977). Shallow oceanic circulation between Antarctica and Australia may have begun at that time. Furthermore, the northward motion of India, which became much more rapid than it had been previously, may have allowed true oceanic circulation in the proto-Indian Ocean south of the subcontinent. Whatever the cause, some important change in oceanic circulation across Kerguelen–Broken Ridge Plateau is implicated in the large increase of the fluxes of biogenic sediments. Northward plate motion of the plateau itself was minimal during the Late Cretaceous, so any new circulation patterns would have influenced regions at fairly high latitudes in the southern proto-Indian Ocean.

The great oceanic rises, when they project up into the realm of the ocean surface circulation, cause bathymetrically-induced upwelling as those currents are forced upslope. Nutrients are thereby brought into the photic zone and productivity is en-

Table 1 (continued).

Age (Ma)	ΔT (m.y.)	Depth (mbsf)	ΔZ (m)	Linear sedimentation rate (cm/1000 yr)	Dry-bulk density (g/cm^3)	Mass-accumulation rate (g/cm^2/1000 yr)
Hole 754A						
0.0–1.9	1.9	0.0–6.3	6.3	0.33	0.89	0.30
1.9–2.2	0.3	6.3–7.3	1.0	0.33	[d]0.91	0.30
2.2–2.6	0.4	7.3–10.4	3.1	0.78	0.93	0.73
2.6–3.5	0.9	10.4–16.0	5.6	0.62	1.05	0.65
3.5–3.8	0.3	16.0–18.4	2.4	0.80	1.00	0.80
3.8–5.0	1.2	18.4–24.0	5.6	0.47	0.98	0.46
5.0–6.5	1.5	24.0–33.4	9.4	0.63	1.00	0.63
6.5–12.0	5.5	33.4–47.5	14.1	0.26	0.96	0.25
12.0–14.4	2.4	47.5–75.2	27.7	1.15	1.07	1.23
14.4–15.4	1.1	75.2–81.6	6.4	0.58	0.97	0.56
15.4–17.1	1.7	81.6–88.2	6.6	0.39	0.90	0.35
17.1–21.5	4.4	88.2–91.3	3.1	0.07	0.86	0.06
21.5–23.7	2.2	91.3–107.8	16.5	0.75	1.00	0.75
23.7–28.2	4.5	107.8–115.3	7.5	0.17	0.97	0.17
28.2–30.2	2.0	115.3–122.2	6.9	0.34	1.19	0.40
Unconformity						
Hole 754B						
74.0–75.0	1.0	224.0–262.8 TD 354.7	38.8	3.88	1.97	7.64
[a]Hole 755A						
0.0–1.9	1.9	0.0–7.1	7.1	0.37	0.96	0.36
1.9–10.0	8.1	71.0–45.8	38.7	0.48	[e]1.00	0.48
10.0–10.8	0.8	45.8–55.5	9.7	1.21	[e]1.00	1.21
10.8–14.9	4.1	55.5–65.6	10.1	0.74	[e]1.00	0.74
Unconformity						
83.0–86.6	3.6	65.6–91.5	25.9	0.72	1.98	1.43
86.6–88.5	0.9	91.5–120.5	29.0	1.53	1.78	2.72
88.5–89.5	1.0	120.5–169.7 TD 208.4	49.2	4.92	1.96	9.64

Note: TD = total depth.
[a] Rotary coring; poor Neogene recovery.
[b] Minimum value only.
[c] Values from equation in Rea (1982).
[d] Average of values above and below.
[e] No data, estimated value.

hanced. In the case of the Kerguelen–Broken Ridge Plateau, this scenario would further imply the development of a drift current in the southern proto-Indian Ocean about 80 m.y. ago—because the plateau was already there. Apparently the increase in carbonate productivity records the evolution of the environment of Kerguelen–Broken Ridge Plateau from a marginal sea, shielded by India, to that of an open ocean, complete with drift currents.

The ash deposited at the Broken Ridge drill sites may have brought micronutrients such as silica to the waters of the northern Kerguelen–Broken Ridge Plateau. Furthermore, a significant landmass can be an important source of nutrients. Drilling on the central Kerguelen Plateau during Leg 120 documented Maestrichtian coarse clastic intervals representing a period of uplift and erosion of the adjacent islands. The increased occurrence of larger shell fragments and scattered indications of current scour in the Maestrichtian sequence on Broken Ridge may reflect this episode of uplift on the central part of the Kerguelen–Broken Ridge Plateau. Runoff from this Late Cretaceous archipelago would have enhanced the ambient nutrient supply.

On a global scale, the Campanian-Maestrichtian was a time of enhanced silica deposition, now preserved as the abundant Upper Cretaceous cherts, and enhanced carbonate deposition, much of it on shallow-water continental margins and inland seas as well as oceanic platforms like Broken Ridge. On this scale the elevated flux of silica and carbonate requires that more Si and Ca be delivered to the oceans per unit time. These elements can come from either chemical weathering of the continents or from enhanced seafloor hydrothermal activity engendered by the Late Cretaceous spreading-center rearrangements. Fluxes of the biogenic components at the Kerguelen–Broken Ridge Plateau also require a local regional enhancement of the ambient oceanic nutrient supply to account for the Maestrichtian carbonate fluxes (Table 2 and Fig. 9).

Depositional Environments at the Cretaceous/Tertiary Boundary

The Cretaceous/Tertiary boundary was recovered at Hole 752B. The rock record of this important event must be interpreted with caution. The recovered materials are in the form of "drilling biscuits," 4–10-cm cylinders of rock that twist off during the coring process and are captured by the core barrel. There is no way of knowing how much material is missing between biscuits. Core 121-752B-11R, the boundary core, recovered 52% of the drilled 9.7 m of sediment. The only chert recovered occurs

Table 2. Paleogene and Cretaceous fluxes of major sedimentary components.

Hole	Age (Ma)	Total mass-accumulation rate (g/cm^2/1000 yr)	Abundance (%)			Mass-accumulation rate (g/cm^2/1000 yr)		
			Calcium carbonate	Opal	Ash	Calcium carbonate	Opal	Ash
753A	47.0–48.8	1.16	89	2	9	1.03	0.02	0.10
752A	55.3–57.8	3.06	81	6	13	2.48	0.18	0.40
	57.8–59.2	2.95	73	9	18	2.15	0.26	0.53
	59.2–60.0	3.06	82	9	9	2.51	0.28	0.28
	60.0–61.6	2.32	68	16	16	1.58	0.37	0.37
	[a]61.6–62.0	[a]15.25	73	13	14	[a]11.13	[a]1.98	[a]2.14
752B	63.8–64.8	5.17	62	19	19	3.21	0.98	0.98
	64.8–65.9	1.64	58	21	21	0.95	0.34	0.34
	65.9–66.4	1.43	30	5	65	0.43	0.07	0.93
	66.4–69.0	4.86	81	4	15	3.94	0.19	0.73
754B	74.0–75.0	7.64	61	6	33	4.66	0.46	2.52
				Glauconite			Glauconite	
755A	83.0–86.6	1.43	25	1	74	0.36	0.01	1.06
	86.6–88.5	2.72	18	2	80	0.49	0.05	2.18
	88.5–89.5	9.64	13	20	67	1.25	1.93	6.46

[a] Short zone at core bottom is unreliable and was averaged with zone above for plotting.

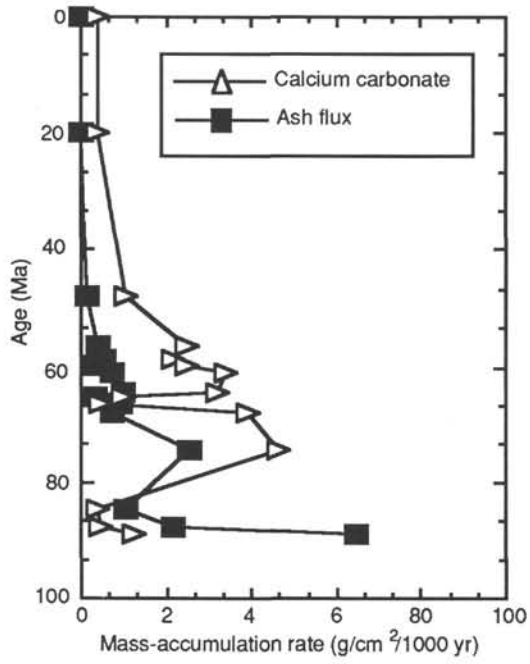

Figure 9. Mass-accumulation rates of the major sediment components on Broken Ridge through time, from the mid-Cretaceous to the present.

in the middle of the 23-cm-long transition zone between subboundary Cretaceous flora and fauna and supraboundary Tertiary flora and fauna (Fig. 7). In general, most of the recovery loss is associated with cherts, so important components of the Cretaceous/Tertiary boundary section may be missing from Core 121-752B-11R. Bearing this in mind, the sediments of the Cretaceous/Tertiary boundary section seem little different than those above or below. Light gray, mottled, and faintly laminated chalks record open-ocean deposition at rates of 4 g/cm^2/1000 yr, implying continuing high productivity. The chalks terminate at a biscuit boundary, above which is a large burrow structure capped by an ash layer, in turn overlain by chalk exhibiting soft-sediment deformation or slump structures. Above the next biscuit boundary is 8 cm of gray chert and porcellanite in the form of a few pebbles. Above the chert pebbles, a light gray chalk layer grades upward into another ashy unit that occurs in two biscuits. Above the ash layer is 23 cm of gray chalk in six biscuits (Fig. 7). There are a total of ten biscuit boundaries in the interval of core that contains the boundary. The depositional environment is characterized by moderate energy, horizontal laminations in the ash layers, oxygenated bottom waters, burrows and mottles, and continuing ash influx.

Immediately overlying this boundary section is an ash layer that may exceed 6 m in thickness, the thickest ash unit in the upper Campanian through middle Eocene part of the sequence. Magnetic susceptibility information (see "Paleomagnetics" section) suggests that this thick unit may represent a compound ash layer, composed of several individual ash-fall events. This unique deposit may represent either a sudden, somewhat greater, influx of volcanic debris or the normal, ongoing ash flux in the context of greatly reduced carbonate input. The flux data permit differentiation between these possibilities (Table 2 and Fig. 9). The flux of volcanic ash increases from 0.7 g/cm^2/1000 yr in the uppermost Maestrichtian zone to 0.9 g/cm^2/1000 yr in the lowest Paleocene zone, an increase smaller than the errors of our calculations. At the same time, the mass-accumulation rate of calcium carbonate falls from 3.9 to 0.4 g/cm^2/1000 yr just above the boundary, almost an order of magnitude reduction of flux. The important change in sedimentation at the Cretaceous/Tertiary boundary, therefore, is the rate of deposition of the biogenic component. Ash flux may increase only moderately.

The significant implication of this scenario is that the carbonate flux at Kerguelen–Broken Ridge Plateau was greatly reduced through the initial two zones of the Tertiary, a period of about 1.5 m.y. The flora preserved in the thick ash unit comprises an assemblage of opportunistic "survivor species" that bloomed when previously dominant groups were no longer competitive or were absent (see "Biostratigraphy" section, this chapter). Therefore, the record is of an oceanic ecosystem lasting

more than a million years where the combination of nutrient supply and the ambient carbonate-secreting organisms was suddenly insufficient to precipitate previously normal amounts of calcite (Zachos and Arthur, 1986). Normal productivity resumed between 63.8 and 64.8 Ma (Table 2 and Fig. 9).

Paleoenvironments of the Early Paleogene

The Paleocene and Eocene chalks record open-ocean, high-latitude deposition on the then gradually subsiding northern margin of the Kerguelen–Broken Ridge Plateau. Sediment mass-accumulation rates remained high. Volcanic ash accumulated at up to 1.0 g/cm^2/1000 yr, still at a large input value, and recorded the waning eruptive cycle that began in the Mesozoic.

Biogenic components continued to accumulate at rapid sedimentation rates of about 2.4 to 4.2 g/cm^2/1000 yr. Sediments of middle to late Paleogene age are enriched in diatoms and radiolarians, and opal exceeds 30% of the sediment. The opal flux during these times was as much as 1.0 g/cm^2/1000 yr (Table 2), which is a high rate for open-ocean silica productivity. The preservation of the fragile silica tests implies a lack of mechanical abrasion and, hence, a generally quiet depositional environment.

Information from foraminifers, both from the benthic assemblages and the planktonic to benthic ratios, suggests that the lower Paleocene material accumulated in rather shallow water depths, probably on the upper slopes. Water depths, as determined from these considerations, gradually increased throughout the Paleocene and into the Eocene, reaching perhaps 1000 to 1500 m. The sedimentary structures in the lower and middle Paleocene materials (horizontal laminae with scoured lower contacts, cross bedding, and graded bedding) are a direct indication of current velocities above the threshold of motion of silt, approximately 20 cm/s.

The short middle Eocene section encountered at Site 753 provides the last glimpse of the north slope of the broad Kerguelen–Broken Ridge Plateau. The environment did not change, remaining fairly shallow, perhaps middle to lower bathyal, in open oxygenated waters and receiving dominantly pelagic material. Ash accrued at only 0.1 g/cm^2/1000 yr or less, a more normal value for Eocene sediments; the long eruptive history of the nearby volcanic center was over. In the 5 m.y. represented by the unrecovered sediments below the bottom of Hole 753A and above the Paleogene material in Hole 752A, the flux of carbonates dropped to about 1.0 g/cm^2/1000 yr, which is low by Kerguelen–Broken Ridge Plateau standards but well within the normal range of fluxes observed on other oceanic plateaus. Perhaps the ongoing subsidence at that time lowered the platform such that bathymetrically-induced upwelling no longer provided a significant flux of nutrients to the photic zone. Alternatively, the event could record reduced intensity of oceanic surface circulation or migration of the sub-polar convergence away from the site.

Lacunae and Hiatuses

Two distinct limestone pebble layers, each representing an important unconformity, were found at Sites 752 and 754. The older layer denotes the major angular unconformity atop Broken Ridge (Fig. 2) and, at Site 752, separates underlying lower Eocene chalk from overlying upper Eocene ooze. The age of oldest material above this unconformity is about 38 Ma, and the youngest material below, recovered at Site 753, is about 45 Ma, so the timing of this event denoting the uplift of Broken Ridge during rifting is well constrained. The amount of uplift must have exceeded 2000 m over the course of, at most, 2 or 3 m.y. or possibly much more rapidly. Exposed Cretaceous limestone and chert sequences were subjected to subaerial erosion and shed clastics down the north-facing dip slope. Both of these lithologies are represented in the Eocene pebble layer. Open-water carbonate deposition resumed with the ensuing subsidence. The earliest deposition took place in shallow conditions, as evidenced by the benthic foraminifers, some of which have suffered mechanical abrasion, and the large rounded quartz grains in the upper Eocene ooze.

The sediment overlying the lower pebble layer is brown at the Broken Ridge sites, as a result of staining by iron oxide. The sudden increase in iron flux may have resulted from weathering of the uplifted Cretaceous and Paleogene sediments. Alternatively, increased iron fluxes are associated with suddenly enhanced seafloor hydrothermal activity, which has been shown elsewhere to increase by as much as an order of magnitude at times of ridge jumps and rift initiation (Owen and Rea, 1985; Lyle et al., 1987).

The younger pebble layer marks a disconformity that separates upper Eocene ooze from upper Oligocene ooze. The oldest age of the overlying sediment is about 30 Ma, and the youngest age of the underlying material is about 38 Ma. Lower to upper Oligocene flora are mixed in with this pebble layer. The Oligocene hiatus on Broken Ridge could result from either a relative fall in sea level or an intensification of ocean circulation. Kennett (1982) suggested that ocean circulation in the Southern Hemisphere became more intense at the time of the ice volume increase at the Eocene/Oligocene boundary, presumably in response to heightened pole-to-equator temperature gradients. He noted widespread early Oligocene hiatuses in support of this suggestion (Kennett, 1982). The presence of the pebble layer implies a change in relative sea level as the cause of this event because the alternative cause, an increase in oceanic current velocity, would not expose the rocks of Broken Ridge to further erosion or occasion the transport of pebbles.

The relative drop in Oligocene sea level almost certainly exceeds at least 100 m. Cretaceous and Paleogene rocks and sediments were again exposed to erosion and transported down the then gentler north-facing dip slope. Because Broken Ridge subsided very slowly in the Oligocene, the relative fall in sea level must represent a true eustatic sea-level fall, the 30 Ma sea-level fall depicted on the "Vail curves" (Haq et al., 1987).

Neogene Currents

Above the Oligocene disconformity is a condensed but apparently complete Neogene section of foraminiferal and nannofossil oozes. This section accumulated at average rates of 0.35 to 0.5 g/cm^2/1000 yr (Table 1), which are much lower than rates in the underlying Paleogene section. The combination of shallow depths, a high percentage of foraminifers, and a low carbonate MAR are all consistent with the interpretation of the DSDP Leg 26 scientists that this unit is a winnowed foraminifer nannofossil silt and sand layer (Davies, Luyendyk, et al., 1974). If this interpretation is correct, then the bulk grain size of these sediments should provide a crude indication of current velocity across Broken Ridge.

The subsidence history of Broken Ridge began about 100 m.y. ago. The late Eocene uplift events were mechanical rather than thermal in nature, and the measured heat flow (see "Physical Properties" section, this chapter) is characteristic of old ocean crust, so the thermal subsidence curve was not reset during the Eocene rifting event. Seafloor older than 70 or 80 Ma subsides at a rate slower than the simple square root of time relationship observed for oceanic lithosphere, so the maximum anticipated Neogene subsidence at Broken Ridge is about 300 m. Sclater et al. (1985) calculated 316 m of subsidence for Broken Ridge since 22 Ma, based on the assumption of 85-m.y.-old crust. Our determination of 100-m.y.-old crust means that the calculated Neogene subsidence would be somewhat less than this amount.

If the only process affecting the winnowing energy across the crest of Broken Ridge was gentle subsidence, then the sediment

grain size would be expected to display a smooth, upward-fining sequence. Any additional character in the grain-size curve represents additional processes. Two such processes that are especially likely are changes in relative sea level and fluctuations in the velocity of ocean currents. Rises in relative sea level would result in a lower-energy seafloor and deposition of smaller size grains, whereas an upward-coarsening sequence might reflect a fall in sea level. Similarly, stronger ocean currents would be expected to remove finer grains from the depositional site, leaving a lag deposit of coarser sediment.

Complete recovery of the winnowed pelagic section above the middle Oligocene disconformity by the APC at three sites provides an opportunity unique in the annals of DSDP/ODP to investigate the actual physical record of past oceanic surface circulation. The Pleistocene record of Antarctic Bottom Water flow through the Vema Gap in the Rio Grande Rise in the South Atlantic has been determined on the basis of changing sediment grain size (Ledbetter, 1979), as has the nature of abyssal reworking of Miocene nannofossil ooze in the southeast Pacific (Rea and Janecek, 1986). Leg 121 Sites 752, 753, and 754 all recovered apparently complete sections of the ooze. The downcore grain-size determinations of those sediments show fluctuations that are temporally coherent from site to site (Fig. 5). We presume that these fluctuations are real indications of the winnowing energy at Broken Ridge over the past 28 m.y.

The size of the winnowed grains decreased during the late Oligocene and earliest Miocene from 28 to 20 Ma, increased during the late early Miocene from 20 to about 16 Ma, decreased from 16 to 13 Ma, increased through the middle and late Miocene from 13 to about 6 Ma, decreased to a low in the early Pliocene at about 2.5 or 3 Ma, and may have increased during the Pleistocene. The transition most probably related to a change in relative sea level is the lowermost, upward-fining sequence of the upper Oligocene and lowermost Miocene. This change, which begins with the mid-Oligocene pebble layer, apparently reflects the increase in water depths on Broken Ridge as eustatic sea level rose, following the 29 to 30 Ma lowstand, to a relative high at 21 Ma (Haq et al., 1987). Although we can not completely discount the effects of ensuing lesser eustatic sea-level changes, the remaining changes in grain size are interpreted to reflect changes in the circulation intensity of the wind-driven geostrophic drift current on the southern side of the Southern Hemisphere subtropical gyre. Since 28 m.y. ago, the Broken Ridge platform has moved north through about 15° of latitude, starting from about 46°S.

The grain-size data suggest that ocean circulation intensity increased three times during the Neogene, at 20–16, 13–6, and since 2.5 Ma. Decreases in current speed occurred at 16–13 and 6–2.5 Ma. The important climatic changes that occurred in the Miocene are usually linked with episodes of ice volume growth on Antarctica. Paleoclimatologists have generally assumed that increased ice volume can be equated with colder polar temperatures, steeper pole-to-equator temperature gradients, and thus more vigorous atmospheric and oceanic circulation. The weak link in this presumptive chain is the intuitive coupling of ice volume and temperature at the poles, while the other assumptions are better demonstrated from observation.

A particularly good example of this is the event of 16 to 13 Ma, when an ice volume increase significant enough to cause a 1‰ enrichment of oceanic ^{18}O values for benthic foraminifers occurred on Antarctica (Woodruff et al., 1981; Vincent et al., 1985). This event would also have caused a eustatic sea-level fall and, presumably, significantly intensified atmospheric and oceanic circulation. Both of these consequences would tend to result in a coarser grain size for the winnowed deposits, yet this was most clearly a time of increasingly finer grains at all three of these Broken Ridge sections (Fig. 5). Although the middle to late Miocene is thought to be a time of steady or perhaps decreasing ice volume, there was a constant coarsening of the winnowed grains from 12 to 6 Ma. These observations suggest that the circulation intensity of the ocean is not directly linked to polar ice volume. The intensity of Southern Hemisphere atmospheric circulation also appears to have increased at this later time, between 11 and 9 Ma, rather than earlier during the ice volume increase (Rea and Bloomstine, 1986). The uppermost Miocene Southern Hemisphere ice buildup event at about 5 Ma also corresponds to a time of decreasing grain size on Broken Ridge, so the pattern is consistent.

The implications are that a moisture supply threshold (Ruddiman and McIntyre, 1984) may be important for significant ice buildup, instead of any further reduction in the temperature of polar regions. Southern Hemisphere temperature reductions may follow ice buildup by a few million years, as snow-covered and high-albedo regions slowly increase in area. The Northern and Southern hemispheres may behave differently in this respect because Antarctic high-albedo regions are effectively limited by the ocean, while the continents of the Northern Hemisphere permit the rapid expansion of high-albedo regions.

The lower Pliocene grain-size minimum corresponds with the last-known time of equitable climates before the onset of Northern Hemisphere glaciation at 2.4 or 2.5 Ma. The change in Southern Hemisphere ice volume during the past 2.5 m.y. is not clear.

Summary

The Kerguelen–Broken Ridge Plateau was formed by constructional volcanism during the mid-Cretaceous, presumably the Albian, on the basis of dated dredged basalts and drill hole basement ages. This broad depositional platform has remained within 1 or 2 km of sea level throughout its history while accumulating a dominantly biogenic sedimentary section of limestones, chalks, and cherts. At the very northern edge of this broad submarine bank, a strong local volcanic center provided voluminous ash deposits for over 30 m.y., from 90 to 60 Ma.

In Turonian through Santonian time most of the Kerguelen–Broken Ridge Plateau was a shallow open-ocean carbonate bank, receiving a low to moderate flux of calcium carbonate at about 0.7 g/cm^2/1000 yr, and the site of extensive glauconite formation. The nearby volcanic center became active sometime after the inception of this depositional environment and poured ash onto a small part of the northern edge of the platform at a rate of up to 6.5 g/cm^2/1000 yr.

At approximately 80 Ma some climatic or tectonic event occurred, or some threshold was crossed, to greatly increase the biological productivity of the overlying waters, because the flux of carbonate increased to about 4.7 g/cm^2/1000 yr in the lower Maestrichtian limestones and chalks (Fig. 9). These Late Cretaceous carbonate fluxes are among the highest ever recorded on oceanic plateaus and require a continuing environment of high biological productivity. Deposition of these carbonates and cherts therefore denotes a combination of increased oceanic circulation, perhaps the result of widening of the proto-Indian Ocean, and of bathymetrically-induced upwelling of the surface waters. The Broken Ridge drill sites lie on what was the northern edge of this broad platform, probably in a setting equivalent to the upper continental slope. Consistent with this scenario are sediment-accumulation rates commonly higher than on the adjacent shallow platform, 2 km of mid-Cretaceous through Eocene sediments, indications of moderate overburden, microfaults, and limestone, dolomite, and chert formation. The Broken Ridge

volcanic center continued to be a source of important amounts of ash during the latest Cretaceous, contributing 2.5 g/cm²/1000 yr (Fig. 9).

The Cretaceous/Tertiary boundary was recovered in Hole 752B. These sediments consist of the normal chalk-chert-ash layer sequence deposited preceding that time for about 10 m.y. The mass-accumulation rate of calcium carbonate dropped sharply at the boundary and remained low for the first 1.5 m.y. of the Tertiary, indicating a significant reduction in the overall rate of biological productivity. At the same time the input of volcanic ash rose slightly (Fig. 9).

Rates of carbonate and opal deposition recovered from the low values that existed immediately following the Cretaceous/Tertiary boundary and continued high through the Paleocene, providing an expanded and fossiliferous high-latitude section. Carbonate accumulated at 2.1 to 3.2 g/cm²/1000 yr, and the volcanic input was reduced to 0.5 g/cm²/1000 yr, indicating the waning of the long period of volcanic activity on the northern Kerguelen–Broken Ridge Plateau. By middle Eocene time these fluxes had been reduced to about 1.0 g/cm²/1000 yr for carbonate and 0.1 g/cm²/1000 yr for volcanic material, both of which are normal values for oceanic shallow-water depositional settings. The Late Cretaceous through middle Eocene record is one of decreasing ash input, waning biological productivity (from very high to normal values), and gentle subsidence (Fig. 9).

An episode of uplift and erosion occurred in the middle Eocene. The various sedimentary units were tilted gently northward and eroded, producing the striking angular unconformity seen in the seismic profiles (Fig. 2). Clastics, mostly pebbles of limestone and chert mixed with sand from the uplifted sediments, were shed northward along the exposed surface of the ridge and reworked into sand and gravel layers as it subsided below sea level. The total amount of vertical uplift may have exceeded 2000 m.

The Oligocene to Pleistocene history of Broken Ridge is one of gentle subsidence and northward drift to its present location at 30° to 31°S. A middle Oligocene disconformity occurs within the pelagic unit atop the ridge, perhaps recording the fall at 30 Ma in eustatic sea level. Upper Oligocene through Pleistocene carbonate oozes were deposited on this shallow platform at rather low flux rates of about 0.35 to 0.5 g/cm²/1000 yr and have been subjected to winnowing during the past 28 Ma. The winnowing record suggests, among other things, reduced ocean circulation intensity during times of Southern Hemisphere ice volume increase, but this observation contradicts the general assumption of significant polar cooling at times of ice volume increase.

TEPHRA

The common occurrence of ash fragments and layers in the Broken Ridge sediments of Late Cretaceous to Eocene age provides an important opportunity to evaluate (1) compositional variations between the ash layers with time and (2) possible sources for the volcanic ashes. The proximity of the Kerguelen hot spot to Broken Ridge at that time period suggests that the ashes may be associated with the hot spot; if this can be ascertained, it provides the opportunity to study a nearly continuous record of hot-spot volcanism with a temporal resolution on the order of a few million years.

Lithology

Traces of volcanic glass are present in every core recovered from Broken Ridge, although visible discoloration due to ash content in the split cores is most pronounced below the Eocene unconformity. The discoloration is very pale brown in the youngest oozes and grades to green and commonly black in the lower chalks and limestones, with the darkest layers reflecting the largest ash concentration. Smear slide analysis suggests that in most cases ash concentration does not exceed 20%, with an average of 6%. Concentrated ash layers (containing more than 50% glass; see the following text) occur in Cores 121-752B-10R and 121-752B-11R above the Cretaceous/Tertiary boundary, as well as in Cores 121-755A-5R to 121-755A-12R, 121-755A-18R, and 121-755A-19R. Ash concentrations reaching 94% are in the interval from 103 to 106 cm in Section 121-754B-9R-6 and in vitric tuff layers in Core 121-755A-19R. Ash was detected only in trace amounts in the chert layers recovered in Cores 121-754B-19R through 121-754B-25R, although this is probably the result of the poor recovery or perhaps the alteration of the ash in these silica-rich layers.

The ash-rich layers occur in three configurations: (1) sharp or only mildly diffuse lower contacts and very gradational upper contacts, (2) sharp upper and lower contacts, and (3) zones of composite ash layers totaling more than 1 m thick.

The first layer type is characterized by sharp lower contacts, rarely disturbed by burrowing, and by diffuse gradational upper contacts. The concentration of ash decreases gradually upward, and the size and shape of the glass particles appear constant within a given layer; however, crystal content in the layers seems to increase near the lower contact. The average thickness of the layers is 40 cm, with none more than 1 m thick. The layers, which resemble ashes commonly recorded in other deep-sea cores (Norin, 1958; Ruddimann and Glover, 1982), are thought to represent ash falls that have been strongly bioturbated. Visible burrows and fossil fragments found in and above the ash demonstrate that bioturbation has been an important post-depositional process (Fig. 10).

The second type of layer consists of ash transported and deposited in small local turbidity flows. These layers have sharp upper and lower contacts, and some are weakly graded. They show limited amounts of bioturbation and are only 10 cm thick or less. The layers occur sporadically in the cores from Sites 752, 753, and 754. The concentrated ash layer at 103–106 cm in Section 121-754B-9R-6 is a reworked layer of this type.

The third type of ash layer is large composite ash deposits that total 1 m or more in thickness and occur both as bioturbated and reworked layers. Layers of this type are present immediately above the Cretaceous/Tertiary boundary in Core 121-752B-11R and also in Cores 121-755A-18R and 121-755A-19R. The thick ash layer in Core 121-752B-11R probably resulted from a drop in the accumulation rate of biogenic material just above the Cretaceous/Tertiary boundary. The composite ash layers in Hole 755A may have resulted from an increase in volcanic activity at those times.

The calculated mass-accumulation rates of the ashes ("Sedimentation" section, this chapter) decrease upsection from a maximum of 6.46 g/cm²/1000 yr for the tuffs of Hole 755A, to 2.52 g/cm²/1000 yr in Hole 754B, to 0.40 g/cm²/1000 yr at about 56 Ma in Hole 752A, with a minimum of 0.10 g/cm²/1000 yr at about 45 Ma in Hole 753A. These data indicate a decrease in ash deposition on Broken Ridge with time in the Late Cretaceous and Paleogene. Subaerial basaltic volcanism typically does not distribute ash more than 100 km from the source vent (Kennett, 1981); however, phreatic activity, or magma/water interaction, can create larger eruption columns and thus have a larger distribution of tephra.

Based on the color and refractive index of volcanogenic glass in smear slides, the method of Schmincke (1981) suggests that most of the glass observed in the smear slides is of basic composition, a conclusion supported by X-ray-fluorescence (XRF) analysis (see the following). Some glass with a lower refractive index was observed as a trace component at all of the sites, with the most notable occurrence in a concentrated layer at 77–80 cm in Section 121-754B-7R-1. This clear glass is more silicic. The

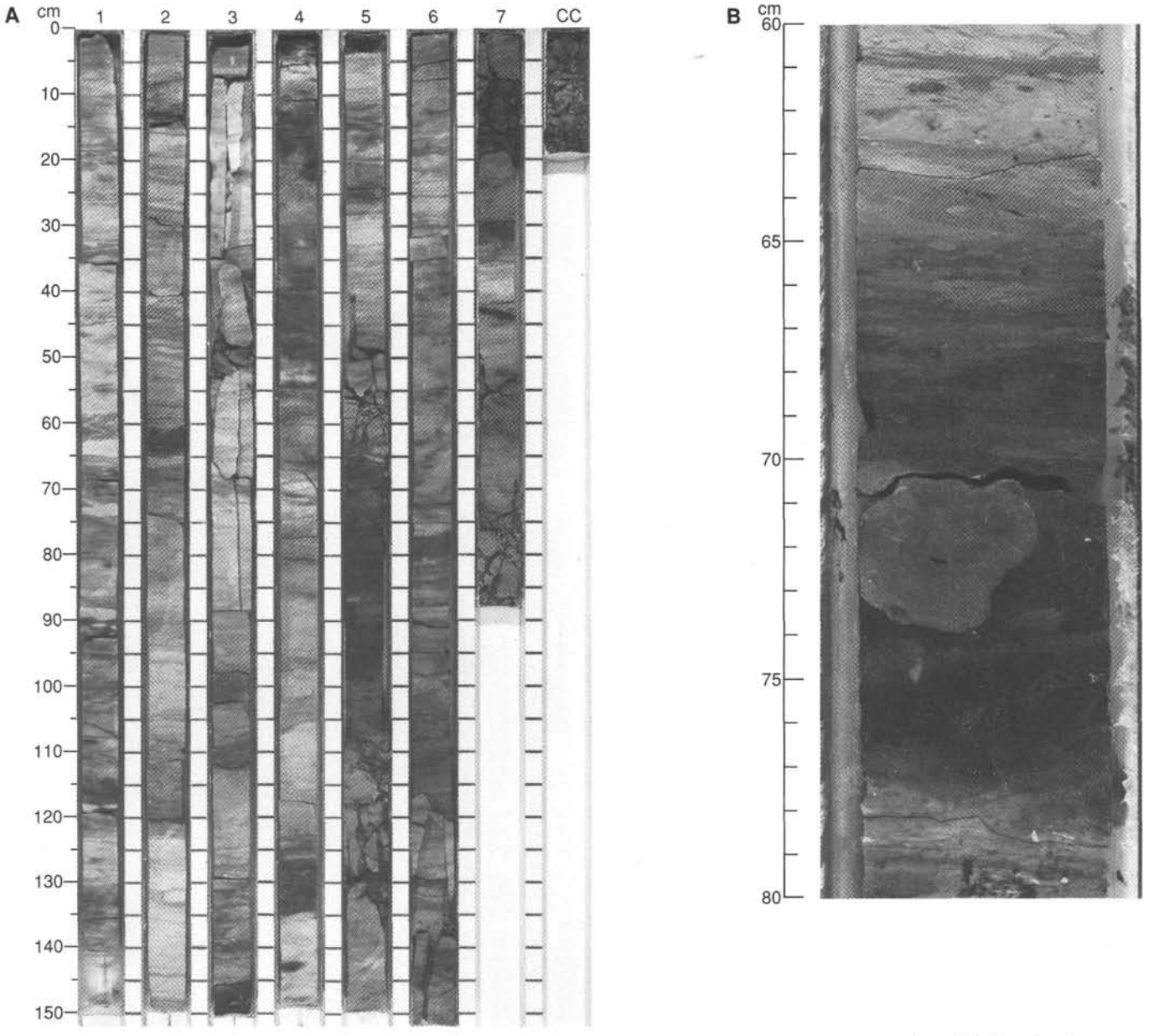

Figure 10. **A.** Alternating ash layers in a limestone matrix (Core 121-754B-14R). The ash horizons are less than 1 m thick, with sharp basal contacts and gradational upper contacts. **B.** Close-up photograph of Section 121-754B-15R-1, 60–80 cm, shows burrowing in the ashes.

observance of rare grains exhibiting myrmekitic texture, an intergrowth of quartz and potassium feldspar, again suggests silicic volcanism. The presence of these grains and glass shards is probably the result of far-field large silicic eruptions.

The glass is commonly altered, usually to palagonite and clays. Smectite is common in a poorly crystalline form, and while it was rarely observed in the smear slides, it is visible in photomicrographs taken with the scanning electron microscope (SEM). Zeolites were observed as trace components in the lower part of the stratigraphic section. Quartz and plagioclase crystals occur as common trace components in the smear slides, and pyroxene crystals were noted at 106 cm in Section 121-754B-9R-6. Apatite is also a common trace component, occurring in quantities as high as 5% in Core 121-755A-19R.

Glass shards were studied with the SEM. The shards are primarily vesicular pumice fragments or are blocky with few vesicles. The blocky shards suggest a lower volatile content in the magma. Also seen were tear-drop pumice shards (Fig. 11), which are typical of basaltic eruptions, and solid glass spherules, for which no origin has been determined. Separation planes as well as poorly crystalline, curled plates of smectite are visible on the highly altered glass shards (Fig. 12). The large volume of clays and the fine fraction of glass seen with the SEM could account for the discrepancy between the low amount (6%) of observed glass in the smear slides and the calculated amount of volcanogenic material in the cores based on chemical studies (see the following).

Major and Trace Element Geochemistry of the Ash Layers

Thirty-six samples of ash-rich sediment were analyzed from the cores of Holes 752A, 752B, 754A, 754B, and 755A using the

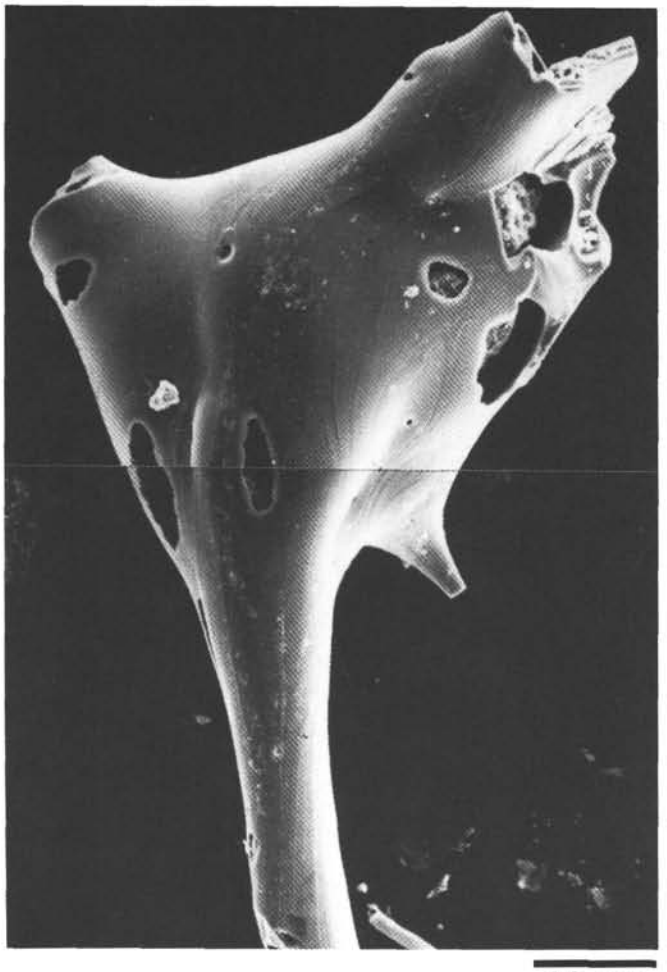

Figure 11. SEM photomicrograph of a tear-drop pumice shard from Section 121-752A-14H-CC (J. Smit).

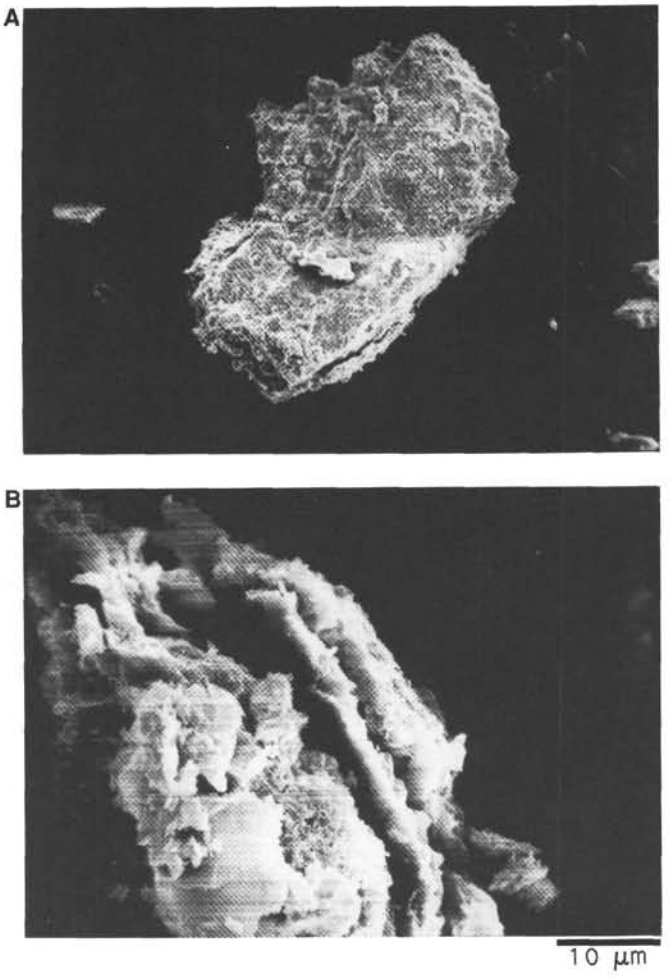

Figure 12. SEM photomicrographs of Sample 121-754B-9R-6, 106 cm. **A.** Blocky glass shard coated with smectite. **B.** Parting planes and plates of smectite on an altered pumice fragment.

shipboard XRF. For comparative purposes, geochemical data are available for Kerguelen Plateau basaltic lavas over a wide range of ages (40 to 6 Ma; Weis et al., 1987b; Gautier et al., 1987; M. Storey and A. D. Saunders, unpubl. data) and for Ninetyeast Ridge DSDP Sites 214, 216, 253, and 254 from 40 to 80 Ma.

Analytical Approach

Ash-rich samples were identified and selected on the basis of their dark color and, in the case of the more basic ashes, on the basis of their high magnetic susceptibility. All analyzed samples are mixtures of ash and calcareous oozes and chalks; the principal contaminant is biogenic calcium carbonate, although siliceous biogenic material is also present, usually in amounts less than 10%. Six samples were analyzed for major elements (Table 3), one ash-poor sample was analyzed for trace elements (Table 4), and all 36 ash samples were analyzed for trace elements (Table 5). All samples were analyzed for CO_2 content, and the trace element data are reported on a calcium carbonate-free basis.

Carbonate-rich Sample 121-752B-8R-3, 148–151 cm (77.5 wt% $CaCO_3$ based on CO_2 content), was analyzed to assess its trace element content (Table 4). Except for Sr and Ba, the trace elements analyzed in the sample are at very low concentrations, which are considered negligible for our present purposes. Therefore, the carbonate component is only a dilutant for most of the trace elements analyzed. The abundances of some elements, such as Y and Ni, are slightly higher than expected in a pure carbonate sample. This implies that either the sample is not pure calcium carbonate (a small amount of ash or another component, such as dolomite or apatite, is present) or the carbonate fraction contains a small concentration of these elements.

We evaluated the effect of removing the calcium carbonate by acid dissolution, but complete leaching could not be achieved. Furthermore, cold HCl dissolution does not remove the biogenically-produced silica-rich components or dolomite.

Results

Major Elements

The major element oxide data are listed in Table 3. The six samples analyzed were selected on the basis of their low carbonate content (less than 20% $CaCO_3$). Except for Sample 121-754B-7R-1, 77–79 cm, which is trachytic in composition, the ashes have basaltic compositions. The high CaO content (>15%) of two of the samples reflects the presence of a large organic carbonate component. The other four samples have CaO contents typical of basalts. A small but significant amount of the carbonate calcium appears to be derived from the volcanic material.

Table 3. XRF major element analyses of representative ash-rich horizons, Hole 754B.

	7R-1, 77–79 cm	9R-6, 103–105 cm	11R-1, 80–81 cm	13R-4, 106–109 cm	14R-5, 93–95 cm	15R-5, 25–28 cm
SiO_2	59.2	51.4	49.1	46.8	50.1	51.6
TiO_2	0.87	2.19	2.26	1.52	1.52	1.65
Al_2O_3	15.4	12.0	11.5	10.8	9.9	12.1
Fe_2O_3*	10.7	13.1	12.6	11.8	11.0	11.9
MnO	0.01	0.04	0.03	0.06	0.06	0.00
MgO	7.9	7.6	8.0	6.6	6.8	9.5
CaO	1.2	7.5	10.2	16.0	15.2	6.7
Na_2O	2.8	3.3	2.7	3.4	2.7	2.7
K_2O	1.20	1.68	1.13	1.28	1.50	0.72
P_2O_5	0.12	0.17	0.14	0.14	0.14	0.07
	99.40	98.88	97.66	98.40	98.92	96.94

Table 4. Trace element analysis of ash-poor carbonate Sample 121-752B-8R-3, 148–151 cm.

$CaCO_3$ (wt%)	77.5
TiO_2 (wt%)	0.08
Nb (ppm)	0.4
Zr (ppm)	6
Y (ppm)	14
Sr (ppm)	718
Rb (ppm)	3
Zn (ppm)	8
Cu (ppm)	17
Ni (ppm)	11
Cr (ppm)	<1
V (ppm)	12
Ce (ppm)	1
Ba (ppm)	912
Zr/Nb	14.0
Ti/Zr	85.6
Zr/Y	0.4
[a](Ce/Y)n	0.2

Note: Approximate age of samples is 64 Ma.
[a] Chondrite-normalized ratio.

Trace Elements

Table 5 includes trace element data based on the presence and absence of carbonate. We focused on Ti, Zr, Nb, Y, V, Cr, and Ni because these elements have low abundances in pure $CaCO_3$, and they are relatively immobile during alteration of basaltic glass by seawater.

Most of the samples have Ni and Cr contents greater than 50 ppm (Table 5), indicating that they are dominantly basaltic ash. This conclusion is consistent with the relatively constant (~90 to 110) Ti/Zr ratios of basaltic lavas (Fig. 13); 27 of the 36 ash layers analyzed have Ti/Zr ratios ranging from 80 to 120. Sample 121-754B-7R-1, 77–79 cm, is an obvious exception, with >700 ppm Zr. This sample is not basaltic (Ni = 27 ppm, Cr = 0 ppm, and Ti/Zr = 6.7) and is discussed separately.

Some specific trace element abundance ratios are commonly used to discriminate between basaltic lavas produced in different tectonic settings. In particular, Zr/Nb ratios are a sensitive indicator of the tectonic eruptive setting, with characteristically low values (5–15) in ocean island basalts and higher values in mid-ocean-ridge basalts and island arc lavas. In these latter settings, the Zr/Nb ratio commonly exceeds 17 and may be as high as 40. In Figures 14 and 15, the overlap of the Broken Ridge ash data with those of the early, transitional flood basalts from the Kerguelen Island, Ninetyeast Ridge, and Kerguelen Plateau lavas is striking, but not unique. These ratios of 3.4 to 17.1 are consistent with ocean island magmatism in general. The proximity of the Kerguelen hot spot to Broken Ridge during pre-Eocene, pre-rifting time, however, makes the hot spot a likely source. It is noteworthy that the strongly alkaline, incompatible-element-enriched volcanic rocks erupted during the late Tertiary on Kerguelen (<26 Ma) and Heard islands (group 1 on Figs. 13 through 15), and which were recovered at Site 748 on the Kerguelen Plateau (Leg 120 Scientific Drilling Party, 1988), are not within the analyzed suite of Broken Ridge tephra, thereby implying that such magmas were not an important source for the pyroclastic material.

Relative abundances of rare earth elements also distinguish mid-ocean-ridge basalts from oceanic island basalts. Trends in light rare earth element/heavy rare earth element ratios are important in understanding mixing between hot-spot- and ridge-derived lavas (Schilling et al., 1983), and Ce/Y ratios are a measure of this fractionation. In the studied ashes, chondrite-normalized Ce/Y ratios range from 0.92 to 10 (Table 5), indicating source magmas that are relatively enriched in light rare earth elements. This indication is consistent with an ocean island basaltic source.

The spread of data on Figures 13 through 15 is not due to dilution by biogenic calcite or silica, but reflects magmatic fractionation instead. For example, Ni and Zr show a weak inverse correlation, typical of fractionation in basaltic rock series resulting from removal of mafic phases from the basaltic liquid (Fig. 16). A simple dilution of basaltic tephra by Ni- and Zr-free carbonate or silica would produce a collinear relationship between these two elements.

Sample 121-754B-7R-1, 77–79 cm, is petrographically and compositionally distinct from the other ash layers. It is almost carbonate free (0.5%) and is composed mainly of colorless glass in various stages of alteration. This sample has low magnetic susceptibility (low Fe?); very low Sr, Ba, Ni, and Cr contents; and an anomalously low Ti/Zr ratio (Table 5). These geochemical features are characteristic of more acid lavas, such as the microsyenites or trachytes of Kerguelen Island (Giret, 1983). The Zr/Nb ratio is indistinguishable from the bulk of the ratios of the analyzed tephra samples (Fig. 15), which is consistent with the sample being a high-level fractionate of the more basaltic components.

Temporal Variations in Ash Compositions

Table 5 includes an approximate age of deposition for each of the analyzed ash layers. The age range of the selected samples is limited (58 to 90 Ma). No systematic variations in ash composition can be discerned from these data. Determination of whether this invariable character is due to insufficient sampling, particularly in the younger sections of core, or to mask-

ing of subtle variations among the ash samples by the effects of carbonate and other contaminants awaits detailed shorebased studies.

Magnetic Susceptibility Studies of the Ash Layers

Ash layers within the Eocene to Upper Cretaceous calcareous platform sediments of Broken Ridge have physical and chemical properties that contrast markedly with those of the enclosing sediments. The large number of core measurements of one such property, magnetic susceptibility, provides important information on such features as (1) the proportion of ash in the sediments recovered, (2) changes in the overall pattern of volcanism with time, and (3) possible cyclicity in sedimentation or volcanism. The magnetic susceptibility measurement procedures and data are presented in the "Explanatory Notes" and Broken Ridge site chapters in this volume. Here, we emphasize application of these data to understanding the features of the ash layers.

Results from the Broken Ridge cores confirm that the volume susceptibility is a sensitive indicator of basaltic ash content, particularly where the ashes are intercalated in a low-susceptibility carbonate matrix. Figure 17 shows the susceptibility signal produced by the basaltic ash horizons, with susceptibility increasing by an order of magnitude to more than 500×10^{-6} cgs units where the ash content of the layer exceeds 50%. A detailed visual comparison of photographs of more than 25 m of core (121-754B-13R through 121-754B-15R) with the susceptibility measurements shows a similar correlation of the lithology with the susceptibility data. The routine susceptibility observations every 5 cm readily detect the thin basaltic ash layers that were degraded by bioturbation to form diffuse 5-cm-wide zones containing only 20% ash. Chemical analyses of the ash-rich horizons show that susceptibility values greater than about 800×10^{-6} cgs units indicate basaltic ash contents as high as 90%.

Although changes in the volume susceptibility reflect the changing proportion of ash in the sedimentary section, the absolute level of the susceptibility is also controlled by the mineralogy and thus by the composition of the ash. Figure 18 demonstrates the relationship of susceptibility to the TiO_2 content of the ash layers, as determined by XRF procedures. Part of the variation in the TiO_2 concentration is a function of varying degrees of dilution by biogenic material. However, there is also variation in the primary composition of the ash layers (see the previous discussion). Higher TiO_2 contents appear to be associated with higher total iron concentrations, which probably reflect higher modal percentages of ferromagnetic minerals.

Of the 36 Broken Ridge ash-rich samples analyzed by XRF during Leg 121, all but one are basaltic in composition. A single thick, more acidic, ash layer in Section 121-754B-7R-1, 77–81 cm, is associated with relatively low susceptibility values of less than 100×10^{-6} cgs units; however, low concentrations of $CaCO_3$ (Table 5), together with a high content of colorless glass, indicate an ash concentration for this sample of nearly 100%. These measurements show that susceptibility observations are only an accurate reflection of ash content if the ashes are of basaltic composition; silicic ash horizons may not have a strong susceptibility signature.

The susceptibility data from sections of the core where recovery was high provide a detailed continuous log of the proportion of basaltic ash in the section. Cores 121-754B-13R through 121-754B-15R constitute such a sequence in which the susceptibility data indicate that the proportion of ash varies rapidly; more than 25 discrete ash-rich horizons are identified within this upper to lower Maestrichtian sequence. Initial observations of the core indicated that the distribution of ash layers in this part of the stratigraphic section might not be random, but cyclic. A shorebased statistical analysis of the continuous susceptibility data, with possible accounting for variations in sedimentation rates, would allow assessment of cyclicity in the section.

The more than 7000 measurements of volume susceptibility of the middle Eocene to Upper Cretaceous limestones and chalks from Broken Ridge (refer to the chapters for Sites 752 through 755, this volume) provide a chronological record of the intensity of volcanism. These relations are shown in Figure 19, in which the median magnetic susceptibility for each core is plotted against stratigraphic depth in the section. The results indicate that the median volume susceptibility declines from about 100×10^{-6} cgs units in the Turonian at the base of the studied section to a median value of about 10×10^{-6} cgs units at the top of the section in the middle Eocene chalks at Site 753. This plot provides a picture of the changing influence of volcanism on sedimentation at Broken Ridge and the general decline in the proportion of volcanic material in the sediments with decreasing age.

The susceptibility values are also plotted against percentage of carbonate, using more than 100 measurements of total carbonate in core samples. Volume susceptibility was estimated from measurements made at 5- or 10-cm intervals in the cores. The results (Fig. 20) suggest that a nonmagnetic, noncarbonate component, probably biogenic silica, composes at least 10% of the bulk succession. Smear slide observations and logging results indicate that some parts of the section have much higher silica contents, particularly in lithologic Subunit IIB (see "Lithostratigraphy and Sedimentology" section, "Site 752" chapter). Thus, the Cretaceous to Eocene rocks have at least three significant components: (1) carbonate, (2) volcanic material, and (3) biogenic silica. The susceptibility results indicate that the percentage of volcanic material in the studied section declines significantly, from more than 50% at the base of the section to perhaps 10% at the top of the section at Site 753. These percentages are much higher than those estimated by smear slide analysis: microscopic analysis measures only the proportion of glass and volcanic detritus in the section and a significant clay-mineral fraction is unreported. The large volcanic component accounts, in part, for the high sedimentation rate during the Paleocene and Late Cretaceous.

Interpretation of the downhole logging results is helped by the very close spacing of the magnetic susceptibility data for the recovered core. Correlations are apparent in a display of the two types of data side by side. As the relation of the susceptibility data to the drilled lithology is known, we can deduce the relationships of the logs to lithologic variation at the two logged Broken Ridge sites (752 and 754). An example of this comparison is shown in Figure 21. Further work using relationships of this type is planned.

Conclusions

1. Volcanism was a major factor in the evolution of the sedimentary succession at Broken Ridge, and volcanic ash contributed significantly to the high sedimentation rates during the late Mesozoic and early Tertiary.

2. The intensity of volcanism declined significantly over the 40 Ma period from Turonian time.

3. The analyzed ashes within the section are dominantly basaltic and comparable in composition to rocks from Ninetyeast Ridge, the Kerguelen Plateau, and the older parts of the Kerguelen Islands.

4. Subordinate intermediate and felsic ashes make up less than 5% of the sampled volcanic material.

5. A composite 6-m-thick sequence of ash layers above the Cretaceous/Tertiary boundary and the tuffs of Hole 755A appear to mark a period of drastically reduced biogenic production of calcium carbonate and/or periods of increased volcanic activity.

Table 5. Trace element analyses of Leg 121 ash-rich sediments.

	752A-19X-3, 70–74 cm	752B-7R-4, 100–110 cm	752B-8R-2, 124–126 cm	752B-10R-7, 25–28 cm	752B-11R-1, 41–44 cm	752B-11R-2, 78–80 cm	752B-16R-3, 83–85 cm	754A-21N-1, 79–81 cm	754A-23N-1, 70–72 cm	754B-5R-2, 24–25 cm
Approximate age (Ma)	58	64	64	66	67	66	67	67	67	66
$CaCO_3$ (wt%)	30.2	47.6	29.7	24.2	4.0	9.5	37.0	51.5	25.0	59.6
TiO_2 (wt%)	0.73	0.79	1.17	1.52	1.89	1.66	0.83	0.91	1.51	0.61
Nb (ppm)	3.6	2.6	4.1	13.5	8.7	8.9	2.5	14.3	13.1	<1
Zr (ppm)	46	40	70	139	122	110	40	48	108	31
Y (ppm)	18	17	22	29	31	29	27	27	15	14
Sr (ppm)	490	902	753	883	777	994	1042	722	517	817
Rb (ppm)	15	10	13	26	36	26	13	11	12	17
Zn (ppm)	75	77	66	128	103	84	76	107	122	51
Cu (ppm)	72	71	90	47	86	91	70	81	110	54
Ni (ppm)	53	41	49	63	51	57	57	56	55	32
Cr (ppm)	95	73	51	15	29	29	14	38	11	91
V (ppm)	130	141	215	154	289	257	170	175	305	144
Ce (ppm)	8	10	14	35	35	31	12	17	63	17
Ba (ppm)	744	961	753	2685	1266	2021	466	810	396	690
Zr/Nb	12.8	15.4	17.1	10.3	14.0	12.4	16.0	3.4	8.2	12.0
Ti/Zr	95.1	118.4	100.2	65.6	92.9	90.5	124.4	113.7	83.8	118.0
Zr/Y	2.6	2.4	3.2	4.8	3.9	3.8	1.5	1.8	7.2	2.2
[a](Ce/Y)n	1.1	1.4	1.5	2.9	2.7	2.6	1.1	1.5	10.0	2.9
Calculated carbonate-free										
TiO_2 (wt%)	1.05	1.51	1.66	2.00	1.97	1.83	1.32	1.88	2.01	1.51
Nb (ppm)	5	5	6	18	9	10	4	29	17	<1
Zr (ppm)	66	76	100	183	127	122	64	99	144	77
Y (ppm)	26	32	31	38	32	32	43	56	20	35
Zn (ppm)	107	147	94	169	107	93	121	221	163	126
Cu (ppm)	103	136	128	62	89	101	111	167	147	134
Ni (ppm)	76	78	70	83	53	63	91	115	73	79
Cr (ppm)	136	139	73	20	30	32	226	78	15	225
V (ppm)	186	269	306	203	301	284	270	361	407	356
Ce (ppm)	11	19	20	46	36	34	19	35	84	42
Zr/Nb	12.8	15.4	17.1	10.3	14.0	12.4	16.0	3.4	8.2	—
Ti/Zr	95.1	118.4	100.2	65.6	92.9	90.5	124.4	113.7	83.8	118.0
Zr/Y	2.6	2.4	3.2	4.8	3.9	3.8	1.5	1.8	7.2	2.2
[a](Ce/Y)n	1.1	1.4	1.5	2.9	2.7	2.6	1.1	1.5	10.0	2.9

[a] Chondrite-normalized ratio.

6. Studies of the ash layers in pelagic limestones are greatly aided by magnetic susceptibility observations. Such observations should be closely spaced (<5 cm) and routinely made prior to splitting the core when volcanic ash is expected or encountered unexpectedly in the section.

BIOSTRATIGRAPHY

The objectives of drilling on Broken Ridge, to understand its uplift and subaerial erosion through the flexural response of the lithosphere to rifting, were met. Evidence for the timing of tectonic "events," the age of the sediments, and the water depth of sediment deposition is provided through faunal analysis. Both calcareous nannofossils and planktonic foraminifers were used to date (1) the subhorizontal sedimentary cap above the unconformity, (2) the age of the unconformity, and (3) the dipping and truncated sedimentary sequence beneath the unconformity (Fig. 4). Benthic foraminifers were used throughout to determine the water depths in which sediment deposition took place.

Neogene calcareous nannofossils are abundant. Throughout the Pleistocene, Pliocene, and Miocene sediments, nannofossil preservation is generally good. Strong overgrowth of the discoasters combined with the lack of zonal markers because of latitudinal effects made zonal assignments of the lower and middle Miocene sections more difficult. Paleogene nannofossils are similarly abundant, though with poorer preservation. In the Maestrichtian and upper Campanian(?), however, preservation is poor. Santonian to Turonian sediments were recovered only at Site 755, but the nannofossils are poorly preserved throughout the sediments of Hole 755A.

Neogene planktonic foraminifers are abundant and well preserved, with assemblages showing Southern Ocean, high-latitude affinities. The Eocene, Paleocene, and Maestrichtian planktonic foraminifer assemblages are also of a temperate nature. The absence of low-latitude marker species makes it impossible to apply known tropical zonation schemes.

Well-preserved benthic foraminifer assemblages were encountered throughout the Cenozoic.

Rare specimens of Neogene diatoms are present only at a few levels in Hole 754A. Well-preserved diatoms were found in the middle Eocene at Site 753 and in the lower Eocene to Paleocene at Site 752. This is the first documentation of early to middle Eocene age diatoms in the Indian Ocean. Cretaceous diatoms are rare, although a few were recorded at Hole 754B. Radiolarians, silicoflagellates, and sponge spicules are also present wherever diatoms occur.

A generally complete Neogene sequence of pelagic, foraminifer nannofossil ooze was recovered from Holes 752A, 753A, and 754A. As shown in Figure 2, the Neogene cap on the crest of Broken Ridge thins toward the south and north, away from a depocenter in the vicinity of Site 754. The nature of the benthic foraminifer assemblages suggests deposition of the sediments took place at middle to lower bathyal depths during the Neogene.

Two erosional surfaces, each characterized by pebble layers, bound an upper Paleogene interval on Broken Ridge at Sites 754 and 752. The two pebble layers coalesce and form a single hiatus to the north at Site 753 and to the south at Site 755.

An upper disconformity separates upper Eocene foraminiferal sands from those of late Oligocene or early Miocene age.

Table 5 (continued).

754B-7R-1, 25–28 cm	754B-7R-1, 28–30 cm	754B-7R-1, 77–79 cm	754B-9R-2, 78–80 cm	754B-9R-2, 132–135 cm	754B-9R-5, 69–71 cm	754B-9R-6, 82–83 cm	754B-9R-6, 103–105 cm	754B-9R-6, 107–108 cm	754B-10R-3, 133–134 cm	754B-11R-1, 80–81 cm	754B-12R-CC, 0–2 cm
67	67	67	68	68	68	68	68	68	68	69	69
56.9	51.7	0.5	59.8	35.7	64.1	58.9	9.1	21.8	51.5	14.1	66.6
0.78	0.92	0.79	0.38	1.20	0.57	0.68	2.09	2.1	0.71	2.15	0.48
4.4	5.1	58.5	2.9	5.8	3.7	5.2	9.8	11.3	4.1	9.8	3.3
53	66	707	28	75	32	62	125	114	45	137	37
25	26	25	21	22	23	25	23	28	32	23	29
818	811	239	652	953	827	811	654	882	786	416	868
14	20	12	14	21	16	15	15	10	20	11	20
98	100	108	71	138	74	78	115	141	114	152	75
65	68	14	31	68	42	50	150	153	64	144	41
41	43	27	33	48	31	32	60	57	43	50	24
8	9	<1	15	35	10	20	22	26	14	40	14
144	174	29	66	178	735	93	339	266	126	346	89
10	10	84	<1	16	<1	15	32	28	7	35	13
1023	1157	33	3266	914	1262	1070	266	576	1560	200	1999
12.9	12.1	9.7		12.9	8.6	11.9	12.8	10.1	11.0	14.0	11.2
88.2	83.6	6.7	81.4	95.9	106.8	65.8	100.2	110.4	94.6	94.1	77.8
2.1	2.5	28.3	1.3	3.4	1.4	2.5	5.4	4.1	1.4	6.0	1.3
1.0	0.9	8.0	—	1.7	—	1.4	3.3	2.4	0.5	3.6	1.1
1.81	1.91	0.79	0.95	1.87	1.59	1.65	2.30	2.69	1.46	2.50	1.44
10	11	59	7	9	10	13	11	14	8	11	10
123	137	711	70	117	89	151	138	146	93	159	111
58	54	25	52	34	64	61	25	36	66	27	87
227	207	109	177	215	206	190	127	180	234	177	225
151	141	14	77	106	117	122	165	196	132	168	123
95	89	27	82	75	86	78	66	73	89	58	72
19	19	0	37	54	28	49	24	33	29	47	42
334	360	29	164	277	204	226	373	340	260	403	266
23	21	84	<1	25	<1	36	35	36	14	41	39
12.0	12.9	12.1	9.7	12.9	8.6	11.9	12.8	10.1	11.0	14.0	11.2
88.2	83.6	6.7	81.4	95.9	106.8	65.8	102.0	110.4	94.6	94.1	77.8
2.1	2.5	28.3	1.3	3.4	1.4	2.5	5.4	4.1	1.4	6.7	1.3
1.0	0.9	8.0	—	1.7	—	1.4	3.3	2.4	0.5	3.6	1.1

Up to 25% of the assemblages within samples above the disconformity are composed of reworked, late Eocene age forms such as *Globigerinatheka* sp. The benthic foraminifer assemblages suggest that deposition occurred at upper bathyal depths.

A lower, older erosional surface separates upper from lower Eocene foraminiferal sands in Hole 752A and from upper Maestrichtian sands in Hole 754A. This lower interval of erosion is represented by a layer of gravel and sand containing limestone, chert, and shell fragments. Within this "hardground," 90% of the assemblages are composed of planktonic foraminifers. Fifty percent of the planktonic foraminifers and nannofossils are reworked, iron stained, and moderately to poorly preserved. These forms are of P14/CP14 age. The other 50% of the planktonic foraminifers and nannofossils are "fresh" late Eocene age (P15 and P16) forms that show few signs of abrasion. This establishes the age of latest reworking. The absence of Oligocene and Neogene forms further indicates that reworking occurred during the Eocene. The high percentage of fresh, moderately preserved to well-preserved planktonic foraminifers suggests hemipelagic/pelagic deposition, whereas the benthic foraminifers indicate deposition at upper bathyal depths.

Shell and bryozoan fragments, shallow-water benthic foraminifers (e.g., *Amphistegina*), and ostracodes comprise 5% of the hardground assemblage. All of the fossils, however, show a high degree of abrasion because of reworking and transportation from shallower, calmer waters, presumably from the higher flanks to the south. Within the hardground are large (10–15-mm), fine-grained clasts containing a 100% reworked, middle Eocene planktonic foraminifer assemblage of P14 age (latest middle Eocene). This indicates the youngest age at which erosion of sediments occurred.

The presence of middle Eocene (P11/CP13c) sediments below the unconformity and sediments of P15/CP15 age above confines the interval of uplift and erosion to latest middle Eocene, P11 to P14 (i.e., a duration of 3.5 to 7.5 m.y.). This would mean that the 2 km of uplift related to rifting was fairly rapid, as was the ensuing subsidence that re-established hemipelagic deposition in the late Eocene. The subsequent return to normal pelagic deposition, at upper to lower bathyal depths, commenced in the late Oligocene.

The size of the clasts and the coarsest grains suggests that reworking of the sediment took place in a high-energy regime, whereas the angularity of the fragments suggests little transportation from their source. Therefore, Broken Ridge was probably uplifted to within wave base to provide enough energy to truncate the dipping sequence of sediments. The presence of *Braarudosphaera* is consistent with a shallow-water origin for the upper Eocene sediments directly overlying the dipping units. We found little direct evidence to suggest that Broken Ridge was subaerially exposed during the middle Eocene. The iron oxide deposits on the reworked planktonic foraminifers suggest a nearby subaerial environment providing iron oxide detritus. The lower Santonian limestones immediately beneath the unconformity are oxidized only at the southernmost Site 755. However, burrows and/or rootlet horizons were not found in the limestones, as would be expected if the limestone surface represents a weathered horizon.

The middle Eocene to Paleocene sediments recovered below the lower unconformity at Sites 754, 752, and 753 are characterized by high planktonic/benthic ratios that indicate pelagic deposition. These sediments also contain a benthic foraminiferal assemblage that includes *Stensioina beccariiformis, Cibicidoi-*

Table 5 (continued).

	754B-13R-3, 50–54 cm	754B-13R-4, 106–109 cm	754B-14R-5, 93–95 cm	754B-15R-3, 96–98 cm	754B-15R-3, 102–104 cm	754B-15R-5, 25–28 cm	755A-6R-1, 56–58 cm
Approximate age (Ma)	69.5	69.5	70	70	70	70	73–78
$CaCO_3$ (wt%)	22.5	20.5	19.5	25.9	27.1	7.4	20.2
TiO_2 (wt%)	1.81	1.48	1.46	1.3	1.00	1.61	1.99
Nb (ppm)	11.3	5.3	5.9	6.6	4.7	7.4	8.0
Zr (ppm)	139	76	86	91	62	93	103
Y (ppm)	34	20	25	24	21	18	26
Sr (ppm)	1221	1024	900	560	568	344	295
Rb (ppm)	15	12	14	20	19	7	20
Zn (ppm)	119	113	145	103	75	77	136
Cu (ppm)	111	119	107	83	77	99	91
Ni (ppm)	49	63	49	54	43	65	44
Cr (ppm)	23	59	31	45	30	85	49
V (ppm)	261	250	240	199	197	302	261
Ce (ppm)	40	21	26	18	11	21	31
Ba (ppm)	489	219	711	1549	1428	317	115
Zr/Nb	12.3	14.3	14.6	13.8	13.2	12.6	12.9
Ti/Zr	78.1	116.7	101.8	85.6	96.7	103.8	115.0
Zr/Y	4.1	3.8	3.4	3.8	3.0	5.2	4.0
[a](Ce/Y)n	2.8	2.5	2.5	1.8	1.3	2.8	2.8
Calculated carbonate-free							
TiO_2 (wt%)	2.34	1.86	1.81	1.75	1.37	1.74	2.5
Nb (ppm)	15	7	7	9	6	8	10
Zr (ppm)	179	96	107	123	85	100	129
Y (ppm)	44	25	31	32	29	19	33
Zn (ppm)	154	142	180	139	103	83	171
Cu (ppm)	143	150	133	112	106	107	114
Ni (ppm)	63	79	61	73	59	70	55
Cr (ppm)	30	74	39	61	41	92	61
V (ppm)	337	314	298	269	270	326	327
Ce (ppm)	52	26	32	24	15	23	39
Zr/Nb	12.3	14.3	14.6	13.8	13.2	12.6	12.9
Ti/Zr	78.1	116.7	101.8	85.6	96.7	103.8	115.0
Zr/Y	4.1	3.8	3.4	3.8	3.0	5.2	4.0
[a](Ce/Y)n	2.8	2.5	2.5	1.8	1.3	2.8	2.8

des velascoensis, Cibicidoides spp., *Pullenia* spp., and *Osangularia* spp., which indicates that sediment deposition took place at lower to middle bathyal depths prior to uplift in the middle Eocene. No significant faunal change occurred through the Paleocene to late Maestrichtian. The Maestrichtian benthic foraminifers indicate middle to lower bathyal depths.

Cretaceous assemblages of Santonian to Turonian age recovered from Site 755 contain low planktonic/benthic ratios (30/70) and a low-diversity benthic fauna without deep-water agglutinated forms. This indicates that deposition occurred in an upper bathyal environment, at a water depth shallower than 600 m.

A comparison of ages and depths of the pelagic cap above the unconformity at the Broken Ridge Sites is presented in Figure 22. Sedimentation rates throughout the Neogene on Broken Ridge are shown to have been about 1 cm/1000 yr.

For the composite age vs. depth plot of the middle Eocene to Turonian strata below the sedimentary cap at Broken Ridge in Figure 23, the depth scale of the composite stratigraphic distances is given in terms of depth below the unconformity between the middle Eocene and the Neogene at Site 753. Sedimentation rates in the middle Eocene to Turonian are shown to have been high, in the range of 2.5–3.0 cm/1000 yr, with rates from 3 to 5 cm/1000 yr in the Coniacian-Turonian. The lower Paleocene interval is an exception, with lower sedimentation rates at 1 cm/1000 yr. A gap of about 200 m, as deduced from the seismic stratigraphy, separates Site 753 from Site 752 stratigraphically. Extrapolating the early Eocene to Paleocene sedimentation rates at 3 cm/1000 yr to Site 753 gives the same distance.

Calcareous Nannofossils

Neogene

Neogene sections containing abundant calcareous nannofossils were recovered at all sites drilled on Broken Ridge. Nannofossil preservation is generally good in the Pliocene-Pleistocene sediments but poor in the Miocene. Strong overgrowth of discoasters in the Miocene sections impeded quick and easy identification. This combined with the lack of middle Miocene age-diagnostic forms made zonal assignments difficult and necessitated the combination of several of the zones of Okada and Bukry (1980). The Neogene section, although condensed, appears to be fairly complete at Site 754. At Site 752, only the *Sphenolithus belemnos* Zone (CN2) could not be identified. The Neogene section at Site 753 is highly condensed (44.0 m thick) and requires detailed work to determine which, if any, biozones are missing. At Site 755, the Neogene section was washed through except for two cores of middle Miocene Zones CN5 and CN6, which were taken directly above the unconformity separating the sediments of the Neogene cap from the underlying dipping units.

Pleistocene sediments on Broken Ridge are usually contained within the first core from each hole. Abundant *Pseudoemiliania lacunosa, Calcidiscus macintyrei*, and forms of the genus *Gephrocapsa* along with common *Oolithotus fragilis* and *Rhabdosphaera clavigera* are typical components of the Pleistocene sediments.

Latest Miocene and Pliocene age assemblages include nearly all the taxa necessary to accurately zone the recovered sequences.

Table 5 (continued).

755A-7R-2, 72–75 cm	755A-9R-1, 128–131 cm	755A-12R-1, 1–4 cm	755A-13R-3, 75–78 cm	755A-14R-2, 62–65 cm	755A-18R-6, 123–125 cm	755A-19R-6, 127–130 cm
73–78	73–78	73–78	88	88	90	90
13.1	16.6	18.7	20.7	18.8	1.7	2.7
0.62	0.96	0.77	1.15	1.07	2.87	1.92
5.2	6.2	7.3	6.8	6.6	23.5	25
57	60	66	86	89	189	228
19	16	18	18	13	39	46
152	286	191	254	307	702	768
12	17	21	27	16	26	18
64	62	55	81	58	153	141
30	46	26	39	23	127	87
41	39	36	35	29	61	73
34	54	50	76	35	68	107
74	161	95	185	125	326	280
17	17	22	25	26	73	63
318	349	560	118	89	12	67
9.8	9.7	9.0	12.6	13.5	7.4	9.1
65.2	95.9	69.9	80.2	72.1	91.0	50.5
3.0	3.8	3.7	4.8	6.8	4.8	5.0
2.1	2.5	2.9	3.3	4.8	4.5	3.3
0.71	1.15	0.95	1.45	1.32	2.92	1.97
7	7	9	9	8	26	26
66	72	81	109	110	192	234
22	19	22	23	16	40	47
74	74	68	102	71	156	145
35	55	32	49	28	129	89
47	47	44	44	36	62	75
39	65	62	96	43	69	110
85	193	117	233	154	332	288
20	20	27	32	32	74	65
9.8	9.7	9.0	12.6	13.5	7.4	9.1
65.2	95.9	69.9	80.2	72.1	91.0	50.5
3.0	3.8	3.7	4.8	6.8	4.8	5.0
2.1	2.5	2.9	3.3	4.8	4.5	3.3

Discoaster brouweri, Discoaster pentaradiatus, Discoaster surculus, Discoaster tamalis, and *Reticulofenestra pseudoumbilica* were noted, as well as common amauroliths and scyphospheres.

Miocene nannofossil assemblages on Broken Ridge are characterized by low diversity and poor preservation. The lack of the delicate age-diagnostic forms of discoasters made it necessary to combine Zones CN7 through CN9a, as we had combined Zones CN5 and CN6. The assemblages of the combined Zones CN7 through CN9a include few to common *D. pentaradiatus, Discoaster variabilis, D. brouweri*, and abundant *R. pseudoumbilica* and *Reticulofenestra* sp. The zonal combination is defined by the first occurrence of *D. pentaradiatus* to the first occurrence of *Amaurolithus primus*. The combined Zones CN5 and CN6 are assigned to sediments containing discoasters related to *Discoaster exilis*. These forms typically have six strongly tapering rays. The remaining assemblage includes *D. variabilis, Cyclicargolithus floridanus*, and *Discoaster deflandrei*. The latter two species decrease in abundance upsection and are not nearly as abundant in middle Miocene sediments as in the lower Miocene strata.

In addition to *C. floridanus* and *D. deflandrei*, lower Miocene sediments of Zones CN3 and CN4 contain abundant *Sphenolithus heteromorphus, Sphenolithus conicus, Reticulofenestra* sp., and *Coccolithus pelagicus*. Assemblages of Zones CN1 and CN2 are similar, but with the addition of the zonal marker *Sphenolithus belemnos* in Zone CN2. The low-latitude, early Miocene marker species *Helicosphaera ampliaperta, Discoaster druggii*, and *Triquetrorhabdulus carinatus* were not recognized in the Broken Ridge sediments.

The Oligocene/Miocene boundary at Sites 752 and 754 is approximated by the last occurrence of *Zygrhablithus bijugatus* and *Reticulofenestra bisecta*. Usually the last occurrence of *Sphenolithus ciperoensis* is used to denote this boundary according to the Okada and Bukry (1980) scheme, but this low-latitude species was not noted in the Broken Ridge sediments. The placement of this boundary using our method may, in retrospect, be above where it would normally be placed. Examination of the Ninetyeast Ridge sediments revealed that the last *Z. bijugatus* and *R. bisecta* lie slightly above the last occurrence of *S. ciperoensis*.

The presence of abundant reticulofenestrids and *C. pelagicus* in combination with the low diversity among the discoasters in the Broken Ridge sediments is indicative of cooler waters and may reflect the ocean circulation changes brought about by the Oligocene establishment of the Antarctic Circumpolar Current (Kennett and Burns, 1972). Apparently Broken Ridge moved north of the influence of these cooler waters during the late Miocene and into a zone of higher productivity, as indicated by the increase in diversity among the amauroliths, discoasters, and especially the scyphospheres. This same change in diversity was noted by Müller (1977) in previously studied Indian Ocean sediments. Although diversity was high during the latest Miocene through Pleistocene, a full subtropical to tropical assemblage never completely developed, as indicated by the lack of common to abundant ceratoliths. *Ceratolithus acutus* and *Ceratolithus rugosus* were noted, but their occurrence is rare.

Paleogene

Paleogene oozes and chalks were recovered at Sites 752, 753, and 754 on Broken Ridge. Calcareous nannofossils are abundant, and their preservation is generally moderate to good through most of the sections.

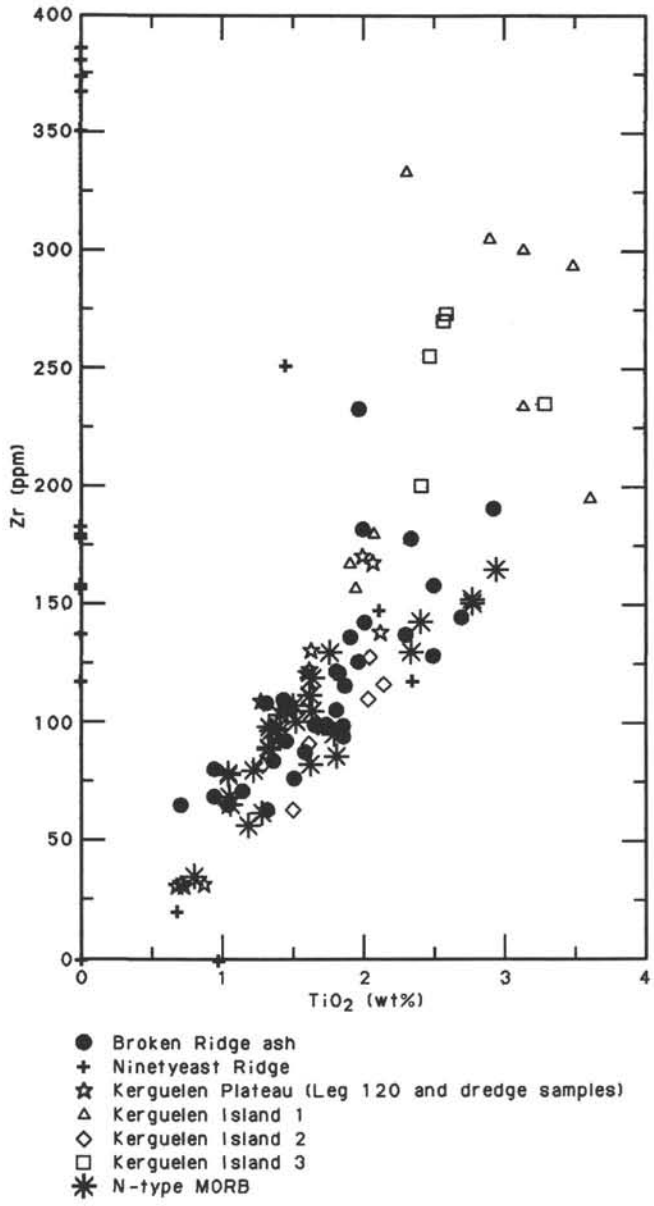

Figure 13. Zr vs. TiO_2 for volcanic ash layers recovered from Holes 752A, 752B, 754A, and 754B on Broken Ridge and for basaltic rocks from the Indian Ocean and other areas: Ninetyeast Ridge and Kerguelen Island (M. Storey and A. D. Saunders, unpubl. data), Kerguelen Plateau (Leg 120 Scientific Drilling Party, 1988; F. A. Frey, unpubl. data; Ludden et al., 1980; Weis et al., 1987b); N-type or "normal" mid-ocean ridge basalt (MORB) (Indian Ocean Triple Junction—Price et al., 1986; DSDP Leg 65, East Pacific Rise 23°N—Saunders, 1983; DSDP Legs 45 and 46, Mid-Atlantic Ridge, 22°N—Bougault et al., 1979a, 1979b). Kerguelen groups 1, 2, and 3 refer to distinct magma suites found on Kerguelen Island; 3 represents older, transitional flood basalts (D. Weis, unpubl. data; Weis et al., 1987a). All ash data are from Table 5 and are plotted on a carbonate-free basis.

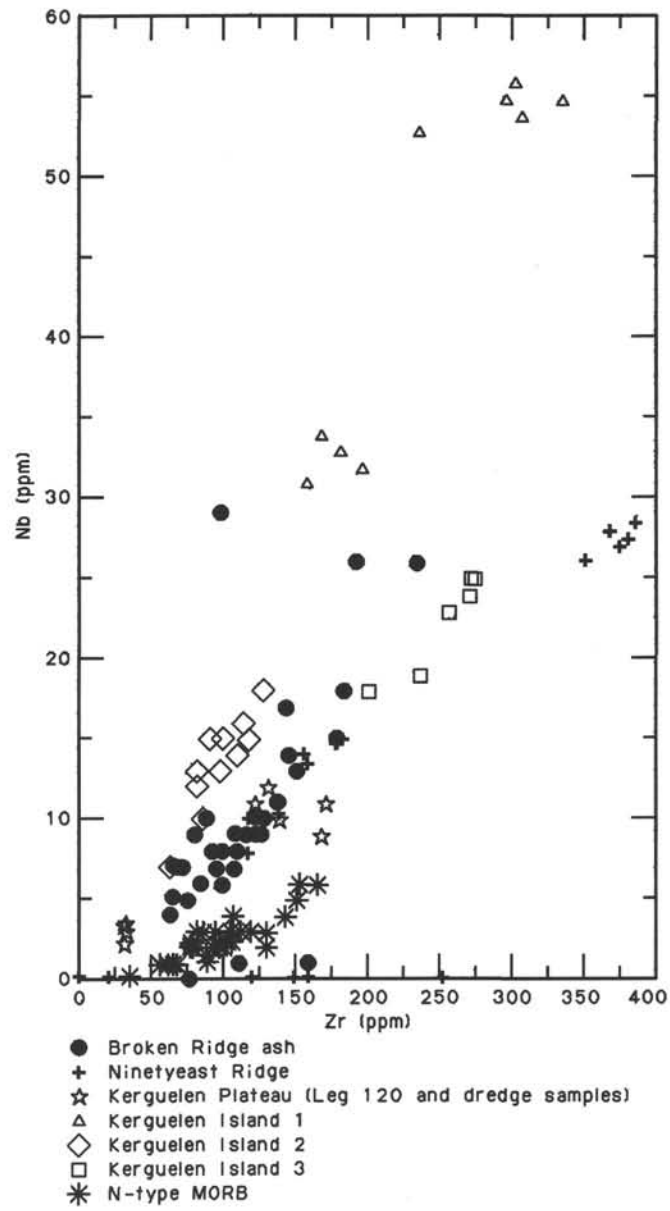

Figure 14. Nb vs. Zr for volcanic ash layers recovered from Holes 752A, 752B, 754A, and 754B on Broken Ridge and for basaltic rocks from the Indian Ocean and other areas. Data sources as in Figure 13. All Broken Ridge data presented on a carbonate-free basis.

Fourteen meters of upper Oligocene (CP19) sediments was recovered at Site 754, and 3 m was recovered at Site 752. The high-latitude late Oligocene age assemblage includes abundant *R. bisecta, Z. bijugatus, C. floridanus, Reticulofenestra* sp., and common *Chiasmolithus altus*. The low-latitude index marker *S. ciperoensis* was not found in these Broken Ridge sediments. The upper Oligocene sediments at these sites disconformably overlie shallow-water sediments of late Eocene age, with Oligocene Zones CP16 through CP18 missing.

At Sites 752 and 754, the upper Eocene sediments assigned to Zone CP15 contain abundant *Reticulofenestra umbilica, R. bisecta*, and *Z. bijugatus* and the common high-latitude index species *Isthmolithus recurvus* and *Chiasmolithus omaurensis*. Low-latitude species such as *Discoaster saipanensis* and *Discoaster barbadiensis* are rare in these sediments, as is *Braarudosphaera*. Reworking is common in these units because the middle Eocene forms *Coccolithus grandis*, *Coccolithus solitus*, and *Neococcolithus dubius* are commonly present. The presence of *Braarudosphaera* is consistent with a shallow-water origin for the upper Eocene sediments directly overlying the dipping units of Broken Ridge. At Site 754, the dipping units immediately below the unconformity are of late Maestrichtian age whereas at Site 752, farther north, the sediments are of early Eocene age.

At Site 753, the objective was to sample the youngest dipping sediments below the prominent unconformity. The calcareous

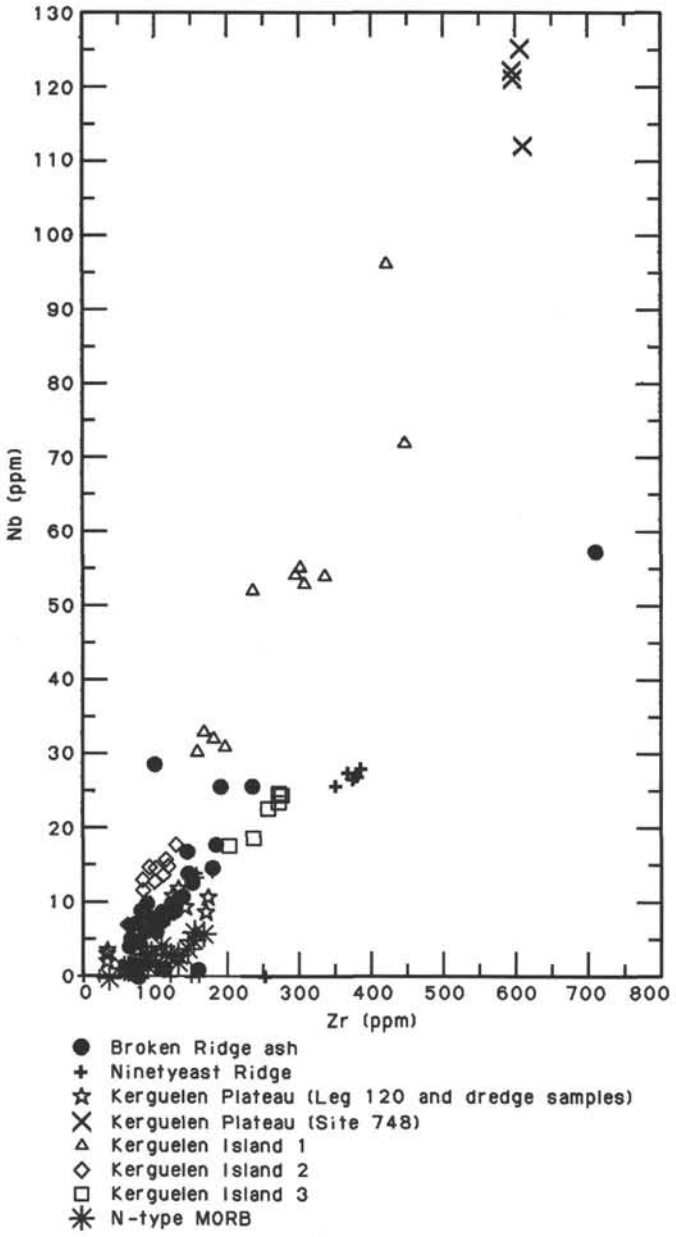

Figure 15. Nb vs. Zr for volcanic ash layers recovered from Holes 752A, 752B, 754A, and 754B on Broken Ridge and for basaltic rocks from the Indian Ocean and other areas. Data presented as in Figure 13, but with compressed axes to include the evolved ash Sample 121-754B-7R-1, 77–79 cm.

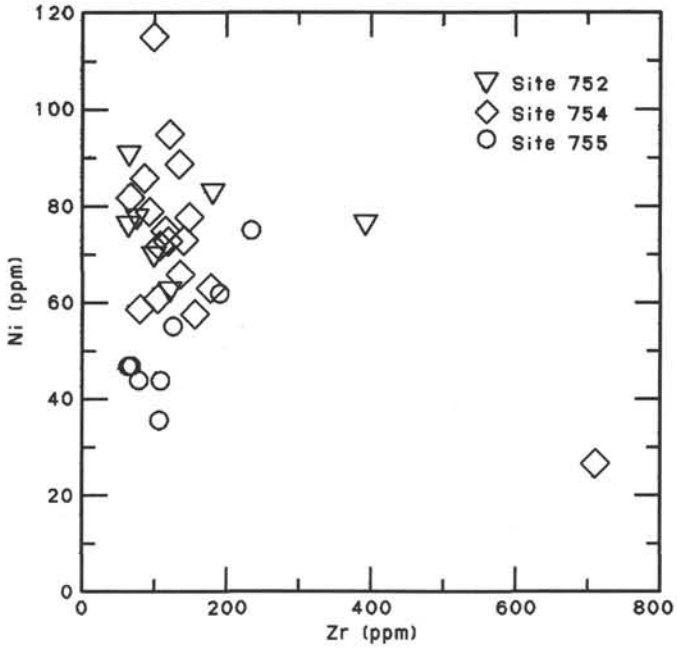

Figure 16. Ni vs. Zr for tephra-rich horizons, Broken Ridge. Data from Table 5 are plotted on a carbonate-free basis.

chalks retrieved in only two cores from below the unconformity contain a middle Eocene assemblage that includes the Subzone CP13b index species *Chiasmolithus gigas*. Also present are abundant *C. solitus* and *Z. bijugatus*, common *Coccolithus formosus, Reticulofenestra samodurovii, N. dubius*, and *C. grandis*, and few *D. saipanensis* and *Nannotetrina* sp. This assemblage is typical for middle- to high-latitude middle Eocene sediments, with abundant chiasmoliths and reticulofenestrids and a lack of abundant *D. saipanensis* and *D. barbadiensis*. Unfortunately, mechanical problems while drilling a second hole at this site prevented recovery of sediments below this interval. Stratigraphic overlap with the lower Eocene sediments cored at Site 752 was an original objective at Site 753. Time and the mechanical problems eliminated this possibility, which would have been quite valuable for paleontological and paleobiogeographical correlations with the Ninetyeast Ridge material, as well as with sections from ODP Legs 119 and 120.

The presence of middle Eocene (CP13c) sediments below the unconformity and sediments of CP15 above precisely confines the interval of uplift and erosion to latest middle Eocene (CP14). The duration of this interval is approximately 3 m.y., which means that uplift related to rifting was fairly rapid, as was the ensuing subsidence and subsequent commencement of normal pelagic deposition.

At Site 752, a complete lower Paleocene to lower Eocene sequence of calcareous chalks was recovered. Zones CP1 through CP10 were identified in this sequence. The preservation of calcareous nannofossils is moderate through most of this unit and good through some intervals of the expanded Danian section.

The early Eocene assemblage includes rare *Discoaster lodoensis*, few *Discoaster kuepperi*, and *Discoaster diastypus*. The plexus of *Tribrachiatus bramlettei, Tribrachiatus contortus*, and *Tribrachiatus orthostylus* is present. *Chiasmolithus bidens, C. solitus*, and species of the genus *Toweius* are abundant.

The upper Paleocene sediments (CP5 to CP8) include *Discoaster multiradiatus, Discoaster mohleri, Fasciculithus tympaniformis, Fasciculithus involutus, C. bidens, Toweius eminens, Toweius tovae, Towieus craticulus, Prinsius bisulcus, Heliolithus kleinpellii, Heliolithus reidelii*, and *Heliolithus universus*. The presence of abundant chiasmoliths and *Toweius* sp. in this assemblage is typical of the austral high latitudes. Another typical high-latitude upper Paleocene species, *Hornibrookina australis*, is also present, in addition to its evolutionary precursor, *Hornibrookina teuriensis*, in the Danian sediments.

Early Paleocene assemblages are characterized by abundant *Chiasmolithus danicus, Cruciplacolithus edwardsii, Prinsius martinii*, and *P. bisulcus*. Lower Danian sediments contain abundant *Cruciplacolithus tenuis, Zygodiscus sigmoides, Prinsius dimorphosus, Thoracosphaera*, and *Coccolithus cavus. Neocrepidolithus* sp., *Markalius inversus*, and *Biantholithus sparsus* are present in sediments just above the Maestrichtian/Danian boundary. Austral high-latitude Cretaceous/Tertiary boundary sequences are rare; thus, the expanded and complete Danian section at Site

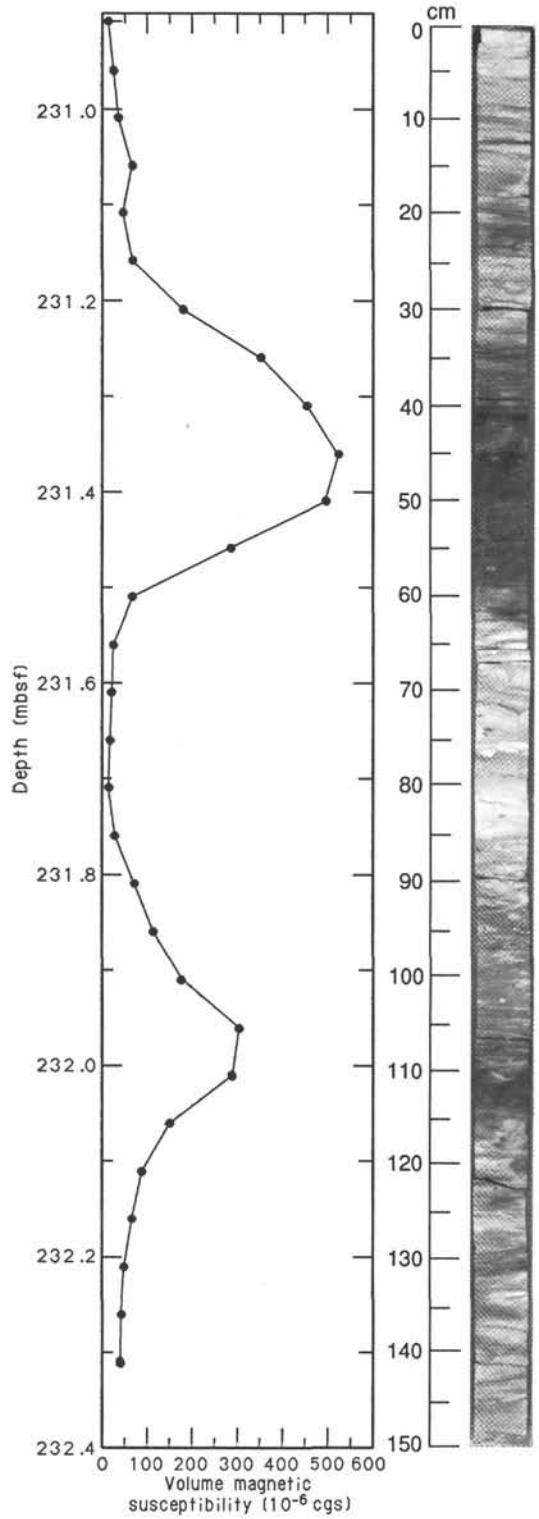

Figure 17. Volume magnetic susceptibility in Section 121-754B-13R-3, with a photograph of the split core taken after measurements were complete. The basaltic ash layers at 231.35 and 232.0 mbsf are clearly visible.

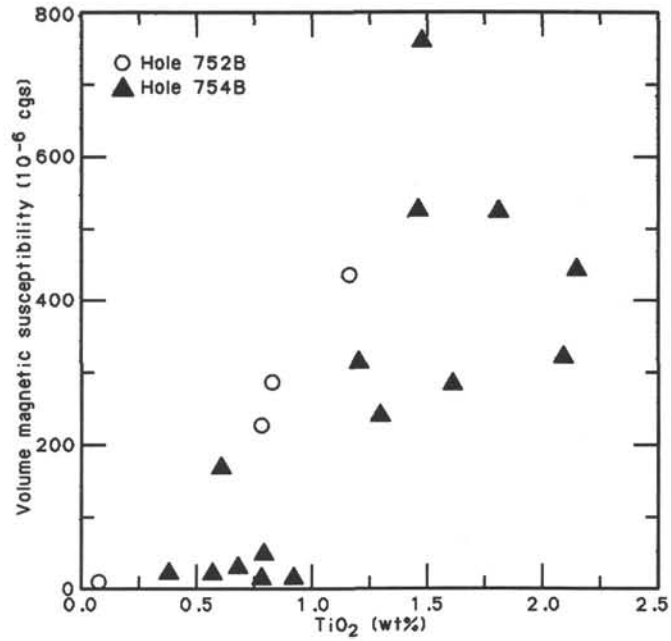

Figure 18. The relationship between TiO_2 and the volume magnetic susceptibility in 35 basaltic ash-rich layers from Broken Ridge ash layers. The concentration of TiO_2 is a readily measured index of the concentration of iron in the basaltic rocks.

752 provides a unique opportunity for paleontological research. The Cretaceous/Tertiary boundary is discussed in more detail in the "Cretaceous/Tertiary Boundary Summary" chapter.

Cretaceous

Upper Cretaceous sediments were recovered at Sites 752, 754, and 755. The calcareous nannofossils range from few to abundant, with diversity appearing to alternate in some sections between low and high. Preservation is generally moderate to poor through the sequence. The alternation between intervals of high and low diversity, as displayed in the Maestrichtian limestones at Site 754, appears to be related partly to preservational factors, but is probably more dependant on some environmental factors.

The upper Maestrichtian sediments of Broken Ridge show a distinct Southern Ocean, high-latitude character. Austral species such as *Biscutum magnum, Biscutum coronum, Biscutum dissimilis, Nephrolithus corystus, Monomarginatus quaternarius,* and *Acuturris scotus* are present, in addition to *Nephrolithus frequens, Arkhangelskiella cymbiformis, Kamptnerius magnificus, Eiffellithus turriseiffeli, Micula decussata*, and *Reinhardtites levis*. Although they are present in varying frequencies, the aforementioned austral taxa never reach the same relative abundances as at previously studied high-latitude sites of the Falkland Plateau (Wise and Wind, 1977) and Maud Rise (Pospichal and Wise, in press).

In the lower Maestrichtian sediments at Site 754, *Tranolithus phacelosus* and *Reinhardtites* aff. *Reinhardtites anthophorous* are characteristic additions to the aforementioned assemblage. A question as to whether the sediments near the bottom of Hole 754B are actually Campanian in age has arisen because the lowest Maestrichtian unit appears to be unusually thick. The high-latitude, late Campanian marker species *Aspidolithus parcus constrictus* was not found in the samples from Hole 754B, which possibly suggests that Campanian sediments were not reached. The assemblages are poor through some intervals, but ecological exclusion of some key marker species cannot be ruled out. Clearly only additional detailed work can resolve this problem.

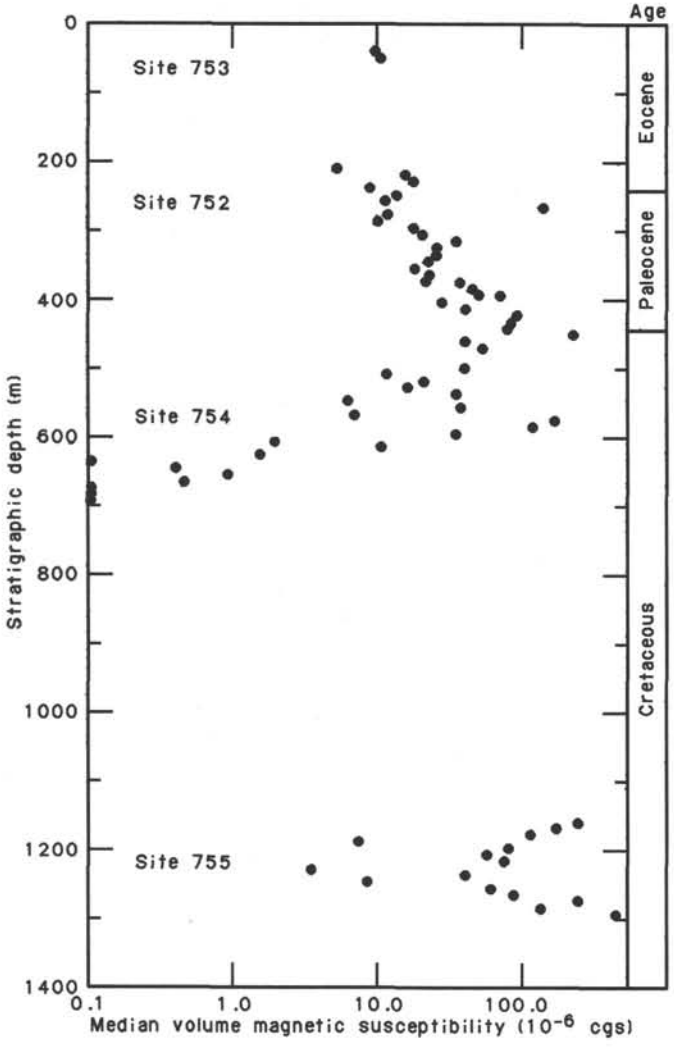

Figure 19. Median volume magnetic susceptibility plotted against stratigraphic depth for the pre-Neogene succession at Broken Ridge. The stratigraphic depth is given in reference to the seafloor at Site 753. The stratigraphic correlation of different sites is on the basis of shipboard seismic, paleontological, and paleomagnetic data. Each susceptibility point represents the median of usually about 50 observations for an individual core. Many of the low susceptibility values recorded at the base of Site 754 are from the cores with poor recovery that contain large amounts of chert.

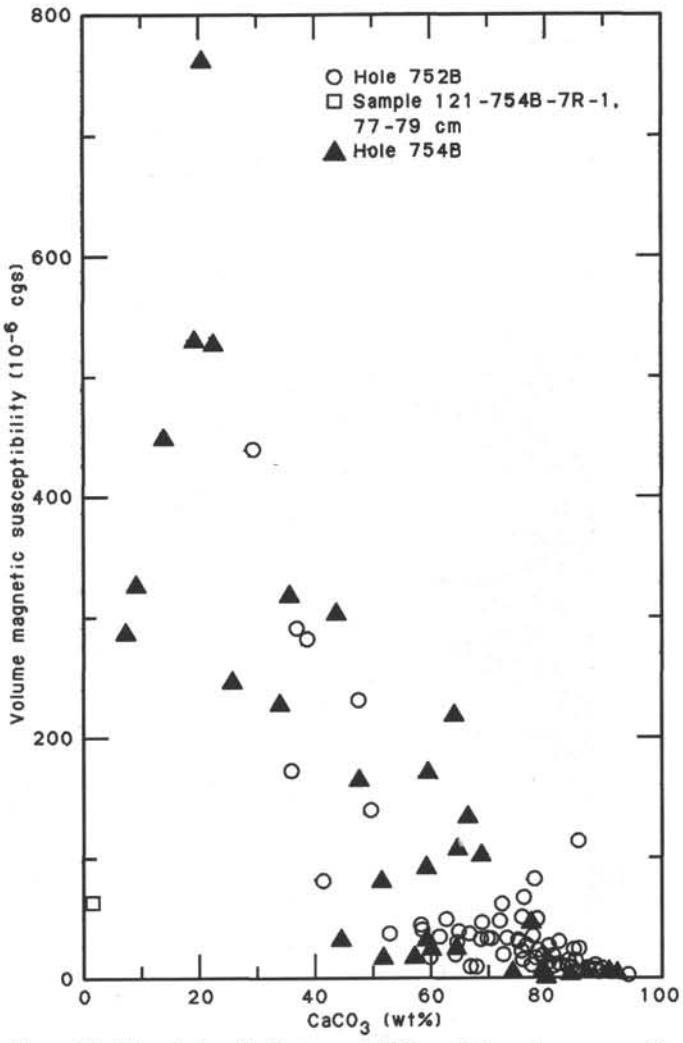

Figure 20. The relationship between $CaCO_3$ and the volume magnetic susceptibility in limestone and ash-rich layers from Broken Ridge.

Turonian to Santonian limestones were recovered at Site 755. For the most part, preservation is poor and calcareous nannofossils are few through this interval. *R. anthophorous, M. decussata, K. magnificus*, and *Aspidolithus parcus expansus* are characteristic of the Santonian sediments on Broken Ridge. Sediments of Turonian/Coniacian age contain *Gartnerago obliquum* and *Lithastrinus floralis*. *Marthasterites furcatus* occurs sporadically through the upper part of this interval. The austral species *Thiersteinia ecclesiastica* is rare in the Turonian limestones of Site 755.

Planktonic Foraminifers

Neogene

Well-preserved Neogene assemblages of planktonic foraminifers were recovered in Holes 752A, 7543A, and 754A. In contrast, the assemblages above and between the erosional surfaces are moderately preserved and show signs of dissolution.

Dominating the Neogene assemblages are typical, middle- to high-latitude, temperate faunas and other more cosmopolitan species. Difficulties arose trying to recognize the zonal boundaries of Blow (1969), Banner and Blow (1965), or Bolli and Saunders (1985) because of the lack of nominate marker species. This is probably the result of latitudinal control on the distribution of the taxa, rather than selective dissolution. The recovered planktonic foraminiferal assemblages have an affinity with other high-latitude, Neogene faunas of the Southern Hemisphere, such as those in southeast Australia (Jenkins, 1960), New Zealand (Jenkins, 1967), the South Atlantic (Jenkins, 1978), and the South Pacific (Kennett, 1973). Because of this apparent low-latitude taxon discrimination, the temperate, zonal scheme of Srinivasan and Kennett (1981) and Kennett (1973) was applied to the Neogene assemblages on Broken Ridge.

Pleistocene

The Pleistocene planktonic foraminiferal assemblages are dominated by *Globorotalia inflata, Globorotalia crassaformis*, and *Globigerina bulloides*. The dominance of *G. inflata*, a species characteristic of a temperate water mass, is typical of other mid-latitude sites in the Indian Ocean (Vincent, 1977). This is in marked contrast to the assemblages recovered from the low-latitude sites on Ninetyeast Ridge, which are dominated by *Globorotalia menardii* (and other tropical species). Of equal impor-

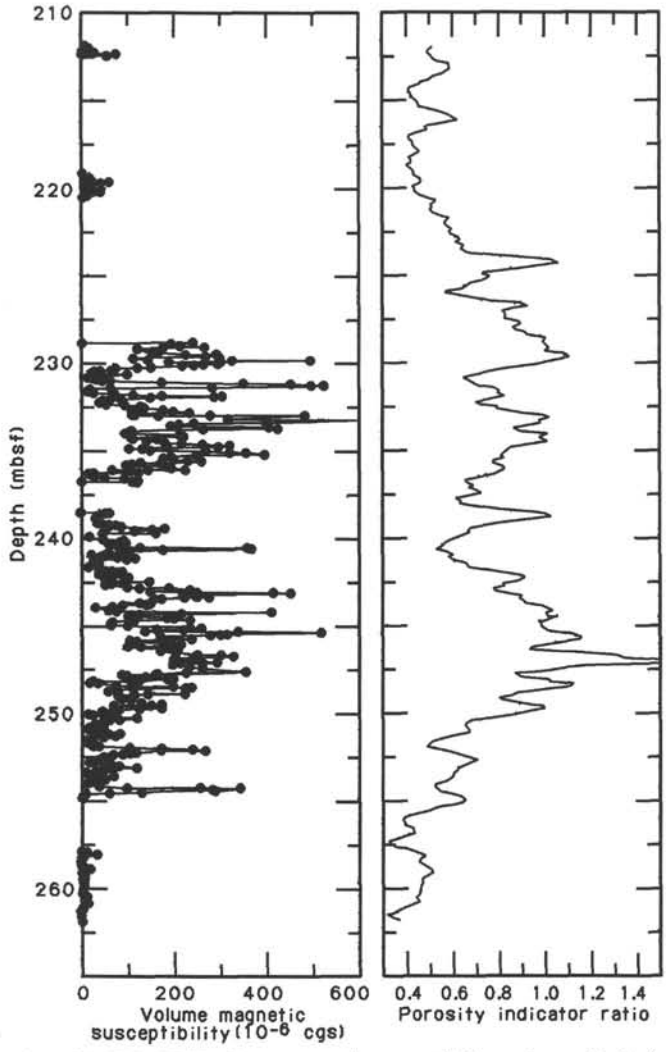

Figure 21. Hole 754B volume magnetic susceptibility and porosity indicator ratio (downhole logging) plots correlate, with higher values indicating increased proportions of ash in the measured 50-m section.

tance is the abundance of *G. bulloides*, which is restricted to transitional and cooler waters at the present (Bé and Tolderlund, 1971). Few tropical forms are present.

Pliocene

The dominant components to the planktonic foraminifer assemblages in the Pliocene are *G. bulloides, Globigerina woodi, Globigerina falconensis, G. crassaformis*, and the species of the *Globorotalia conoidea–G. inflata* lineage, the first occurrences of which are used to zone the Pliocene. With the exception of rare occurrences of *Globigerinoides sacculifer*, none of the warm to tropical forms such as *Globorotalia tumida, Globorotalia tumida flexuosa, Sphaeroidinella dehiscens, Pulleniatina obliquiloculata, Neogloboquadrina dutertrei*, and *Neogloboquadrina humerosa* are present. Preservation throughout this interval is excellent.

Miocene

The upper Miocene planktonic foraminifer assemblages are dominated by *Globigerina nepenthes, G. conoidea, Globorotalia miozea, Globorotalia panda, G. bulloides, G. falconensis*, and *Globoquadrina dehiscens. G. menardii* is present in small numbers.

In the middle Miocene the absence of the low-latitude marker species *Globorotalia praefohsi, Globorotalia fohsi, Globorotalia fohsi lobata*, and *Globorotalia fohsi robusta* testifies to the higher latitudinal position of Broken Ridge at that time. Only the more temperate to subtropical earlier forms of the *G. fohsi* evolutionary lineage, *Globorotalia peripheroronda* and *Globorotalia peripheroacuta*, are present.

Sediments of early Miocene age are characterized by *G. dehiscens, Globigerinoides trilobus, Catapsydrax dissimilis, G. bulloides, Globorotalia incognita*, and *Globorotalia zealandica*.

Paleogene

Oligocene

Oligocene assemblages were recovered only in sediments from Holes 754A and 752A. The assemblages contain midlatitude, temperate faunas of low diversity and moderate preservation. The assemblages also contain up to 40% reworked planktonic foraminifers of late Eocene age.

Eocene to Paleocene

All of the Eocene and Paleocene assemblages are typical for midlatitude, temperate austral areas (Jenkins, 1985). The most typical marker species of the low-latitude zonations, such as the most ornate of the *Morozovella* species, *Morozovella velascoensis* and *Morozovella acuta, Truncorotalia* spp., and *Hantkenina* spp., do not occur.

Throughout the Eocene and Paleocene are low-diversity assemblages of abundant planktonic foraminifers. The middle Eocene assemblages are almost completely dominated by *Acarinina primitiva* and *Acarinina bullbrooki*, along with *Globigerinatheka subconglobata* and *Globigerinatheka index*. Preservation decreases downhole with increasing lithification. Early Eocene age assemblages are dominated by *A. primitiva, Acarinina soldadoensis*, and *Globigerina linaperta*. Some keeled specimens of *Morozovella marginodentata* and *Morozovella subbotinae* indicate an earliest Eocene age. The upper and middle Paleocene are characterized by low-diversity assemblages dominated by globigerinids such as *Globigerina velascoensis* and *G. linaperta*. A few *Morozovella aequa* indicate a late Paleocene age for Cores 121-752A-18X to 121-752A-27X, and *Morozovella angulata* establishes a middle Paleocene age for Cores 121-752A-28X to 121-752A-32X. The lower Paleocene assemblages are generally poorly preserved. Long-ranging species such as *Morozovella pseudobulloides* and *Globigerina triloculinoides* occur in abundance, but the marker species *Morozovella trinidadensis* and *Morozovella uncinata* are absent.

The Cretaceous/Tertiary boundary was recovered in Core 121-752B-11R, at 358.55–358.75 mbsf. The most important feature of the Cretaceous/Tertiary boundary is a 6.1-m-thick dark green, $CaCO_3$-poor unit that is rich in volcanic ash, but extremely poor in planktonic foraminifers. This unit lies directly on the extinction horizon of the Cretaceous globotruncanid-rugoglobigerinid fauna at 358.75 mbsf. The Cretaceous/Tertiary boundary is probably complete biostratigraphically, although faunas of earliest Paleocene age were not positively recognized (see the "Cretaceous/Tertiary Boundary Summary" chapter).

Cretaceous

The Upper Cretaceous section was recovered in two different parts, from the uppermost Maestrichtian to Campanian at Sites 752 and 754 and a Santonian to Turonian section at Site 755. Biostratigraphically, Holes 752B and 754B overlap by about 40 m and are correlated by means of the first appearance of the marker for the uppermost Maestrichtian, *Abathomphalus mayaroensis*. According to the seismic stratigraphy a gap of about 400–450 m separates the sections at Sites 754 and 755.

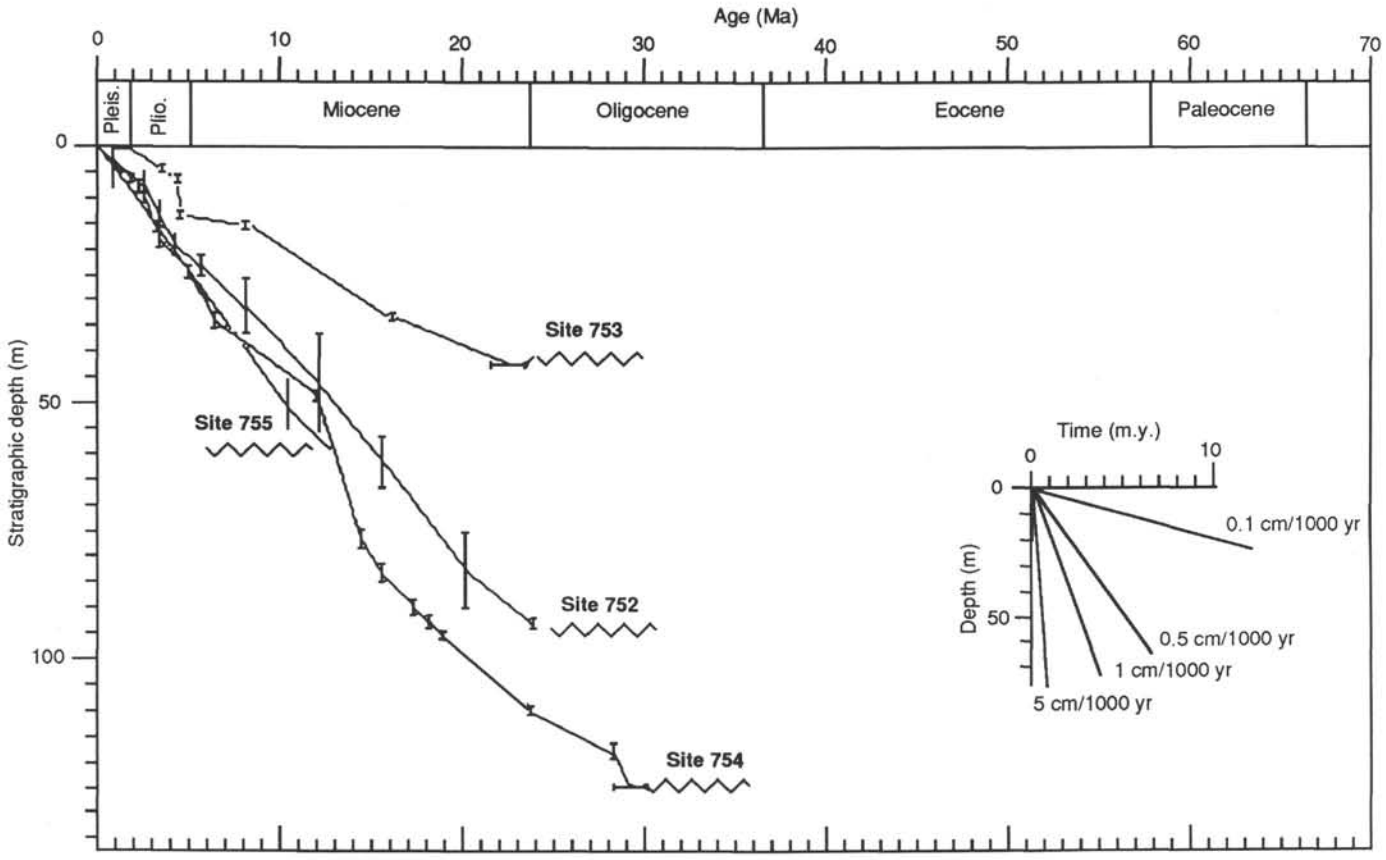

Figure 22. Composite age vs. depth plot of the strata above the unconformity at Broken Ridge Sites 752–755.

Preservation is reasonable in the upper Maestrichtian, but decreases rapidly downsection. In the uppermost Maestrichtian, *Globotruncana arca, Rugoglobigerina rugosa*, and *A. mayaroensis* assign the assemblages to the *Abathomphalus mayaroensis* Zone. A general shallowing downsection, as deduced from lower planktonic/benthic foraminifer ratios, may be responsible for a further decrease of diversity downsection. Down to the upper Maestrichtian the recognition of biostratigraphic zones is relatively easy. Farther downsection the poor preservation and very low diversity make a subdivision into stages, let alone biozones, virtually impossible. The lower Maestrichtian (upper Campanian?) is dominated by *Rugoglobigerina* spp., *Globigerinelloides* spp., hedbergellids, and a few *Globotruncana linneiana*. Globotruncanids are absent in most samples farther downsection, but long-ranging *Heterohelix* spp. and abundant *Globigerinelloides ehrenbergi* dominate all faunas. Site 755 contains a few abundant, but low-diversity, faunas in the few limestone units intercalated in the thick volcaniclastic sequence. Preservation deteriorates farther downhole, and no washed residues could be prepared. The lowermost determinable fauna in Site 755 contains a late Turonian–Santonian age assemblage at 169.7 mbsf (Sample 121-755A-15R-CC), based on the occurrence of double-keeled forms of the *Globotruncana coronata–G. linneiana* group, which reportedly do not occur below the upper Turonian.

Benthic Foraminifers

Benthic foraminifers were examined from all the sites on Broken Ridge to determine its water depth history. Benthic foraminifers are generally well preserved and common throughout most of the samples. At Sites 752, 754, and 755, Pleistocene to Maestrichtian and Santonian to Turonian sediments were recovered. The benthic faunas are generally represented by deep-water forms typical of bathyal depths.

In this report, marine benthic depth zones are based on van Morkhoven et al. (1986): neritic (0–200 m), upper bathyal (200–600 m), middle bathyal (600–1000 m), lower bathyal (1000–2000 m), and abyssal (>2000 m). The upper and lower depth limits of the noted taxa also define the depth ranges described in van Morkhoven et al. (1986) (Fig. 24). Figure 25 summarizes the water depth vs. age at Broken Ridge, based on the depth association of the noted taxa.

Neogene

Pleistocene to Pliocene

The benthic faunas are similar to the present-day southeastern Indian Ocean faunas (Corliss, 1979; Peterson, 1984) and are associated with Indian Deep Water and Indian Ocean Bottom Water.

Miocene

The Miocene faunas are characterized by taxa such as *Globocassidulina subglobosa, Uvigerina* spp., *Cibicidoides* spp., and *Oridorsalis umbonatus*. These forms vary in abundance throughout the Miocene. The differences in abundance appear to result from paleoceanographic changes related to Antarctic ice sheet expansion during the middle Miocene (Woodruff, 1985).

The depth distribution of the main taxa ranges from bathyal to abyssal depths, but their depth associations are middle to lower bathyal. This indicates that the Miocene water depth at Broken Ridge is similar to its present depth.

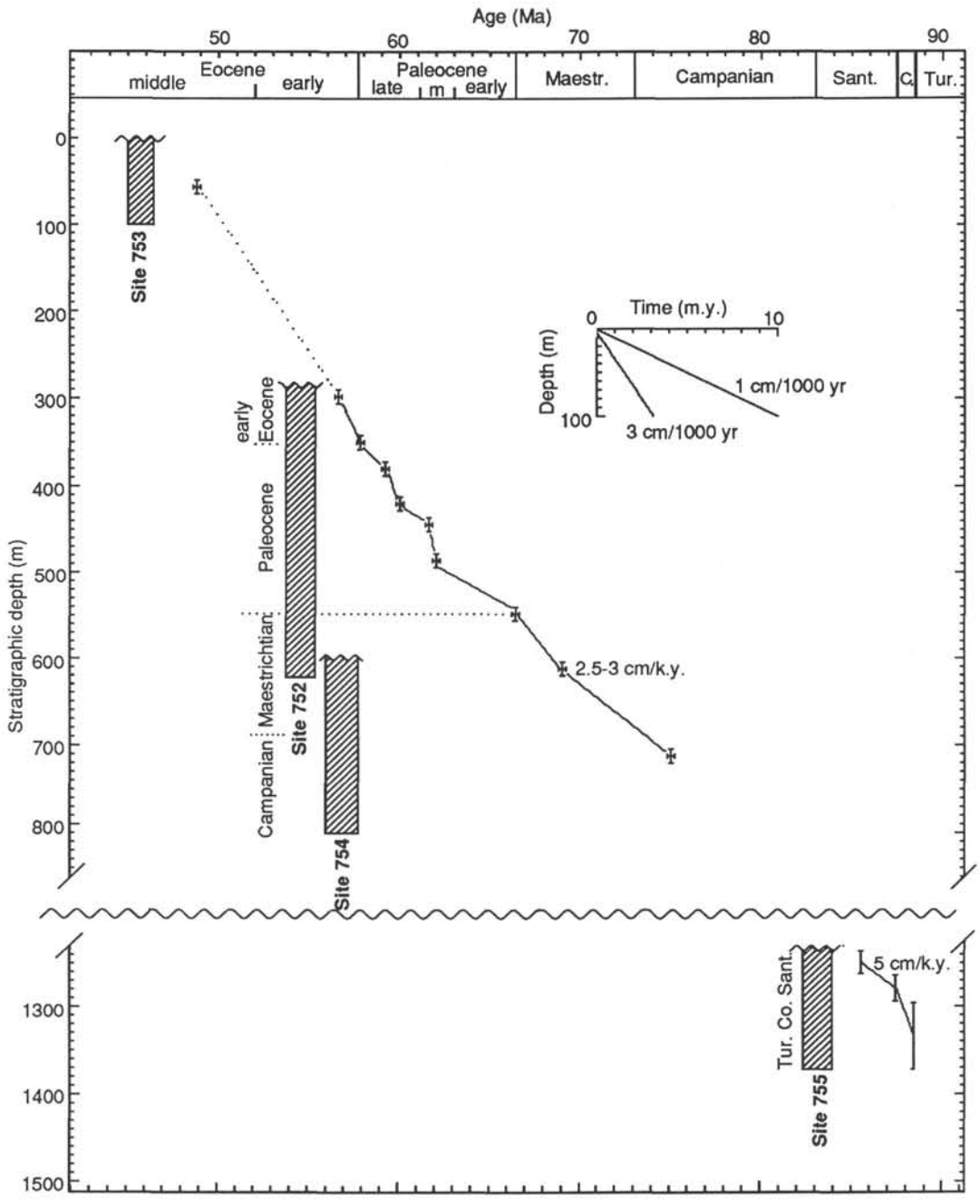

Figure 23. Composite age vs. depth plot of the middle Eocene to Turonian strata below the capping unit and unconformity at Broken Ridge Sites 752–755. Depth is meters below the unconformity between the middle Eocene and the Neogene at Site 753.

Paleogene

Oligocene

Benthic foraminifers in the upper Oligocene are similar to the lower Miocene faunas; however, certain bathyal taxa, suggesting shallower depths, occur in the Oligocene sediments in comparison with the Miocene faunas.

Eocene

Moderately preserved upper bathyal faunas are found in upper Eocene coarse-grained sand and gravels. Badly preserved shallow-water benthic foraminifers such as *Amphistegina*, shells, and bryozoan fragments indicate that deposition resulted from downslope transportation from shallow-water depths.

The early Eocene age faunas found at Site 752 consist of calcareous foraminifers resembling the lower bathyal to abyssal Eocene faunas of the South Atlantic Ocean (Tjalsma and Lohmann, 1983). The faunas of Broken Ridge, however, are usually devoid of abyssal agglutinated forms, which indicates that Broken Ridge was at lower bathyal depths during the early Eocene. The middle Eocene chalks recovered at Site 753, which are assigned to calcareous nannofossil Zone CP13, contain benthic foraminifers similar to the early Eocene faunas and therefore indicate a lower bathyal depth.

Figure 24. Upper and lower depth limits of the benthic foraminiferal taxa at Broken Ridge. Ranges based on van Morkhoven et al. (1986).

Paleocene

Paleocene faunas are dominated by deep-water species such as *Stensioina beccariiformis*. The extinction of this species near the Paleocene/Eocene boundary corresponds to the boundary determined by nannofossils. The depth range of the faunas indicates middle to lower bathyal depths.

Cretaceous

Maestrichtian

No significant faunal change occurred through the Paleocene to the late Maestrichtian. The Maestrichtian faunas indicate middle to lower bathyal depths.

Santonian to Turonian

The faunas of the Santonian to Turonian are characterized by low diversity and low abundance. None of the deep-water taxa present in the Maestrichtian strata were found. The faunas also include fragmented benthic foraminifers, suggesting their displacement from shallower environments. These faunal assemblages indicate upper bathyal depths.

Diatoms

An almost continuous sedimentary record from the middle Cretaceous to the Holocene was recovered at the Broken Ridge sites. From the examination of all core-catcher samples and additional material, it appears that diatoms are consistently present in middle Paleocene through middle Eocene sediments only. Middle Eocene diatom assemblages occur at Site 753. Early Eocene through Paleocene age diatom assemblages occur through a long, continuously cored lower Eocene through Paleocene section at Site 752.

The occurrence of well-preserved early Paleogene diatom assemblages is significant. In fact, our knowledge of Paleogene diatoms is still limited because few deposits containing diatoms are known from the early Eocene–Paleocene time interval (cf. data compiled by Fenner, 1985). Therefore, Sites 752 and 753 offer an exceptional opportunity to document the diatom flora of the lower Paleogene and to determine biostratigraphic diatom datum levels that can be directly correlated to nannofossil and planktonic foraminiferal zonations. In addition, the diatom record from Broken Ridge will represent the first documentation of middle and early Eocene diatoms in the Indian Ocean.

Neogene

Diatoms generally do not occur in Neogene sediments. However, very rare and poorly preserved specimens of *Thalassiothrix*

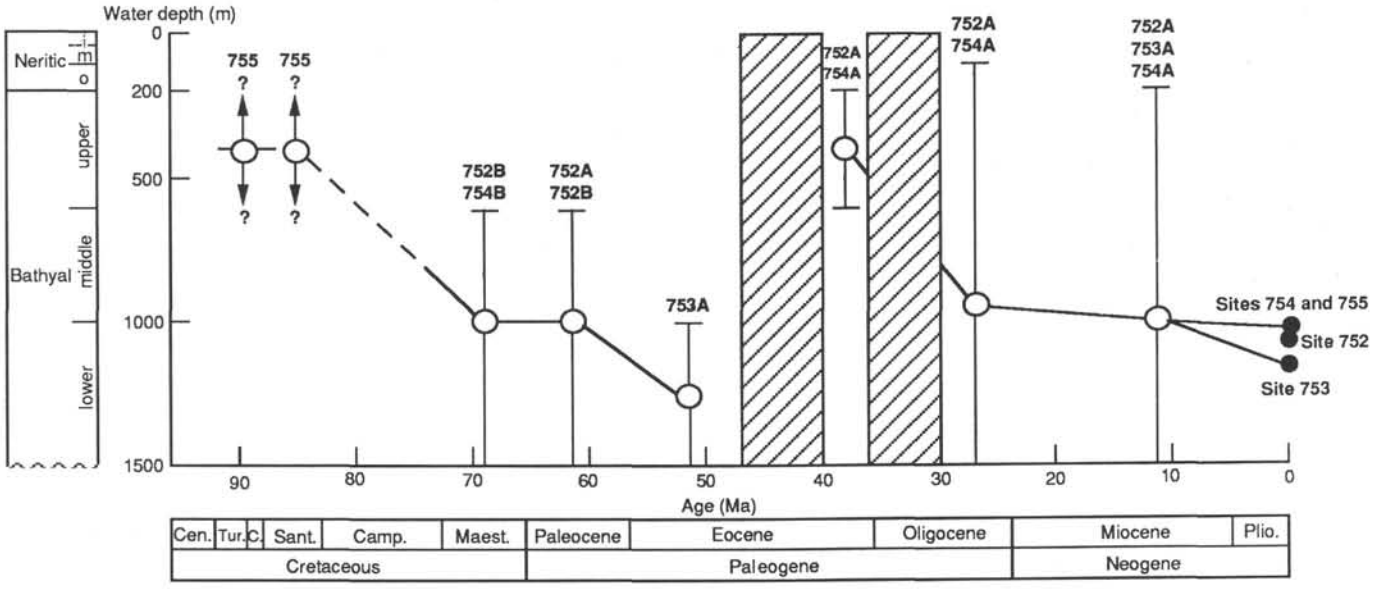

Figure 25. The depth of sediment deposition on Broken Ridge, based on benthic foraminifers. Diagonally ruled areas represent hiatuses.

longissima, Actinocyclus ingens, and *Azpeitia tabularis* were observed in Samples 121-754A-7H-CC and 121-754A-8H-CC. In addition, *Denticulopsis* aff. *dimorpha* occur in Sample 121-752A-3H-CC, of late Miocene age.

Paleogene

Middle Eocene

Moderately preserved to well-preserved diatom assemblages were found in the middle Eocene sediments of Site 753. These assemblages appear similar to those previously described in other ocean basins for the middle Eocene (Fenner, 1984, 1985) and consist mainly of species belonging to the genera *Triceratium, Hemiaulus, Coscinodiscus, Melosira*, and *Stephanopyxis*. The occurrence of *Trinacria excavata* forma *tetragona, Triceratium inconspicuum* var. *trilobata, Triceratium kanayae, Skeletonema barbadense, Melosira architecturalis*, and *Rylandsia biradiata* is consistent with the assignment of this interval to the middle Eocene, according to the diatom biostratigraphy of Fenner (1984).

Lower Eocene

Diatoms are common and moderately to well preserved in Cores 121-752A-13X to 121-752A-17X. Assemblages are similar through the section and consist of *M. architecturalis, Pyxilla gracilis, Hemiaulus polycystinorum, Hemiaulus* sp., *Arachnoidiscus* sp., *Stephanopyxis turris, Stephanopyxis* sp., *Sceptroneis* sp., *Rhizosolenia* sp., *Trinacria simulacrum, T. excavata* forma *tetragona*, and *Triceratium* aff. *cellulosum*.

Paleocene

Middle and late Paleocene age diatoms occur in Hole 752A. Diatoms are common and moderately preserved in Cores 121-752A-28X to 121-752A-31X. Diatoms are abundant and well preserved in Cores 121-752A-18X to 121-752A-27X.

The assemblages are similar to those previously described from upper Paleocene sediments (Gombos, 1977, 1984; Mukhina, 1974, 1976). However, the stratigraphic zonal markers *Hemiaulus inaequilateralus* and *Odontropsis klavsenii* proposed by Gombos (1977) are not present here. The assemblages are dominated by *S. turris, Stephanopyxis* sp., *H. polycystinorum, Hemiaulus incurvus, Hemiaulus* sp., *Rhizosolenia* sp., *Sceptroneis* sp., *Hyalodiscus scoticus* (*sensu* Mukhina 1976), *Hyalodiscus* sp., *T. simulacrum, T. excavata* forma *tetragona, T.* aff. *cellulosum*, and *Triceratium* aff. *tesselatum*.

Some observed upsection changes in the composition of the associations may be useful as stratigraphic markers, and two new zones are proposed for the Paleocene: *Triceratium tesselatum* and *Hemiaulus incurvus* Zones.

Shorebased analyses may reveal whether the diversified genera *Hemiaulus, Hyalodiscus*, and *Triceratium* are of biostratigraphic interest.

No diatoms were found in the lower Paleocene sediments of Site 752.

Cretaceous

Diatoms were found only in Upper Cretaceous Sample 121-754B-25R-CC. Specimens belonging to genera *Triceratium* or *Trinacria* were recognized, but they are too poorly preserved to be identified at the species level.

Other Siliceous Microfossils

Radiolarians, silicoflagellates, and sponge spicules are present and generally well preserved in the same samples where diatoms occur (late middle Paleocene to middle Eocene age). In addition, fragments of radiolarians and sponge spicules were found in some of the Cretaceous sediment samples from Sites 752, 754, and 755.

PALEOMAGNETICS

Magnetostratigraphy

A preliminary magnetostratigraphy was constructed from initial remanence measurements and those made following 9-mT alternating field (AF) demagnetization of archive core halves. Key intervals were checked by discrete sample demagnetization studies (AF demagnetization to 20–30 mT and thermal demagnetization to 500°C). This preliminary magnetostratigraphy will be refined with more rigorous shorebased demagnetization studies.

Capping Sequence (Lithologic Unit I)

Magnetostratigraphic analysis of the upper Eocene to Pleistocene oozes awaits shorebased studies. The whole-core data are not readily correlatable with either the geomagnetic reversal time scale (GRTS) or the preliminary biostratigraphy. Shipboard demagnetization studies on discrete samples were not possible because of the weak natural remanent magnetization (NRM) of most of the unit.

Dipping and Truncated Sequence (Lithologic Unit II)

The ash-bearing carbonate sequence produced an interpretable polarity sequence ranging from Turonian to Eocene (Fig. 26). The Cretaceous normal polarity interval (C34N) was identified in the 145-m-thick Turonian to Santonian section of Hole 755A. The majority of the polarity record consists of a nearly continuous sequence of ten chrons (C32R to C23R), identified in the 485-m-thick lower Maestrichtian to lower Eocene section from Holes 754B, 752B, and 752A. Chron C20 was identified in the 20-m-thick middle Eocene section of Hole 753A, directly below the unconformity separating lithologic Units I and II.

Correlation of the polarity sequence at Site 752 with the GRTS (Fig. 26) is straightforward and in good agreement with biostratigraphic datum levels with the following exceptions:

1. The first occurrence of *Discoaster lodoensis* occurs in an indeterminate polarity interval that we have tentatively identified as C23R. Berggren et al. (1985a, 1985b) correlated this first-occurrence datum with the early part of Chron C24N-1, although a slightly later occurrence (C23R-2) has also been reported (Monechi et al., 1985).
2. The first occurrence of *Nephrolithus frequens* (base of the *N. frequens* Zone) and the *Abathomphalus mayaroensis/Globotruncana gansseri* boundary are both within a reversed chron that we have identified as Chron C31R. The correlation of Bolli et al. (1985) indicates that both markers are approximately coincident with Chron C30R.

Although the overlap between Holes 752B and 752A is easily derived from comparison of the sub-bottom depths and matching susceptibility patterns, the correlation between Holes 754B and 752B is less certain. One possible correlation (option A, Fig. 26) relies on the identification of the *A. mayaroensis/G. gansseri* boundary in the top of Hole 754B (161 mbsf) and at the base of Hole 752B (422 mbsf; "Biostratigraphy" section, "Site 754" chapter, this volume). The implied overlap (13 m) is well within the range (20 ± 20 m) derived from seismic stratigraphy ("Seismic Stratigraphy" sections, "Site 752" and "Site 754" chapters). The similarity of the susceptibility patterns (Fig. 27) may support this correlation. This scheme, however, apparently requires a significant (>4 m) normal event within Chron C31R as well as a change in sedimentation rate from 5.7 m/m.y. during Chron C31N to >32.0 m/m.y. during Chron C31R. The normal interval at the top of Hole 754B may represent a remagnetization related to the unconformity, thus removing this objection to the correlation.

A second correlation is based on the identification of the uppermost normal interval in Hole 754B as Chron C31N. An over-

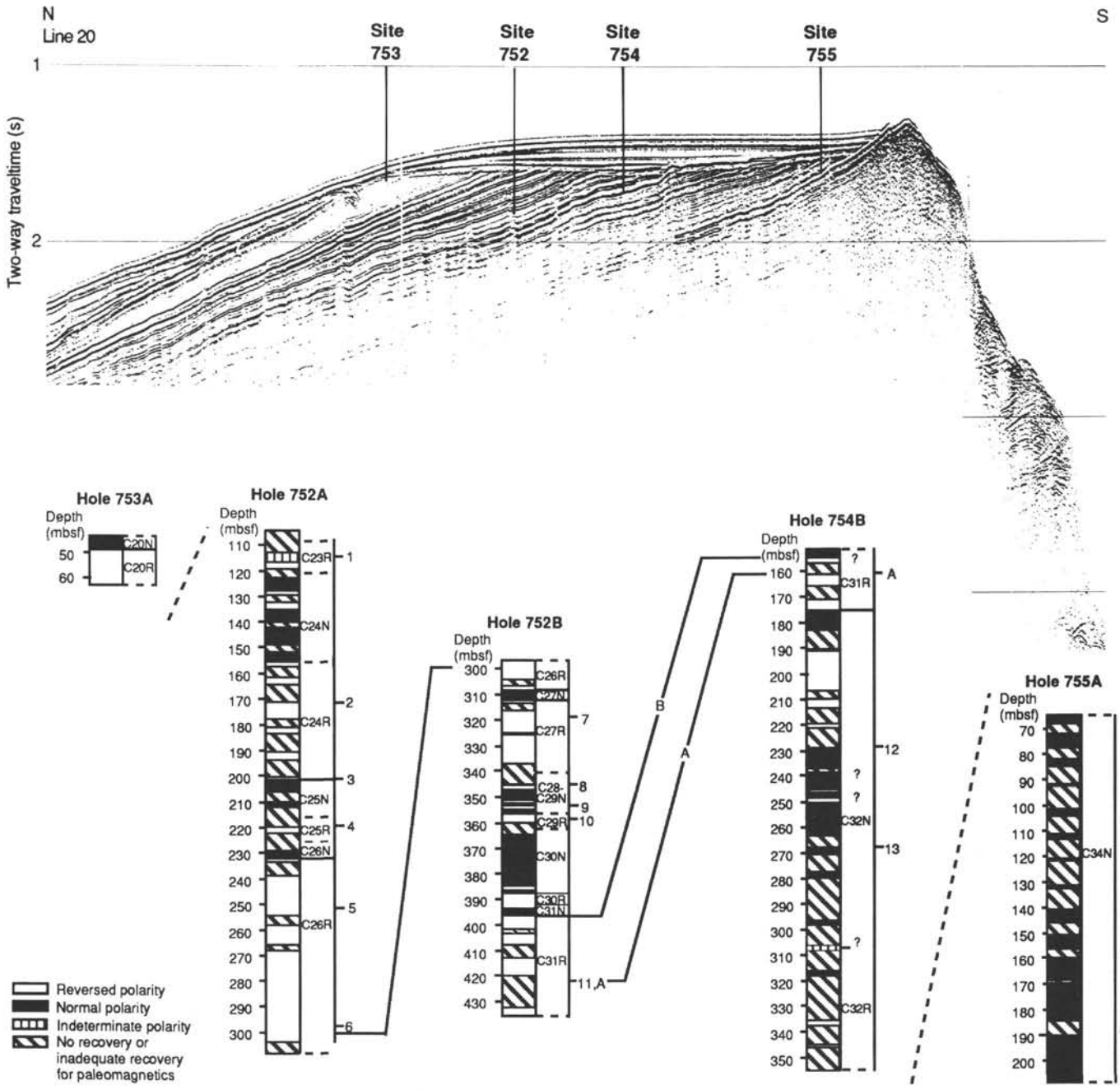

Figure 26. Composite magnetostratigraphic diagram for Holes 755A, 754B, 752B, 752A and 753A. Numbers correspond to the following nannofossil first-appearance datums: 1 = *Discoaster lodoensis*; 2 = *Tribrachiatus bramlettei*; 3 = *Discoaster multiradiatus*; 4 = *Heliolithus riedelii*; 5 = *Heliolithus kleinpellii*; 6 = *Fasciculithus tympaniformis*; 7 = *Prinsius martinii* or *Neochiastozygus saepes*; 8 = *Chiasmolithus danicus*; 9 = *Chiasmolithus tenuis*; 10 = *Biantholithus sparsus*; 11 = *Nephrolithus frequens*. A = boundary between the *A. mayaroensis/G. gansseri* foraminifer zones. Data are insufficient to adequately distinguish between schemes A and B for the correlation of Hole 754B with 752B. Dashed correlations indicate no overlap between sites.

lap of about 40 m between Holes 754B and 752B can thus be inferred from the correlation of the C31R/C31N boundary (option B, Fig. 26). Such an overlap is acceptable within the resolution of seismic correlations. Nonidentification of some critical elements in the *A. mayaroensis* assemblage permits stretching the *A. mayaroensis/G. gansseri* tie point upward to 146 mbsf in Hole 754B (above the recovered interval) and to 397 mbsf in Hole 752B. This correlation requires lateral sedimentation rate changes to account for the relative lengths of C31R in the two holes (10.2 m/m.y. in Hole 752B and >20.4 m/m.y. in Hole 754B). A reasonable susceptibility correlation may also be contrived for this model (option B, Fig. 27). We note that perhaps the best susceptibility correlation (option C, Fig. 27) is in obvious disagreement with polarity determinations and biostratigraphic and seismic correlations. We conclude that the susceptibility data provide no compelling evidence for correlation, and the remainder of the available data are insufficient to distinguish between options A and B.

A number of short (<2 m) polarity intervals that were recognized have no corresponding expression in the GRTS (within Chrons C32R, C30, C28/29, and C24). The interpretation of these short events is at present uncertain. A short event in C24 is

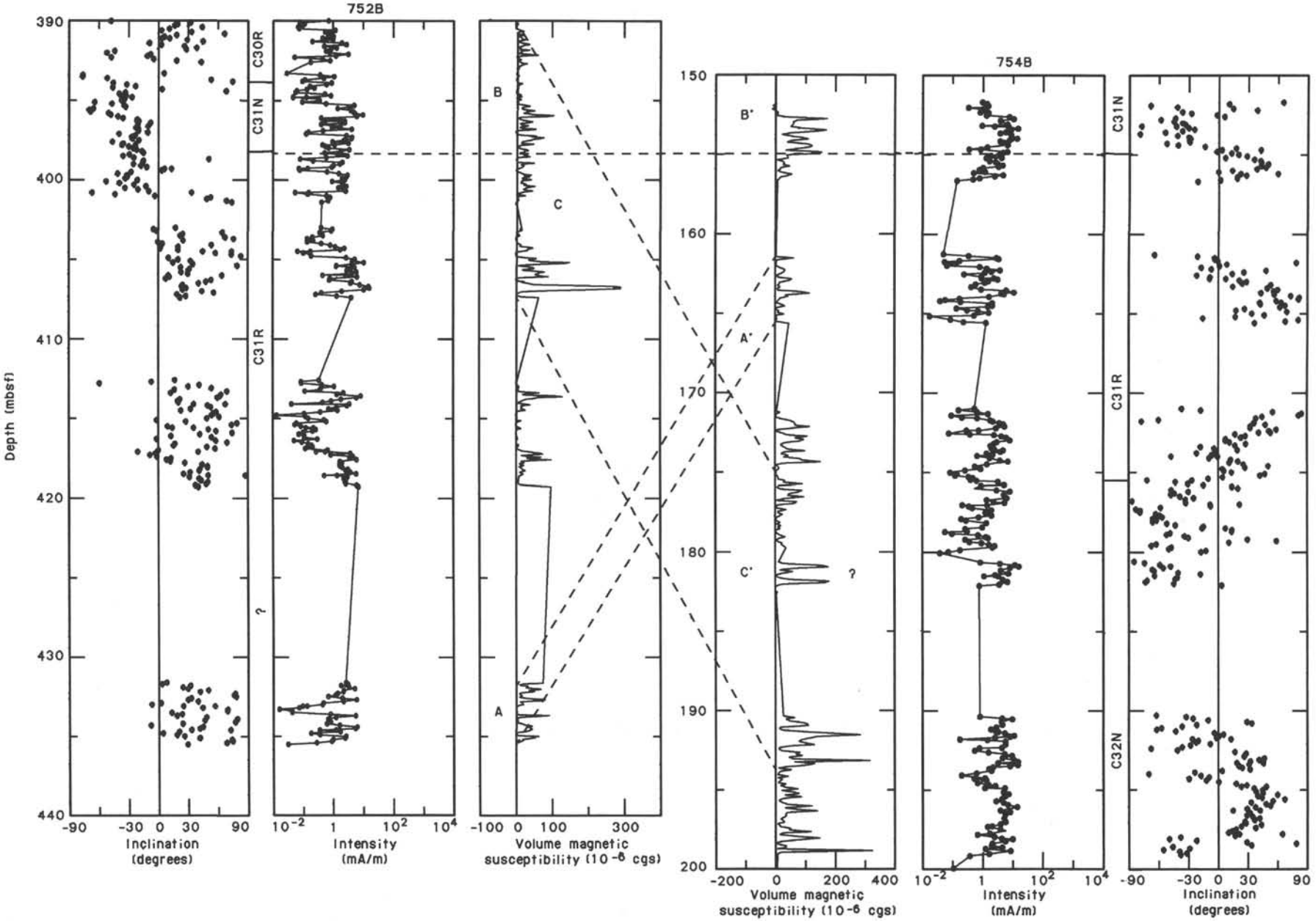

Figure 27. Possible correlation of Hole 752B with Hole 754B, based on segments of their respective susceptibility patterns (remanence after 9-mT AF demagnetization). As discussed in the text, option C should be ruled out on biostratigraphic, seismic stratigraphic, and magnetostratigraphic grounds (cf. Fig. 26).

particularly well documented by discrete sample measurements ("Paleomagnetics" section, "Site 752" chapter). A possible explanation for these extra polarity events may lie in the considerable ash influx and resulting episodically high sedimentation rates. This may have produced a considerably more detailed record of polarity intervals than normally obtained from magnetic anomaly or magnetostratigraphic studies. A number of other explanations are also possible, including (1) misorientation of cores, (2) unrecognized overprints, and (3) locally intense alteration or bioturbation.

Bulk Susceptibility

Susceptibility proved a valuable tool for detailed correlation (e.g., correlation of Holes 752A and 752B; Fig. 11, "Site 752" chapter) and for identification of ash-rich layers. Bulk susceptibility values may be used for semiquantitative estimates of ash content ("Tephra" section). However, care must be taken because susceptibility also depends on factors such as mineralogy (e.g., Ti content in titanomagnetite) and grain size. A more robust quantitative estimate can be obtained from the combined analysis of susceptibility and remanent intensity, which generally do not depend in the same way on grain size and mineralogy. Substantial variations that show up both in the susceptibility and the intensity log can be interpreted more realistically as reflecting variations in ash content.

Such simultaneous variations in NRM intensity and bulk susceptibility may be subjectively interpreted in terms of evolution of volcanic activity, bearing in mind that the ash record is also modulated by sedimentation processes ("Sedimentary Record of Broken Ridge" section). The sudden increase in susceptibility at 254.7 mbsf in Hole 754B (Fig. 28) coincides with a sudden influx of ash near the Campanian/Maestrichtian boundary (upper part of Chron C32). The Leg 120 Scientific Drilling Party (1988) found evidence at Sites 750 and 748 on the Kerguelen Plateau for a major tectonic episode at about that time (dated at 75 and 68 Ma, respectively). This tectonic event corresponds with the onset of a 20-m.y. period of very fast northward movement of the Indian plate. The ash influx is possibly related to the onset of this tectonic event. Because drilling on the Kerguelen Plateau has not recorded any comparable ash influx, the Broken Ridge volcanics must be considered of local origin. More gradual increases in susceptibility (e.g., the upper Maestrichtian to lower Paleocene sediments of Hole 752B; Fig. 29) may be interpreted in terms of large- and small-scale gradual increases in volcanic ash influx leading up to a paroxysmal phase of eruptive activity, followed by a gradual decline.

Additional Observations

No indication was found in our shipboard studies of any systematic magnetic overprint due to Eocene rifting of Broken Ridge and the Kerguelen Plateau (Mutter and Cande, 1983; Mutter et al., 1985), nor did we find clear indication of secondary components attributable to authigenic production of magnetic minerals resulting from devitrification of volcanic ashes ("Inorganic Geochemistry" in "Geochemistry" section, this chapter). If confirmed from shorebased studies, absence of such a rifting overprint markedly distinguishes the Broken Ridge–Kerguelen Plateau rifting process from such events as the Late Cretaceous extensional tectonism in the Tasman Fold Belt, which ultimately led to formation of the Tasman Sea. Paleomagnetic (Schmidt and Embleton, 1981; Klootwijk, 1985) and fission-track (Moore et al., 1986) data from the Tasman Seaboard of southeast Australia suggest a short-lived thermal pulse around 90 Ma may have preceded seafloor spreading by 5 to 10 m.y. The resulting magnetic and fission-track overprints are very prominent. Pending more detailed paleomagnetic and fission-track studies, we provisionally conclude that such a thermal pulse is absent at Broken Ridge. This conclusion is consistent with the uplift record and heatflow studies, which imply that far-field stresses, rather than thermal effects, caused the rifting of Kerguelen/Broken Ridge and the attendant uplift of Broken Ridge.

GEOCHEMISTRY

Inorganic Geochemistry

The objectives of the inorganic geochemistry studies for Leg 121 are given in the "Inorganic Geochemistry" section of the "Site 752" chapter. In short, the principal objective is to understand what causes variations of chemical gradients in a horizontal sense on a scale of a few hundred meters to a few kilometers. The chemical constituent of greatest interest is the calcium ion concentration in the pore waters. This has been most directly related to the alteration of ash in the sediments or underlying basalts.

At Broken Ridge the geochemical problem focuses on variations in pore-water chemistry from site to site on the scale of a few kilometers. It is important to view this problem in the context of the broader scale stratigraphic relationships. Four sites were drilled on a 20-km-long north-south line perpendicular to the strike of Broken Ridge (Figs. 2 and 3). The stratigraphy consists of a 40- to 150-m-thick cap of Neogene and uppermost Paleogene oozes overlying older sediments. An angular unconformity separates the two sequences (Fig. 2, "Sedimentary Record of Broken Ridge" section). The oozes are thickest at the middle Sites 752 and 754. The uppermost underlying sediments that subcrop beneath the oozes are older from north to south, ranging in age from 45 Ma at Site 753 to 86 Ma at Site 755. A middle to late Eocene erosion event caused by rift-related uplift was followed by subsidence through the present to produce the overall stratigraphic relationships on Broken Ridge. The sediments below the unconformity are increasingly lithified from north to south. They are generally slightly indurated at Sites 753 and 752 and highly indurated at Sites 754 and 755.

Discussion

The calcium ion concentration is the chemical constituent in the pore waters that exhibits a systematic trend across Broken Ridge. At Sites 753 and 752 the calcium ion concentration increases steadily with depth. This calcium gradient is moderately high compared to such gradients from the oceans as a whole (see Lawrence and Gieskes, 1981). At Sites 754 and 755 only a slight increase, which became constant below 20 mbsf, was observed (Fig. 30). This major difference between the two pairs of sites can be related to differences in lithology. Relatively soft sediments of Paleogene age that contain volcanic ash are present at Sites 752 and 753. The increase in calcium with depth is directly related to the ongoing alteration of the ash to smectite in these sediments. Most of the ash is below the Eocene unconformity (see "Inorganic Geochemistry" section, "Site 752" chapter). The horizontal lines in Figure 30 represent the depth of the unconformity at each site.

The sediments above the unconformity do not contain significant amounts of ash. Therefore, little or no calcium can be input into the pore waters. The relatively hard and well-lithified sediments below the unconformity at Sites 754 and 755 are so well lithified that no pore waters could be squeezed from them. These Upper Cretaceous sediments contain ash layers, but the ash has been completely altered to smectitic clays and zeolite (see "Inorganic Geochemistry" section, "Site 754" chapter). Apparently the reaction that is the source of calcium to the pore waters, namely the alteration of ash to clay and zeolite, has largely been completed. In view of the high contrast in the degree of lithification above and below the unconformity, it is probable that the alteration may have been completed prior to

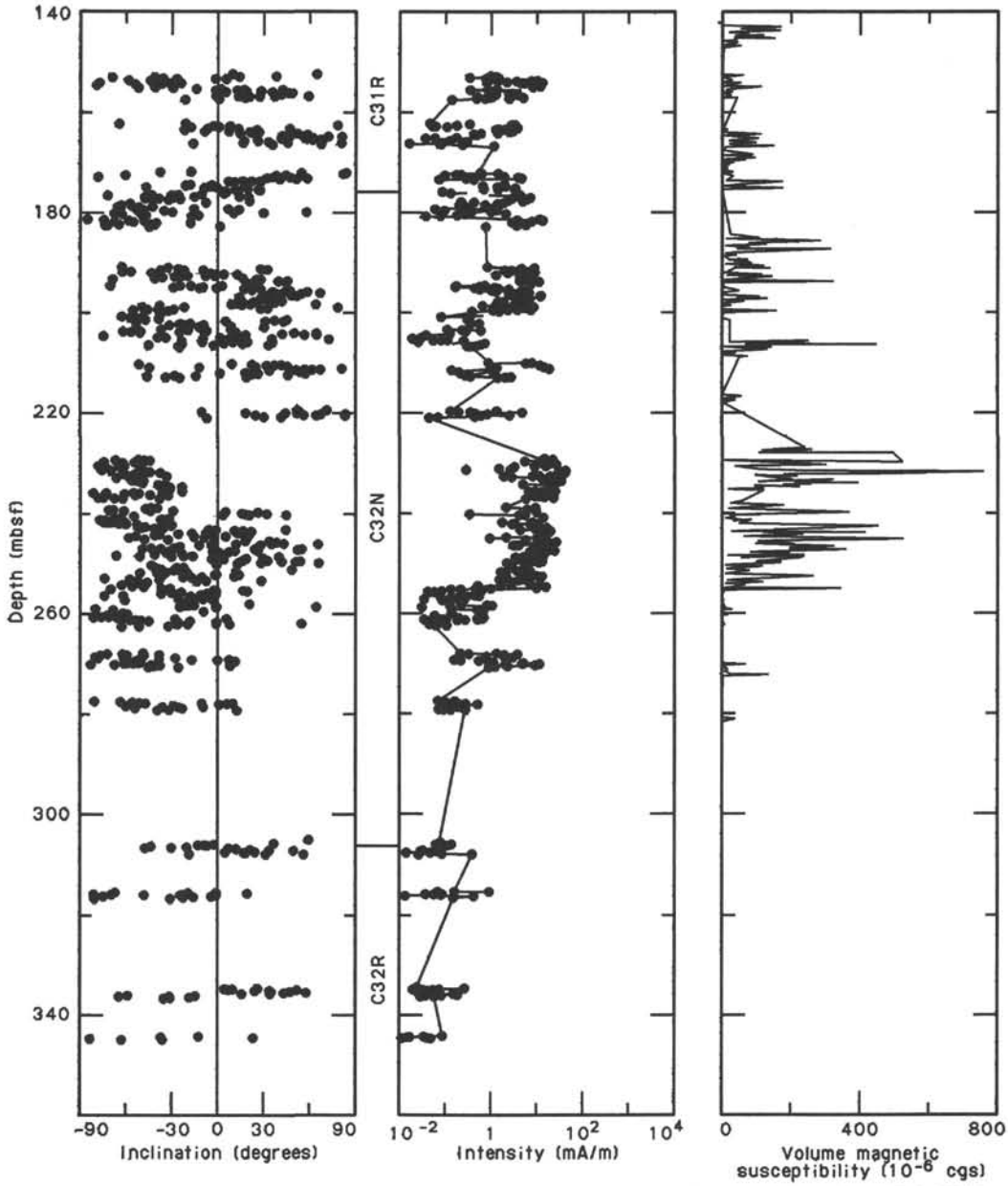

Figure 28. Remanence (after 9-mT AF demagnetization) and volume magnetic susceptibility plots, Hole 754B.

the uplift of Broken Ridge and the formation of the angular unconformity. Another factor of importance is the influence that lithification has on diffusion. Diffusion is very slow through lithified sediments, in contrast to that in oozes.

Other variables, namely magnesium ion concentration and alkalinity, also show corresponding trends with calcium. Magnesium is directly related to the alteration of ash, as is calcium. Alkalinity is indirectly related, and it decreases in response to the increase in calcium ion concentration. This process results in pore-water supersaturation with respect to calcium carbonate and removal of the carbonate ion, which lowers alkalinity. Sulfate and chloride concentrations change little with depth at any of the sites and are unrelated to the other chemical changes.

Organic Geochemistry

Objectives

At Sites 752 through 755 on Broken Ridge, measurements of (1) hydrocarbon gas concentrations, (2) quantities of total carbon and carbonate carbon, and (3) the bulk geochemical composition of the organic matter were performed.

Concentrations of hydrocarbon gases were determined in order to detect traces of either thermally or biogenically generated gas that could eventually create safety problems. Amounts of total carbon and carbonate carbon were analyzed to document the evolution of carbonate percentages and organic carbon contents in a thick sedimentary sequence of Cretaceous to Neogene age. The bulk geochemistry measurements were performed in order to determine whether the organic matter is of marine or terrestrial origin and whether it contains some hydrocarbon generation potential.

Gas Analyses

Methane concentrations varied between 3 and 200 ppm, corresponding to about 10 to 600 μL methane/L rock. In general, they were lower than 50 ppm. In uncontaminated samples, no ethane and propane were detected. No increase of methane concentrations with depth was recorded.

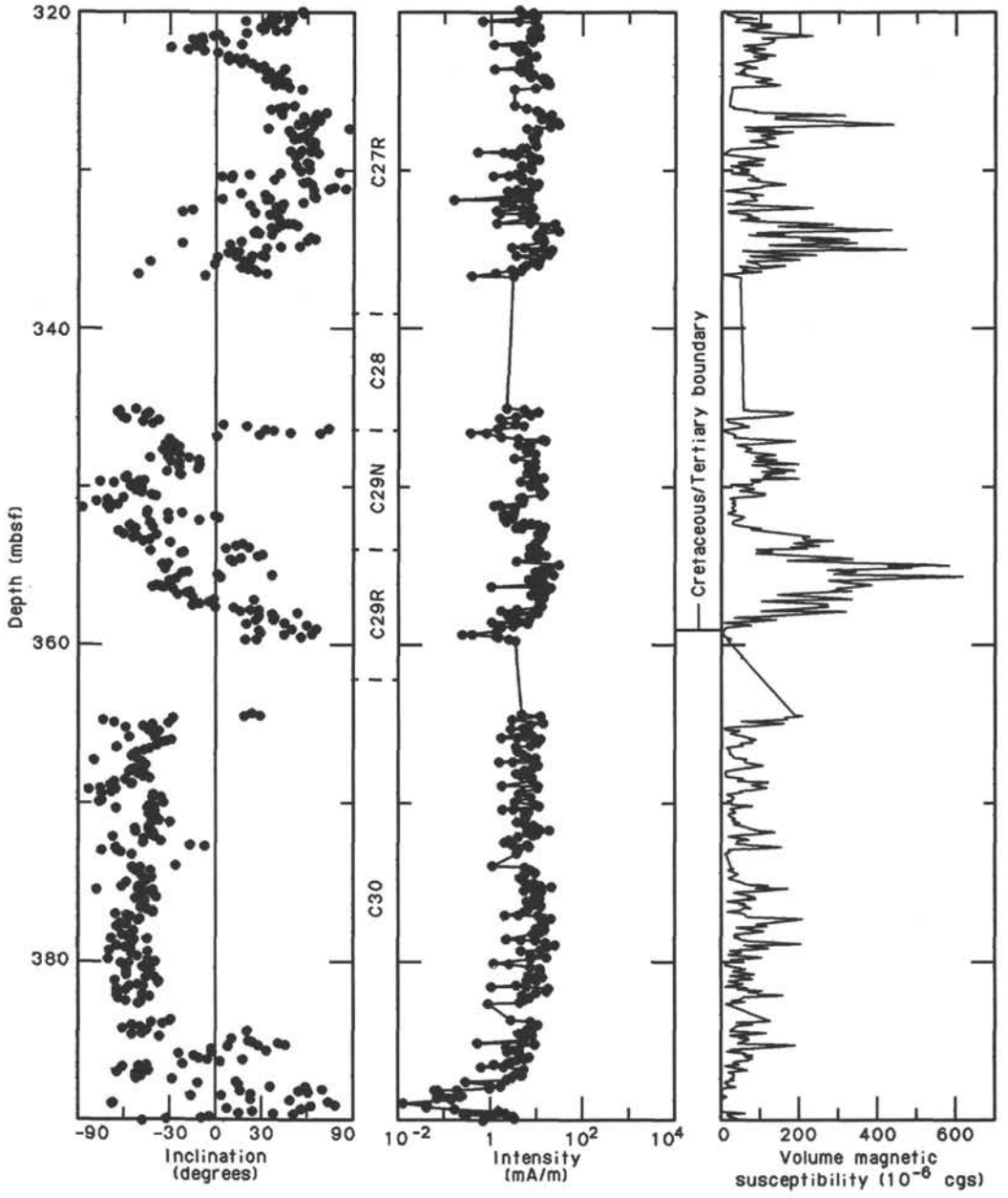

Figure 29. Remanence (after 9-mT AF demagnetization) and volume magnetic susceptibility plots, Hole 752B.

These data indicate that neither the generation of biogenic or thermal gases in the drilled sedimentary sequence nor the migration of gases into the sediments was significant at Broken Ridge.

Organic Carbon Content

Organic carbon contents in the drilled sedimentary sequence rarely exceed 0.2%. Most Neogene samples contain no organic matter at all, with a few exceptions (Fig. 31). As in the Neogene, there is little organic matter in sediments of Oligocene and Eocene age except for the thin, coarse-grained lower Oligocene to upper Eocene layer immediately overlying the truncation surface. For the Paleocene rocks, organic carbon percentages of about 0.3% were recorded. The lowermost Paleocene and upper Maestrichtian sediments are poor in organic matter, whereas the lower Maestrichtian and Santonian to Turonian sequences contain 0.2% organic matter on average.

The small quantity of organic matter in sediments from Broken Ridge is not related to a low bioproductivity but rather to a severe and often complete degradation of the organic matter prior to burial.

Bulk Composition of the Organic Matter

All pyrolysized post-Paleocene samples at Broken Ridge are extremely hydrogen poor (i.e., hydrocarbon release was lower than 30 mg/g organic carbon). Better qualities for hydrocarbon generation were found for samples from the lower Maestrichtian (Fig. 32). About 200 mg of hydrocarbons/g organic carbon could be released from samples in this stratigraphic unit.

Hydrogen percentages in the organic matter from the Paleocene and from the Santonian to Turonian sequence are higher than in the post-Paleocene, but lower than in the lower Maestrichtian. According to microscopic observations of Sample 121-755A-11R-1, 148–150 cm, the bulk of the organic matter

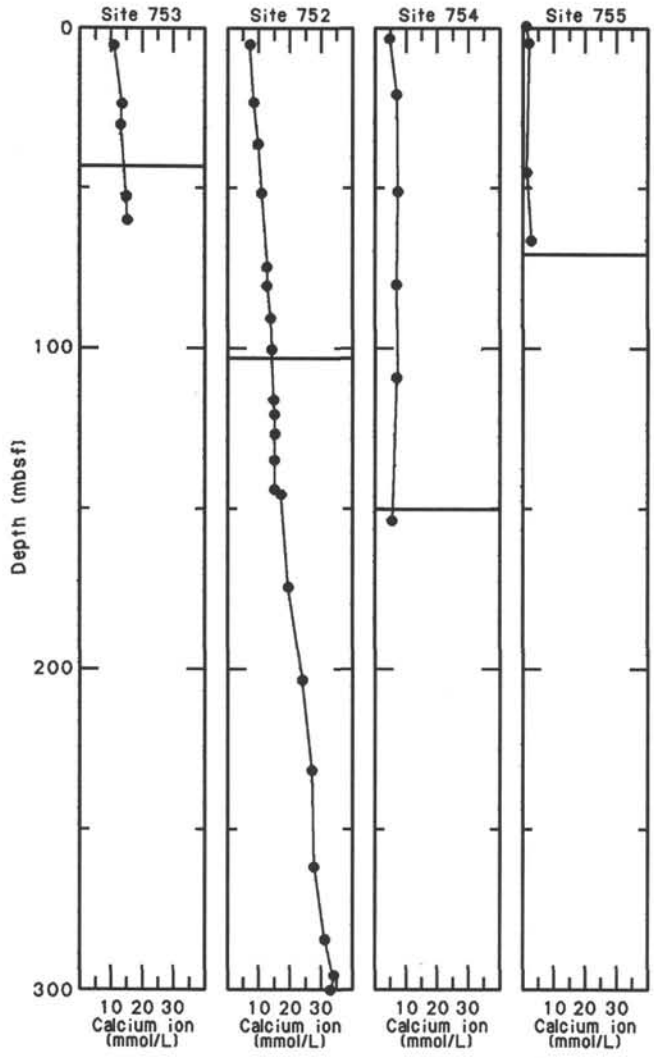

Figure 30. The calcium ion concentration of pore waters from Sites 753, 752, 754, and 755 plotted as a function of depth. The horizontal lines represent the Eocene unconformity at each site.

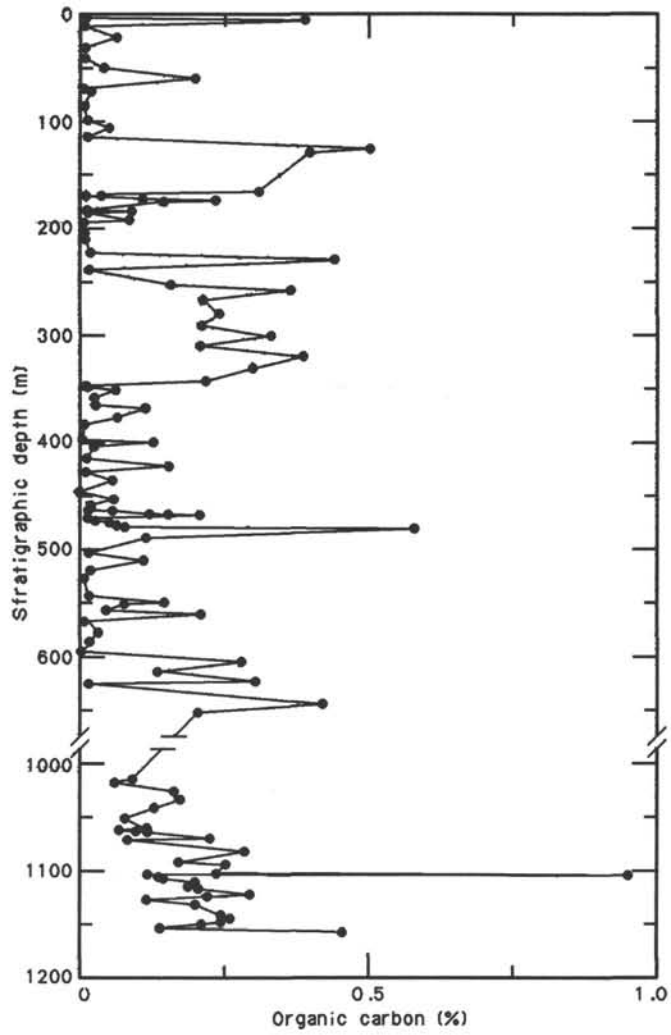

Figure 31. Weight percentages of organic carbon in sediments from Sites 752, 753, 754, and 755. The depths are adjusted assuming an overlap of 20 m between the bottom of Hole 752B and the top of the Cretaceous at Site 754 and a 450 m gap between the lower Maestrichtian at Site 754 and the Santonian at Site 755. Note break in depth scale.

consists of terrestrial debris (i.e., inertinite and vitrinite; Figs. 33A through 33C). The terrestrial organic fragments in this sample are as large as 50 μm, which indicates that the plant particles were not transported over great distances from land to the depositional site. There are also minor amounts of bituminite (Fig. 33D), probably derived from marine organic matter. Further investigation is necessary in order to determine whether all the organic matter at Broken Ridge is derived from the chemically more stable detritus of terrestrial higher plants, or whether there is also a significant input from marine organisms or from bacteria.

Carbonate Content

Carbonates are major constituents in the studied sequence and consist almost entirely of calcite ($CaCO_3$). Some dolomite occurs in the lower Maestrichtian, generally in quantities of less than 10% of the total carbonate. A calcite/dolomite ratio of about 1.5 was recorded by X-ray diffraction (XRD) in Sample 121-754B-22R-1, 21–22 cm.

Carbonate contents in the analyzed samples vary between 0% and 97% and generally decrease with increasing age. In the Neogene, mean carbonate percentages are 96%, with little variation (Fig. 34). There is no significant difference between carbonate values in the Neogene sections drilled at Sites 752, 753, 754, and 755.

Carbonate contents in the lower Oligocene to upper Eocene brown gravel layer that lies immediately below the Neogene ooze and above the angular unconformity vary between 30% and 75%, with a mean of about 60%.

The older sediments of middle Eocene and early Eocene through Paleocene age beneath the unconformity at Sites 753 and 752, respectively, contain between 30% and 90% carbonate. Average carbonate values decrease within the Eocene section down to the top of the ash-rich layer above the Cretaceous/Tertiary boundary (400 m adjusted stratigraphic depth, Fig. 34) from about 85% to about 60%. The ash-rich layers in this sequence are not pure volcanics but mixtures of biogenic carbonates and volcaniclastic particles. On the other hand, even sediments that contain no volcanic material according to visible and microscopic description and XRD analysis are not as rich in

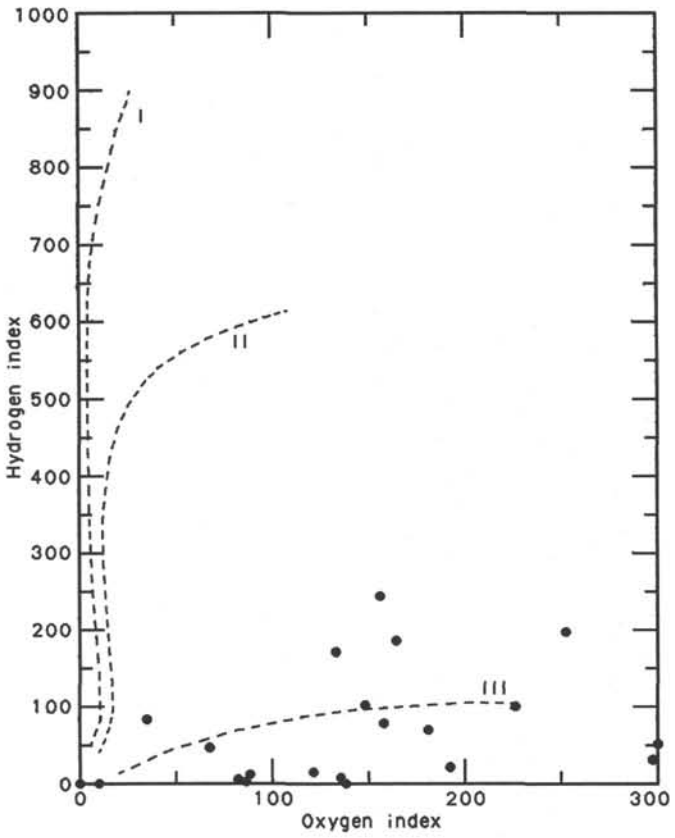

Figure 32. Hydrogen indices vs. oxygen indices of samples from Sites 752, 754, and 755. The highest hydrogen indices are in samples from the lower Maestrichtian at Site 754 and plot between the pathways for type II and type III kerogen. The Neogene samples possess no hydrocarbon generation potential. The hydrogen indices of Paleocene and Santonian-Turonian samples are about 100.

carbonate as the Neogene oozes. They contain, however, a significant proportion of opal derived from the biogenic silica of diatoms and radiolarians.

The carbonate-poor layer above the Cretaceous/Tertiary boundary (at about 400 m adjusted stratigraphic depth in Fig. 34; see Fig. 35) contains a high amount of biogenic silica as well as volcanic fragments. Its composition and thickness clearly differ from those of the other carbonate-poor layers in the Tertiary section. In the underlying Maestrichtian, carbonate percentages vary between 0% and 90%. There is a general trend toward decreasing carbonate contents with increasing age. The lowest carbonate percentages were measured in some cherts, but there are also some volcaniclastic layers with carbonate contents lower than 20%.

In the Santonian to Turonian sequence drilled at Site 755, carbonate values are significantly lower than in the overlying drilled units (Fig. 35). As in the Eocene to Paleocene sequence and in the upper to lower Maestrichtian sequence, carbonate percentages decrease with increasing depth. In the lower 50 m of Hole 755A, values of more than 5% carbonate are rare.

A linear regression calculated for the entire sequence drilled on Broken Ridge shows the increase of carbonate percentages in the sediments since the Turonian (Fig. 36). Reasons for this increase of carbonate contents are (1) a decrease in volcaniclastic deposition and (2) a change in primary production from a mixed calcareous and siliceous assemblage toward a nearly exclusively calcitic assemblage.

PHYSICAL PROPERTIES AND GEOPHYSICAL WELL LOGGING

Drilling at Broken Ridge was aimed at studying the vertical motion of the ridge in relation to lithospheric extension and rifting. The physical-properties and logging efforts at the four Broken Ridge sites were intended to define ties between the seismic stratigraphy and cored lithologies, to understand the history of the sediment section through its physical properties, and to constrain the thermal history through heatflow experiments.

The physical definition of the major lithologies at Broken Ridge is clearly defined through laboratory and logging measurements. Both sets of data agree closely. Extrapolation of the cored lithologies over the western part of Broken Ridge using regional seismic surveys is discussed in the "Broken Ridge Underway Geophysics" chapter (this volume). This section summarizes the physical properties of the stratigraphic section at Broken Ridge.

Pelagic Cap

Coring at Sites 752, 753, and 754 fully sampled the pelagic oozes capping the middle Eocene unconformity overlying the dipping units. Lithologically, the cap is composed of nannofossil/foraminifer to nannofossil ooze. The relatively homogeneous aspect of this material is evident in all index properties, as illustrated by the continuous GRAPE bulk densities (Fig. 37). Bulk density throughout the cap sequence ranges from approximately 1.52 to 1.75 g/cm^3, which is relatively high in comparison to other calcareous ooze sections, such as described by Hamilton (1976).

Low values of compressional-wave velocity and vane shear strength attest to the thixotropic nature of these calcareous sediments. The lack of any cohesion in these sediments results in extremely low strengths that simply reflect intergranular locking during the tests. Velocities near 1500 m/s throughout the cap are also indicative of a material with little rigidity.

Horizons corresponding to the prominent seismic reflectors within the pelagic cap were, unfortunately, those least recovered by coring. A lower Oligocene hiatus occurs at Sites 752 and 754. This same disconformity merges with the middle Eocene unconformity at Sites 753 and 755. Cherty sand, gravel, and shell fragments were recovered overlying the Oligocene unconformity, and the middle Eocene unconformity is a zone of coarse-grained clastic sands and pebbles derived from eroded underlying cherts and chalks to limestones. The physical contrast between these unconformity-related materials and the surrounding calcareous oozes to chalks results in the clear seismic reflectors. Limited logging was achieved only across the lower unconformity at Site 752. There, slightly higher natural gamma counts, which possibly reflect a weathered and oxidized matrix, indicate that the upper Eocene section above the truncation surface extends from 96 to 112 mbsf (see Fig. 32 in "Geophysical Well Logging" section of the "Site 752" chapter).

Other changes in physical properties that are more subtle than the two unconformities occur within the pelagic cap. These slight variations, such as the decrease in bulk density at 60–75 mbsf at Site 752 (Fig. 37), appear to be related to slight sedimentologic changes. A coarse grain-size fraction from 58 to 76 mbsf and these lower densities may attest to sediment winnowing in the lower Miocene section. Another coarsening fraction from 35 to 44 mbsf at Site 753, also in the lower Miocene, matches a general decrease in bulk density. The same slight density decrease occurs between approximately 76 and 90 mbsf at Site 754, where it is correlated with a coarser grain size. The low densities at 28–33 mbsf at Site 752, at approximately 19 mbsf at Site 753, and as poorly distinguished at 35 mbsf at Site 754 are

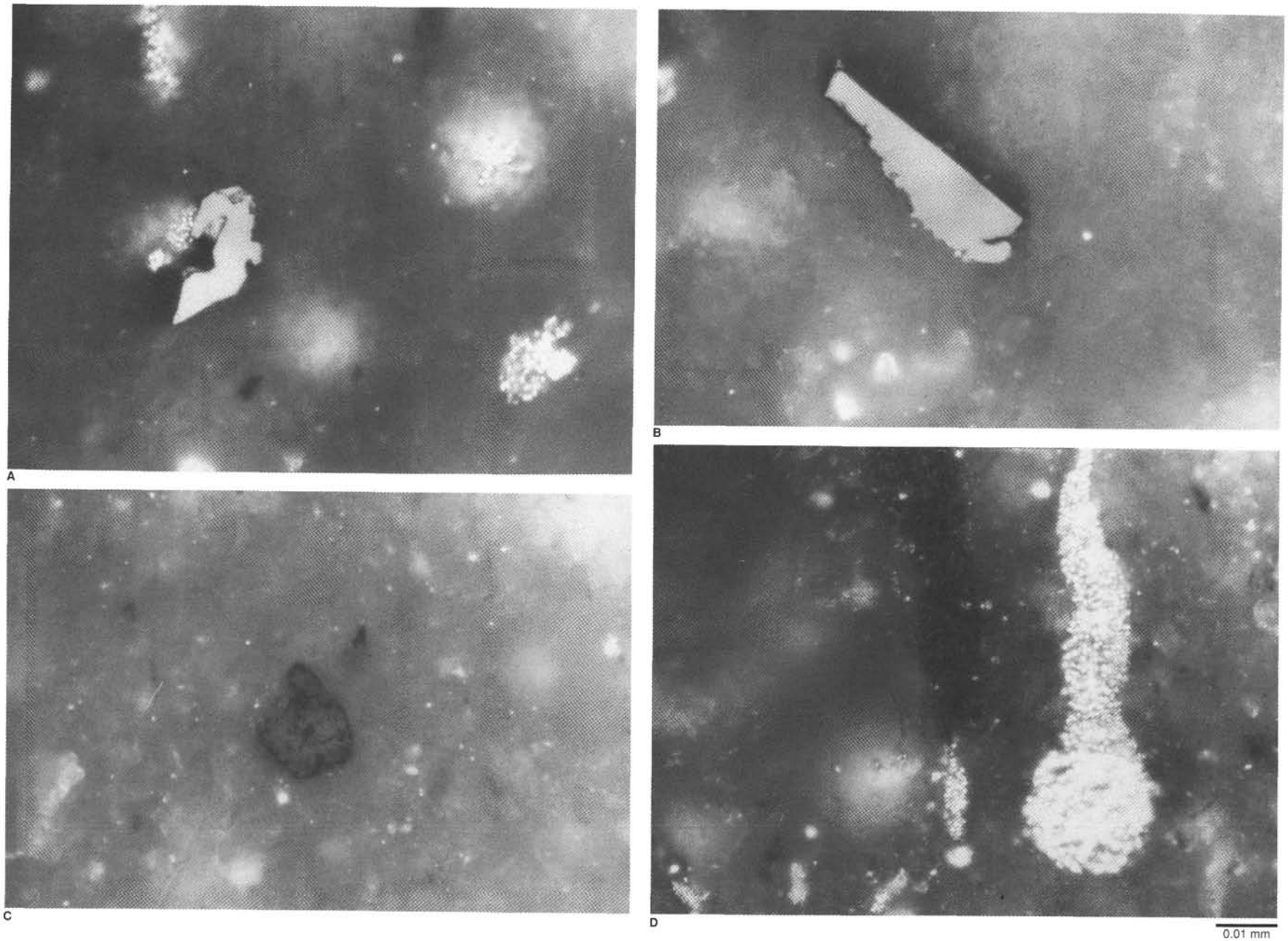

Figure 33. Photomicrographs of Sample 121-755A-11R-1, 148–150 cm. Reflected white light, oil immersion. **A.** Inertinite particle derived from strongly degraded higher plants. Inertinites are the major organic constituents in this sample. **B.** Inertinite particle with a diameter of about 50 μm, indicating a nearby source for the terrestrial particles. **C.** Vitrinite particle. Like inertinites, vitrinites are derived from higher land plants transported to the depositional site. **D.** Bituminite(?) and framboidal pyrite. Bituminites are derived from marine organic matter. Framboidal pyrite, which is very common in this sample, is derived from the early diagenetic activity of sulfate reducing bacteria.

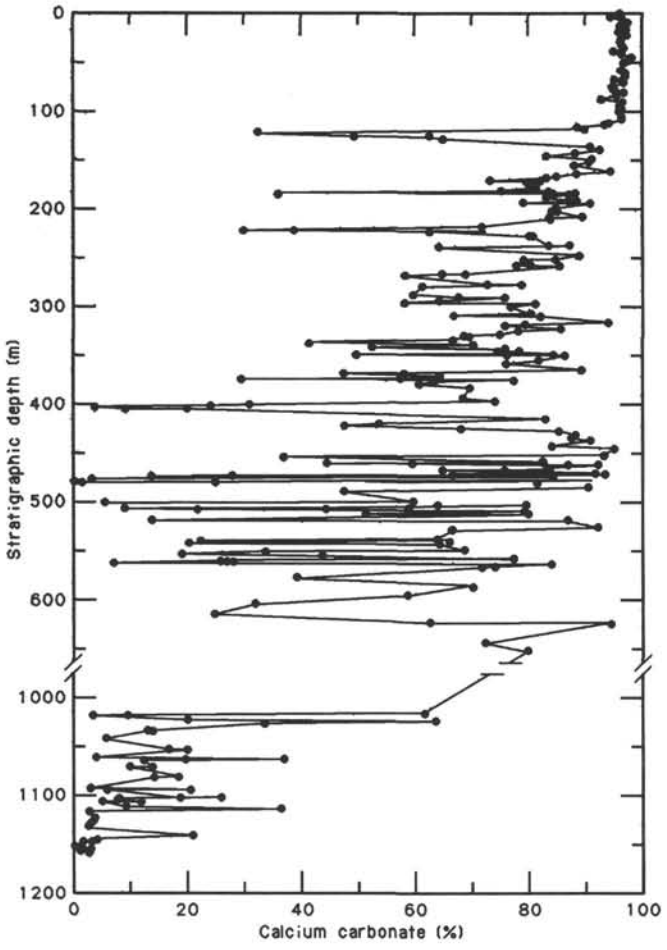

Figure 34. Weight percentages of calcium carbonate calculated from inorganic carbon measurements for samples from Sites 752, 753, 754, and 755. The depths are adjusted assuming an overlap of 20 m between the bottom of Hole 752B and the top of the Cretaceous at Site 754 and a 450 m gap between the lower Maestrichtian at Site 754 and the Santonian at Site 755. Note break in depth scale.

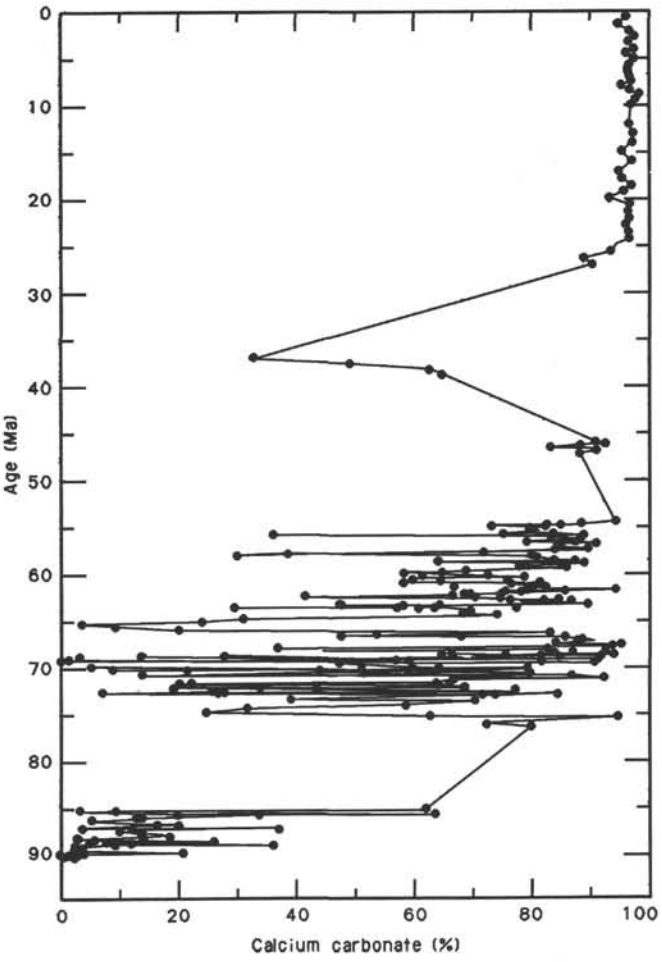

Figure 35. Calcium carbonate percentages at Broken Ridge vs. age. The plot is based on the same data as Figure 36. Ages are adopted from the available paleontological data (see "Biostratigraphy" sections of the Broken Ridge site chapters).

within the middle upper Miocene. These intervals can also be correlated with intervals of coarser grain size. The implication for this section capping Broken Ridge, then, is that slightly lower densities within the almost homogeneous ooze section may reflect a coarsening grain size that is probably the result of winnowing. On a larger scale, however, this pelagic section is more compacted (i.e., lower porosity) than similar oozes in the Pacific (Hamilton, 1976), which may reflect the lower sediment-accumulation rate and some early calcareous diagenesis.

Dipping and Truncated Section

Middle Eocene to Turonian lithologies were recovered from the transect of holes across Broken Ridge. The transition from overlying ooze to underlying chalks was used to delineate lithologic Unit I from Unit II. Coring at Site 752 sampled the thickest chalk interval, represented by a shift from lower to higher bulk densities and velocities relative to those of the pelagic cap. Bulk densities in the chalks range from about 1.70 to 1.90 g/cm^3, which is fairly distinct from the other cored lithologies at Broken Ridge (Fig. 38). The intervals of relatively higher densities within the chalk correspond to intervals in which cherts and porcellanites were recovered. The low density values at 220–240 mbsf correlate with a chalk containing biogenic siliceous material. Initial XRD studies of sediment residues following carbonate analyses show an alteration of opal-A to opal-CT at 280 mbsf at Site 752 and below the unconformity at Site 754. The effect of this transformation on the physical properties is not clear from the shipboard analyses, but will be the topic of later shorebased work. At 290–300 mbsf, ash within the chalk may contribute to the slightly lower densities.

Velocities in the chalk section vary around an average of 2100 m/s, as indicated by the logging results (Fig. 39). Laboratory-measured velocities average about 1900 m/s. The difference is probably a result of rebound and disturbance of sediment samples. Results of the two measurement techniques do indicate similar downhole trends, however. At Site 752, low velocities and densities at 180 mbsf may reflect ash in these chalks (Fig. 39A). Velocities in excess of 2400 m/s at 200–210 mbsf correspond to chert (Fig. 39A).

The consolidation of the calcareous sediments is noticeable in the increase in density and velocity at 300 mbsf in the sediments at Site 752. A smaller density transition occurs at about 200 mbsf at Site 754, which is also a different stratigraphic level. The diagenetic transition from chalk to limestone is readily apparent in the physical properties, whereas visual descriptions may miss these changes. This transition is marked by a density increase to values over 2.25 g/cm^3 and velocities in excess of about 3000 m/s at Site 752. The density change at Site 754 at

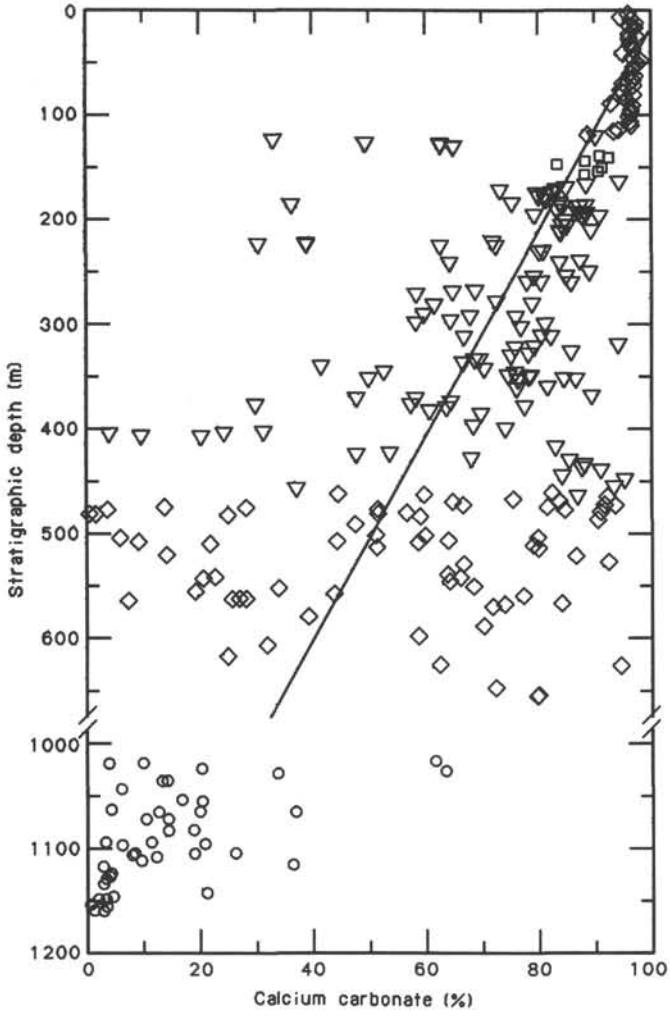

Figure 36. Weight percentages of calcium carbonate plotted for depths adjusted assuming an overlap of 20 m between the bottom of Hole 752B and the top of the Cretaceous at Site 754 and a 450 m gap between the lower Maestrichtian at Site 754 and the Santonian at Site 755. Note break in depth scale. Neogene and Maestrichtian samples from Site 754 are marked by diamonds, middle Eocene samples from Site 753 are marked by open squares, upper Eocene gravels and lower Eocene to upper Maestrichtian samples from Site 752 are marked by inverted triangles, and Santonian to Turonian samples from Site 755 are marked by circles. A linear regression curve shows the general increase of carbonate percentages toward the Neogene.

200 mbsf, however, does not correspond with a velocity contrast because these values are near 3000 m/s where logging began at 165 mbsf (Fig. 39).

An interesting aspect of the Maestrichtian chalks and limestones is their clearly anisotropic velocities. Horizontal (measured along bedding) velocities are consistently greater than those measured perpendicular to bedding. Whether this anisotropy is a result of primary sedimentary structure or an artifact of the consolidation process awaits shorebased analyses.

The lower section cored at Site 752 stratigraphically overlaps with the upper Maestrichtian section cored below the unconformity at Site 754. The interval from about 150–170 mbsf at Site 754 is stratigraphically equivalent to the lower 20 m of Site 752, where logging velocities are greater than 3000 m/s. Opal-CT to quartz diagenesis, which appears to occur at about 380 mbsf at Site 752 and at 320 mbsf at Site 754, may be related to the higher densities observed exclusively below those depths. The velocity change related to the soft to hard chalk, or limestone, transition is lost in the unconformity at Site 754. Thus, the continuous consolidation of this calcareous section is best represented at Site 752.

The continuous stratigraphic section at Broken Ridge can be approximated by stacking cored intervals with corresponding stratigraphic gaps and overlaps between sites. Based on the seismic stratigraphic interpretation, a 190 m gap exists between the cored sections at Sites 753 and 752, Sites 752 and 754 overlap by approximately 20 m, and about 540 m is missing between Sites 754 and 755. (The length of the missing section was subsequently revised to approximately 400–450 m, although not incorporated in Fig. 40.) Using these relationships, the bulk density of the section below the unconformity at Broken Ridge was constructed (Fig. 40). The chalk to limestone transition is quite clear at a stratigraphic depth of 500 m, and the slight consolidation within the chalk sequences can be appreciated by the increase from about 1.6 to 1.8 g/cm^3.

A cross section of the sites drilled along Broken Ridge shows the tie of several physical-properties units defined for each site (Fig. 41). Note, however, that the physical-properties boundaries transcend age and lithologic boundaries. The deepest stratigraphic section, at the base of Site 755, is composed of tuff and tuff with glauconite or with micrite. The physical properties at Site 755 suggest that the ash is cemented, whereas the ash results in intervals of low density and high water content in the chalk and limestone sections (350–375 mbsf, Site 752; 245–264 mbsf, Site 754; Fig. 41). This cementation produces low water contents and high densities comparable to those of the limestones (Figs. 38, 39, and 41), but results in relatively low velocity (see Fig. 14 in the "Physical Properties" section, "Site 755" chapter). This low-velocity interval was an unexpected result of coring at Site 755. Toward the base of Site 755, however, several recrystallized calcite nodules were recovered in the volcanic ash. These have high velocities (4100 m/s) and densities (2.5 g/cm^3) relative to the ash and may represent some of the material underlying the ash sequence. This lithologic and physical-properties contrast might explain the strong seismic reflector at the base of that drill hole (see "Seismic Stratigraphy" section, "Site 755" chapter).

Heat Flow

A point of discussion pertinent to the vertical motion history at Broken Ridge is its thermal history. The middle Eocene uplift and subsequent erosion at Broken Ridge can be attributed to a mechanical response to lithospheric extension and/or thermal rejuvenation of the ridge during rifting. Knowing the regional heat flow, therefore, becomes necessary to discern the relative thermal contribution to the vertical motion of Broken Ridge since the middle Eocene.

Four downhole temperature measurements were made at Sites 752 and 753, yielding three reliable points from bottom-water temperature to 53 mbsf. The thermal gradient calculated from these three values is 33.9°C/km, which results in a heat flow of 44.8 W/m°C (1.04 HFU) in consideration of the thermal conductivities of the pelagic cap. This heat flow lies between two values reported by Anderson et al. (1977). They reported two heatflow measurements from Broken Ridge, one at the juncture with Ninetyeast Ridge and the other near the Leg 121 transect, of 53 and 34 W/m°C, respectively. Hyndman et al. (1974) reported a heatflow value of 1.12 ± 0.22 HFU in sediments below 130 mbsf at DSDP Site 254 on Ninetyeast Ridge. The Leg 121 and the Anderson et al. (1977) results are shown relative to Anderson et al.'s (1977) compilation of heat flow through the Indian Ocean crust older than 40 Ma (Fig. 42). The data suggest that the Broken Ridge crust is thermally consistent with a Cenomanian-Albian age. Although the Broken Ridge heatflow data

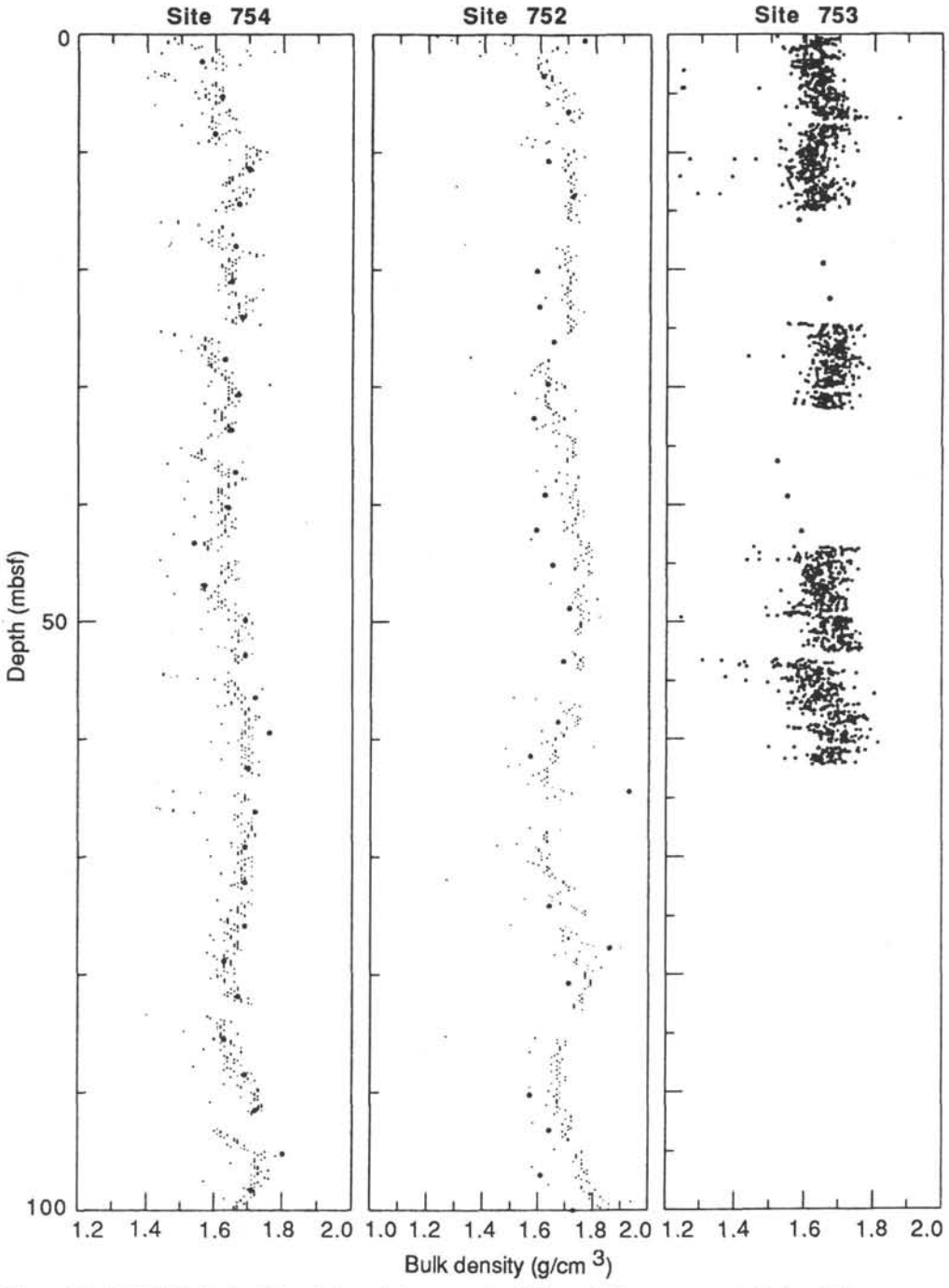

Figure 37. GRAPE bulk densities of the pelagic, nannofossil/foraminifer ooze cap at Broken Ridge.

are not necessarily constrained by Anderson et al.'s (1977) model, the Leg 121 results do not appear to substantiate a significant thermal event there during the middle Eocene.

CONCLUSIONS

1. The Kerguelen-Heard Plateau and Broken Ridge were formed by constructional volcanism during the mid-Cretaceous (Cenomanian to possibly Albian), based on dated dredged basalts and basement drilled on Kerguelen Plateau (Barron, Larsen, et al., in press; Schlich, Wise, et al., in press). These features constituted a large oceanic platform until they were separated in the middle Eocene by rifting and subsequently by seafloor spreading.

2. Broken Ridge, which occupied the northern part of the original broad depositional platform, subsided from outer shelf/upper slope to lower bathyal depths from the Turonian to the middle Eocene, according to benthic foraminifer assemblages.

3. The Turonian to Santonian section is dominantly volcanogenic, reflecting voluminous eruptive activity from a nearby source. Ash-rich layers were found up into the lower Tertiary part of the section. The ash-accumulation rate, however, decreases upsection, perhaps in response to waning volcanic activity or increasing distance between Broken Ridge and the eruptive center ("Ninetyeast Ridge Summary" chapter, this volume). The ashes are primarily basaltic, similar in composition to rocks from Ninetyeast Ridge, the Kerguelen Plateau, and older parts

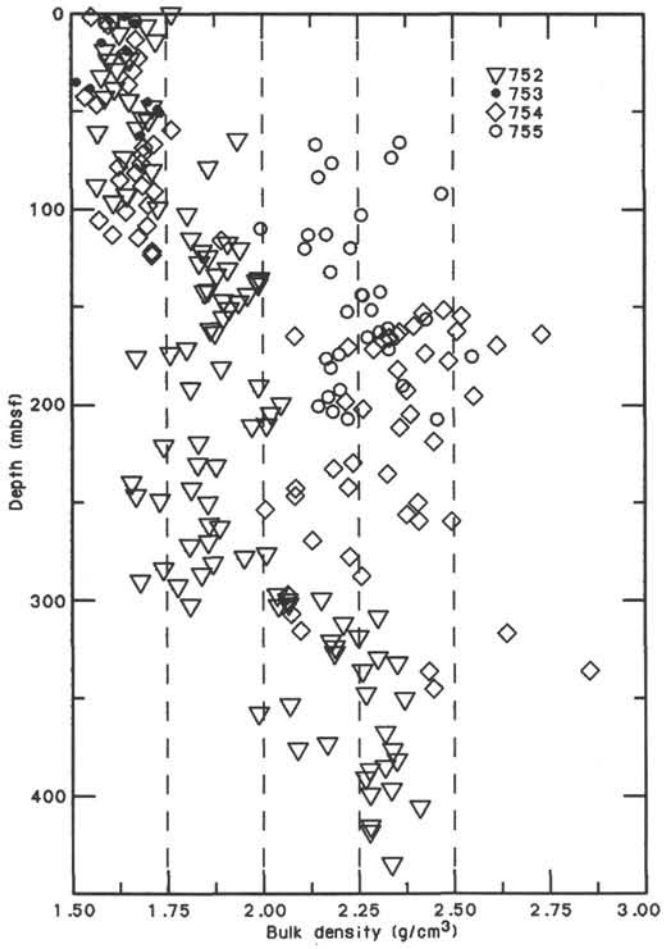

Figure 38. Bulk densities of sediments from all ODP Leg 121 Broken Ridge sites. The distinct groups of densities reflect various steps in calcareous sediment diagenesis.

of the Kerguelen Islands. Microscopic terrestrial organic debris found in the Turonian-Santonian section indicates that some parts of the Kerguelen–Broken Ridge platform were emergent and vegetated at that time.

4. Although the earliest depositional sequences on Broken Ridge were not reached by Leg 121 drilling, the biological productivity of the overlying waters increased rapidly between the early Santonian and early Maestrichtian. We suggest that such enhancement of productivity might reflect a combination of increased oceanic circulation, perhaps as the result of rapid widening of the proto-southern Indian Ocean, and of bathymetrically-induced upwelling. The carbonate-accumulation rates at Broken Ridge are among the highest ever recorded on oceanic plateaus for the Late Cretaceous, and they decreased gradually through the early Tertiary.

5. The Cretaceous/Tertiary boundary was recovered in Hole 752B (see "Cretaceous/Tertiary Boundary Summary" chapter).

6. A rich diatom assemblage is found in the lower Tertiary section of Broken Ridge, allowing direct correlation of diatom datum levels with nannofossil and planktonic foraminiferal zonations. In addition, the diatom record from Broken Ridge will represent the first documentation of middle and early Eocene age diatoms in the Indian Ocean.

7. The youngest sediments below the unconformity are chalks of middle Eocene age (P11/CP13c) at Site 753. Therefore, rifting between Broken Ridge and Kerguelen Plateau and the consequent uplift and erosion of Broken Ridge began at about 45 Ma.

8. Because depositional depths were increasing rather than shoaling before rifting, we conclude that extension was initiated by far-field horizontal stress (passive rifting) rather than by a mantle convective process (active rifting).

9. The oldest sediments above the erosional surface are late Eocene age oozes (P15 and CP15) deposited in upper bathyal depths. About half the microfossil assemblage, however, consists of older reworked forms, some of which are from shallower depths. Clastic debris (shell and bryozoan fragments, pebbles of limestone, and chert mixed with sand from the uplifted sediments), much of it iron-stained, was shed from the exposed surface of Broken Ridge, reworked into sand and gravel layers, and deposited as Broken Ridge subsided through sea level.

10. The water paleodepth data, the geometry of seismic reflectors, and the observed gravity anomalies indicate that Broken Ridge was uplifted by >2 km during rifting.

11. The duration of the rifting event was relatively short (<5 m.y. long) because seafloor spreading was under way between Broken Ridge and Kerguelen Plateau by anomaly 18 time (approximately 42 Ma).

12. Both the brevity of the rifting event and the low present-day heat flow (45 mW/m^2) are consistent with a mechanical, rather than thermal, origin for the uplift at Broken Ridge. The rift flank uplift at Broken Ridge can be explained as flexural rebound following mechanical unloading of the lithosphere during extension (Weissel and Karner, in press). If this explanation is correct, the lithosphere must retain finite mechanical strength (or flexural rigidity) during extension.

13. A disconformity in the pelagic oozes capping Broken Ridge represents a hiatus between the upper Eocene and upper Oligocene at Sites 752 and 754. This hiatus was not found to the north at Site 753 or to the south at Site 755. The disconformity perhaps records the fall in eustatic sea level at 29 Ma (Haq et al., 1987) or is evidence for enhanced surface-current activity related to the opening of the circum-Antarctic seaway (Kennett and Burns, 1972).

14. The upper Oligocene through Pleistocene carbonate oozes in the capping sequence have been subjected to winnowing, as reflected in variations in grain size. The winnowing record suggests, among other things, reduced intensity of ocean circulation during times of Southern Hemisphere ice-volume increase. This suggestion contradicts the general assumption of significant polar cooling at times of ice-volume increase.

15. A silica diagenesis "front" occurs in a 20-m interval below 280 mbsf in the middle Paleocene at Site 752. This interval is marked by the oldest sediment in which diatoms are preserved, a change from opal-A to opal-CT, increases in physical properties such as bulk density and acoustic velocity, and a decrease in water content. We speculate that the lowering of temperature and the decrease in confining pressure following uplift and erosion of the crest of Broken Ridge may have effectively "frozen" this diagenetic boundary at its pre-rift level.

REFERENCES

Anderson, R. N., Langseth, M. G., and Sclater, J. G., 1977. The mechanisms of heat transfer through the floor of the Indian Ocean. *J. Geophys. Res.*, 82:3391–3409.

Banner, F. T., and Blow, W. H., 1965. Progress in the planktonic foraminiferal biostratigraphy of the Neogene. *Nature*, 208:1164–1166.

Barron, J., Larsen, B., et al., in press. *Proc. ODP, Init. Repts.*, 119: College Station, TX (Ocean Drilling Program).

Bé, A.W.H., and Tolderlund, D. S., 1971. Distribution and ecology of living planktonic foraminifera in surface waters of the Atlantic and Indian Oceans. *In* Funnell, B. M., and Riedel, W. R. (Eds.), *Micropaleontology of Oceans*: Cambridge (Cambridge Univ. Press), 105–149.

Berggren, W. A., and Hollister, C. D., 1977., Plate tectonics and paleocirculation—commotion in the ocean. *Tectonophysics*, 38:11–48.

Berggren, W. A., Kent, D. V., and Flynn, J. J., 1985a. Jurassic to Paleogene: part 2. Paleogene geochronology and chronostratigraphy. *In* Snelling, N. J. (Ed.), *The Chronology of the Geological Record*: Mem. Geol. Soc. London, 10:141–198.

Berggren, W. A., Kent, D. V., Flynn, J. J., Van Couvering, J. A., 1985b. Cenozoic geochronology. *Geol. Soc. Am. Bull.*, 96:1407–1408.

Blow, W. H., 1969. Late middle Eocene to Recent planktonic biostratigraphy. *In* Bronnimann, P., and Renz, H. H. (Eds.), *Proc. Int. Conf. Planktonic Microfossils, 1st, Geneva, 1967*, 1:199–421.

Bolli, H. M., and Saunders, J. B., 1985. Oligocene to Holocene low latitude planktic foraminifera. *In* Bolli, H. M., Saunders, J. B., and Perch-Nielsen, K. (Eds.), *Plankton Stratigraphy*: Cambridge (Cambridge Univ. Press), 155–262.

Bolli, H. M., Saunders, J. B., and Perch-Nielsen, K., 1985. *Plankton Stratigraphy*: Cambridge (Cambridge Univ. Press).

Bougault, H., Cambon, P., Joron, L., and Treuil, M., 1979a. Trace elements: fractional crystallization and partial melting processes, heterogeneity of upper mantle material. *In* Dmitriev, L., Heirtzler, J., et al., *Init. Repts. DSDP*, 46: Washington (U.S. Govt. Printing Office), 247–252.

Bougault, H., Treuil, M., and Joron, J. L., 1979b. Trace elements in basalts from 23°N and 36°N in the Atlantic Ocean: fractional crystallization, partial melting, and heterogeneity of the upper mantle. *In* Melson, W. G., Rabinowitz, P. D., et al., *Init. Repts. DSDP*, 45: Washington (U.S. Govt. Printing Office), 493–506.

Corliss, B. C., 1979. Recent deep-sea benthonic foraminiferal distributions in the southeast Indian Ocean: inferred bottom-water routes and ecological implications. *Mar. Geol.*, 31:115–138.

Davies, T. A., Luyendyk, B. P., et al., 1974. *Init. Repts. DSDP*, 26: Washington (U.S. Govt. Printing Office).

Fenner, J., 1984. Eocene-Oligocene planktic diatom stratigraphy in the low latitudes and in the high southern latitudes. *Micropaleontology*, 30:319–442.

_____, 1985. Late Cretaceous to Oligocene planktic diatoms. *In* Bolli, H. M., Saunders, J. B., and Perch-Nielsen, K. (Eds.), *Plankton Stratigraphy*: Cambridge (Cambridge Univ. Press), 713–762.

Gautier, I., Weis, D., Giret, A., and Vidal, P., 1987. The basalts of Kerguelen Islands. *Terra Cognita*, 7:11.

Giret, A., 1983. Le plutonisme océanique intraplaque, exemple de l'archipel des Kerguelen (T.A.A.F.) [Ph.D. thesis]. Paris VI Univ.; *C.N.F.R.A.*, 54.

Gombos, A. M., 1977. Paleogene and Neogene diatoms from the Falkland Plateau and Malvinas Outer Basin, Leg 36, Deep Sea Drilling Project. *In* Barker, P. F., Dalziel, I.W.D., et al., *Init. Repts. DSDP*, 36: Washington (U.S. Govt. Printing Office), 575–687.

_____, 1984. Late Paleocene diatoms in the Cape Basin. *In* Hsü, K. J., LaBrecque, J. L., et al., *Init. Repts. DSDP*, 73: Washington (U.S. Govt. Printing Office), 495–512.

Hamilton, E. L., 1976. Variations of density and porosity with depth in deep-sea sediments. *J. Sediment. Petrol.*, 46:280–300.

Haq, B. U., Hardenbol, J., and Vail, P. R., 1987. Chronology of fluctuating sea levels since the Triassic. *Science*, 235:1156–1167.

Hyndman, R. D., Erickson, A. J., and Von Herzen, R. P., 1974. Geothermal measurements on DSDP Leg 26. *In* Davies, T. A., Luyendyk, B. P., et al., *Init. Repts. DSDP*, 26: Washington (U.S. Govt. Printing Office), 451–463.

Jenkins, D. G., 1960. Planktonic foraminifera from the Lakes Entrance oil shaft, Victoria, Australia. *Micropaleontology*, 6:345–371.

_____, 1967. Planktonic foraminiferal zones and new taxa from the lower Miocene to the Pleistocene of New Zealand. *N. Z. J. Geol. Geophys.*, 10:1064–1078.

_____, 1978. Neogene planktonic foraminifers from DSDP Leg 40 Sites 360 and 362 in the southeastern Atlantic. *In* Bolli, H. M., Ryan, W.B.F., et al., *Init. Repts. DSDP*, 40: Washington (U.S. Govt. Printing Office), 723–739.

_____, 1985. Southern mid-latitude Paleocene to Holocene planktic foraminifera. *In* Bolli, H. M., Saunders, J. B., and Perch-Nielsen, K. (Eds.), *Plankton Stratigraphy*: Cambridge (Cambridge Univ. Press), 263–283.

Kennett, J. P., 1973. Middle and late Cenozoic planktonic foraminiferal biostratigraphy of the southwest Pacific—DSDP Leg 21. *In* Burns, R. E., Andrews, J. E., et al., *Init. Repts. DSDP*, 21: Washington (U.S. Govt. Printing Office), 575–639.

_____, 1981. Marine tephrochronology. *In* Emiliani, C. (Ed.), *The Sea: The Oceanic Lithosphere* (vol. 7): Chicago (Wiley), 1373–1436.

_____, 1982. *Marine Geology*: Englewood Cliffs, NJ (Prentice-Hall).

Kennett, J. P., and Burns, R. E., 1972. Australian-Antarctic continental drift, paleocirculation changes and Oligocene deep erosion. *Nature*, 239:51–55.

Klootwijk, C. T., 1985. Paleomagnetism of the Tasman Fold Belt: indication for mid-Carboniferous large-scale southwards displacment of the New England region. *Third Circum Pacific Terrane Conf., Abstr. Geol. Soc. Aust.*, 14:124–127.

Lawrence, J. R., and Gieskes, J. M., 1981. Constraints on water transport and alteration in the oceanic crust from the isotopic composition of pore water. *J. Geophys. Res.*, 86:7924–7934.

Ledbetter, M. T., 1979. Fluctuations of Antarctic Bottom Water velocity in the Vema Channel during the last 160,000 years. *Mar. Geol.*, 33: 77–89.

Leg 119 Scientific Drilling Party, 1988. Leg 119 studies climatic history. *Geotimes*, 33(7):14–16.

Leg 120 Scientific Drilling Party, 1988. Leg 120 explores origins and history. *Geotimes*, 33(9):12–16.

Ludden, J. N., Thompson, G., Bryan, W. B., and Frey, F. A., 1980. The origin of lavas from the Ninetyeast Ridge, eastern Indian Ocean: an evaluation of fractional crystallization models. *J. Geophys. Res. B*, 85:4405–4420.

Lyle, M., Leinen, M., Owen, R. M., and Rea, D. K., 1987. Late Tertiary history of hydrothermal deposition at the East Pacific Rise: correlation to volcano-tectonic events. *Geophys. Res. Lett.*, 14:595–598.

Monechi, S., Bleil, U., and Backman, J., 1985. Magnetobiochronology of Late Cretaceous–Paleogene and late Cenozoic pelagic sedimentary sequences from the northwest Pacific (Deep Sea Drilling Project, Leg 86, Site 577). *In* Heath, G. R., Burckle, L. H., et al., *Init. Repts. DSDP*, 86: Washington (U.S. Govt. Printing Office), 787–797.

Moore, M. F., Gleadow, A.J.W., and Lovering, J. F., 1986. Thermal evolution of rifted continental margins: new evidence from fission track dating of apatites from southeastern Australia. *Earth Planet. Sci. Lett.*, 78:255–270.

Morkhoven, F.P.C.M. van, Berggren, W. A., and Edwards, A. S., 1986. Cenozoic cosmopolitan deep-water benthic foraminifera. *Bull. Cent. Rech. Explor. Prod. Elf-Aquitaine*, 11:1–421.

Mukhina, V. P., 1974. The Paleocene diatom ooze in the eastern part of the Indian Ocean. *Okeanologiya*, 14:852–858.

_____, 1976. Species composition of the late Paleocene diatoms and silicoflagellates in the Indian Ocean. *Micropaleontology*, 22:151–158.

Müller, C., 1977. Distribution of calcareous nannoplankton in Oligocene to Holocene sediments of the Red Sea and the Indian Ocean reflecting paleoenvironment. *In* Heirtzler, J. R., Bolli, H. M., Davies, T. A., Saunders, J. B., and Sclater, J. G. (Eds.), *Indian Ocean Geology and Biostratigraphy*: Washington (Am. Geophys. Union), 371–395.

Mutter, J. C., and Cande, S. C., 1983. The early opening between Broken Ridge and Kerguelen Plateau. *Earth Planet. Sci. Lett.*, 65:369–376.

Mutter, J. C., Hegarty, K. A., Cande, S. C., and Weissel, J. K., 1985. Breakup between Australia and Antarctica: a brief review in the light of new data. *Tectonophysics*, 114:255–279.

Norin, E., 1958. The sediments of the central Tyrrhenian Sea. *In* Pettersson, H. (Ed.), *Reports of the Swedish Deep Sea Expedition, 1947-1948, 8: Sediment Cores from the Mediterranean Sea and the Red Sea*: Göteborg (Elanders Boktryckeri Aktiebolag), 1–136.

Okada, H., and Bukry, D., 1980. Supplementary modification and introduction of code numbers to the low latitude coccolith biostratigraphic zonation (Bukry, 1973; 1975). *In* Haq, B. U. (Ed.), *Nannofossil Biostratigraphy*: Stroudsburg, PA (Hutchinson Ross), 321–327.

Owen, R. M., and Rea, D. K., 1985. Sea floor hydrothermal activity links climate to tectonics: the Eocene CO_2 greenhouse. *Science*, 227: 166–169.

Peterson, L. C., 1984. Recent abyssal benthic foraminiferal biofacies of the eastern equatorial Indian Ocean. *Mar. Micropaleontol.*, 8:479–519.

Pospichal, J., and Wise, S. W., Jr., in press. Maestrichtian calcareous nannofossil biostratigraphy of Maud Rise ODP Leg 113 Sites 689 and 690, Weddell Sea. *In* Barker, P. F., Kennett, J. P., et al., *Proc. ODP, Sci. Results*, 113: College Station, TX (Ocean Drilling Program).

Price, R. C., Kennedy, A. K., Riggs-Sneeringer, M., and Frey, F. A., 1986. Geochemistry of basalts from the Indian Ocean triple junction: implications for the generation and evolution of Indian Ocean Ridge basalts. *Earth Planet. Sci. Lett.*, 78:379–396.

Rea, D. K., 1982. Fluctuation in eolian sedimentation during the past five glacial-interglacial cycles: a preliminary examination of data from Deep Sea Drilling Project Hole 503B, eastern equatorial Pacific. *In* Prell, W. L., Gardner, J. V., et al., *Init. Repts. DSDP*, 68: Washington (U.S. Govt. Printing Office), 409–415.

Rea, D. K., and Bloomstine, M. K., 1986. Neogene history of the South Pacific tradewinds: evidence for hemispherical asymmetry of atmospheric circulation. *Palaeogeogr. Palaeoclimatol. Palaeoecol.*, 55: 55–64.

Rea, D. K., and Janecek, T. R., 1986. Grain size changes in reworked pelagic sediments, Deep Sea Drilling Project Site 599. *In* Leinen, M., Rea, D. K., et al., *Init. Repts. DSDP*, 92: Washington (U.S. Govt. Printing Office), 341–343.

Reading, H. G. (Ed.), 1978. *Sedimentary Environments and Facies*: Oxford (Blackwell Scientific).

Ruddiman, W. F., and Glover, L. K., 1982. Mixing of volcanic ash zones in subpolar North Altantic sediments. *In* Scrutton, R. A., and Talwani, M. (Eds.), *The Ocean Floor*: New York (Wiley), 37–60.

Ruddiman, W. F., and McIntyre, A., 1984. An evaluation of ocean-climate theories on the North Atlantic. *In* Berger, A., Imbrie, J., Hays, H., Kukla, G., and Saltzman, B. (Eds.), *Milankovitch and Climate: Understanding the Response to Orbital Forcing*: Dordrecht (Reidel), 671–686.

Saunders, A. D., 1983. Geochemistry of basalts recovered from the Gulf of California during Leg 65 of the Deep Sea Drilling Project. *In* Lewis, B.T.R., Robinson, P., et al., *Init. Repts. DSDP*, 65: Washington (U.S. Govt. Printing Office), 591–622.

Schilling, J. G., Zajac, M., Evans, R., Johnston, T., White, W., Devine, J. O., and Kingsley, R., 1983. Petrologic and geochemical variations along the Mid-Atlantic Ridge from 29°N to 79°N. *Am. J. Sci.*, 283: 510–586.

Schlich, R., Wise, S. W., Jr., et al., in press. *Proc. ODP, Init. Repts.*, 120: College Station, TX (Ocean Drilling Program).

Schmidt, P.W., and Embleton, B.J.J., 1981. Magnetic overprinting in southeastern Australia and thermal history of its rifted margin. *J. Geophys. Res.*, 86:3998–4008.

Schmincke, H.-U., 1981. Ash from vitric muds in deep sea cores from the Marianas Trough and fore-arc regions (South Philippine Sea) (Sites 453, 454, 455, 458, 459). *In* Hussong, D. M., Uyeda, S., et al., *Init. Repts. DSDP*, 60: Washington (U.S. Govt. Printing Office), 473–481.

Sclater, J. G., Meinke, L., Bennett, A., and Murphy, C., 1985. The depth of the ocean through the Neogene. *In* Kennett, J. P. (Ed.), *The Miocene Ocean: Paleoceanography and Biogeography*: Mem. Geol. Soc. Am., 163:1–19.

Srinivasan, M. S., and Kennett, J. P., 1981. Neogene planktonic foraminiferal biostratigraphy: equatorial to subantarctic, South Pacific. *Mar. Micropaleontol.*, 6:499–534.

Thiede, J., and Rea, D. K., 1981. Mass accumulation rates of Barremian to Recent biogenic sediments from the Mid-Pacific Mountains (Deep Sea Drilling Project Site 463) and Hess Rise (Sites 464, 465, 466), central Pacific Ocean. *In* Thiede, J., Vallier, T. L., et al., *Init. Repts. DSDP*, 62: Washington (U.S. Govt. Printing Office), 637–651.

Tjalsma, R. C., and Lohmann, G. P., 1983. Paleocene-Eocene bathyal and abyssal benthic foraminifera from the Atlantic Ocean. *Micropaleontology Spec. Publ.*, 4:1–90.

Vallier, T. L., Dean, W. E., Rea, D. K., and Thiede, J., 1983. Geologic evolution of Hess Rise, central North Pacific Ocean. *Geol. Soc. Am. Bull.*, 94:1289–1307.

Vincent, E., 1977. Indian Ocean Neogene planktonic foraminiferal biostratigraphy and its paleoceanographic implications. *In* Heirtzler, J. R., Bolli, H. M., Davies, T. A., Saunders, J. B., and Sclater, J. G. (Eds.), *Indian Ocean Geology and Biostratigraphy*: Washington (Am. Geophys. Union), 469–584.

Vincent, E., Killingley, J. S., and Berger, W. H., 1985. Miocene oxygen and carbon isotope stratigraphy of the tropical Indian Ocean. *In* Kennett, J. P. (Ed.), *The Miocene Ocean: Paleoceanography and Biogeography*: Mem. Geol. Soc. Am., 163:103–130.

Weis, D., Bassias, Y., Gautier, I., and Mennessier, J. P., 1987a. Isotopic study of MD48 basalts (S. Indian Ocean): Kerguelen type signature. *EOS, Trans. Am. Geophys. Union*, 68:1541.

Weis, D., Beaux, J. F., Gautier, I., Giret, A., and Vidal, P., 1987b. Kerguelen Archipelago: geochemical evidence for recycled material. *Nato ASI Workshop, Abst.*, May 25–29, Antalaya, Turkey, 122–125.

Weissel, J. K., and Karner, G. D., in press. Flexural uplift of rift flanks due to mechanical unloading of the lithosphere during extension. *J. Geophys. Res.*

Wise, S. W., and Wind, F. H., 1977. Mesozoic and Cenozoic calcareous nannofossils recovered by DSDP Leg 35 drilling on the Falkland Plateau, southwest Atlantic sector of the Southern Ocean. *In* Barker, P., Dalziel, I.W.D., et al., *Init. Repts. DSDP*, 36: Washington (U.S. Govt. Printing Office), 296–306.

Woodruff, F., 1985. Changes in Miocene deep-sea benthic foraminiferal distribution in the Pacific Ocean: relationship to paleoceanography. *In* Kennett, J. (Ed.), *The Miocene Ocean: Paleoceanography and Biogeography*: Mem. Geol. Soc. Am., 163:131–176.

Woodruff, F., Savin, S. M., and Douglas, R. G., 1981. Miocene stable isotope record: a detailed deep Pacific Ocean study and its paleoclimatic implications. *Science*, 212:665–668.

Zachos, J. C., and Arthur, M. A., 1986. Paleoceanography of the Cretaceous/Tertiary boundary event: inferences from stable isotopic and other data. *Paleoceanography*, 1:5–26.

Ms 121A-113

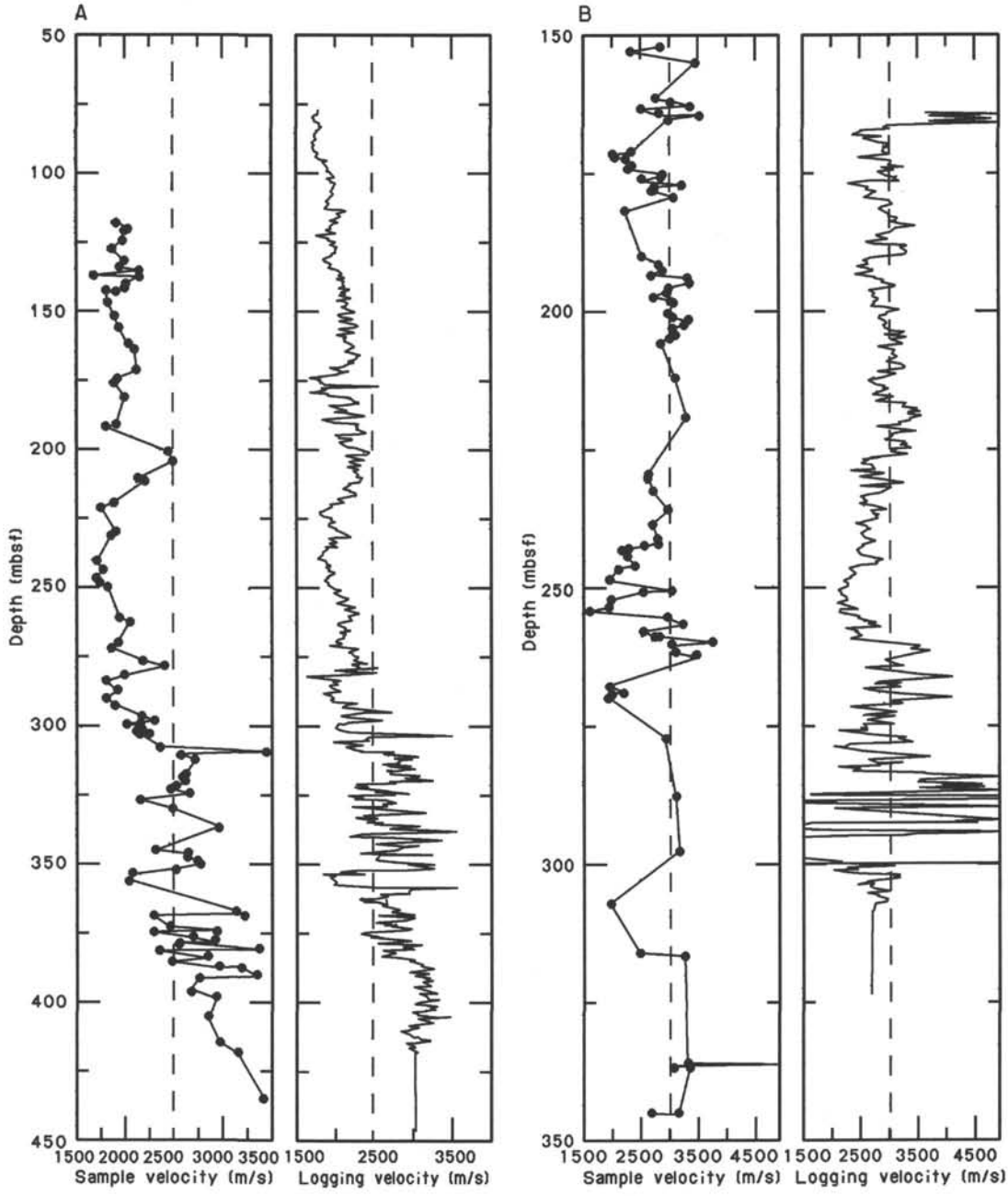

Figure 39. A comparison of laboratory- and logging-measured velocities at Site 752 (**A**) and Hole 754B (**B**). Both methods show the velocity increase related to the formation of "hard" chalk at 300 mbsf at Site 752.

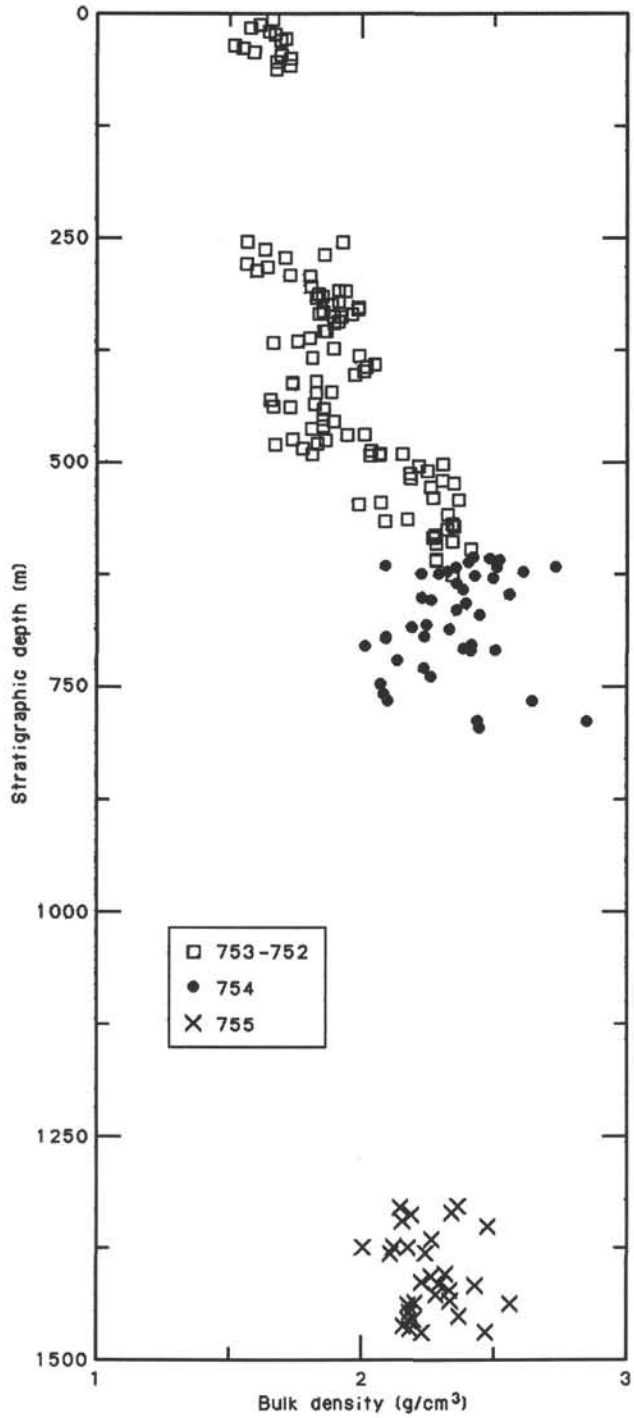

Figure 40. Stratigraphic plot of the bulk densities of the Broken Ridge section. Sites 752 and 753 are shown together, with the pelagic cap separated from the units underlying the unconformity by a gap equivalent to that estimated from seismic stratigraphic interpretation (190 m between the base of Site 753 and lower Eocene sediments at Site 752). Sites 752 and 754 have about 20 m of overlap, and the 540 m gap estimated between Sites 754 and 755 has been subsequently revised to about 450 m.

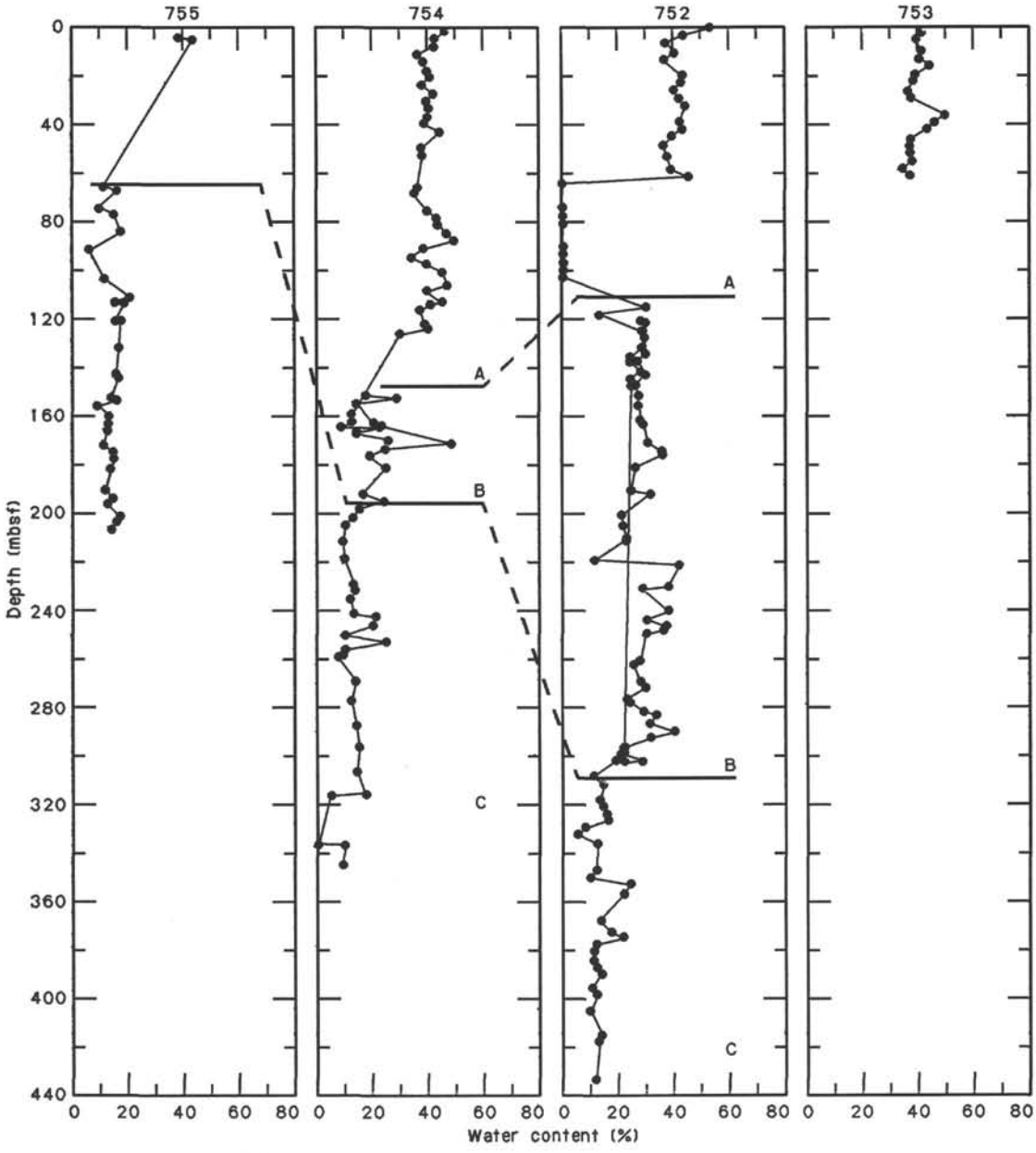

Figure 41. Cross section of sediment water contents measured at the Broken Ridge sites, showing the correlation of physical-properties units defined in the respective site chapters.

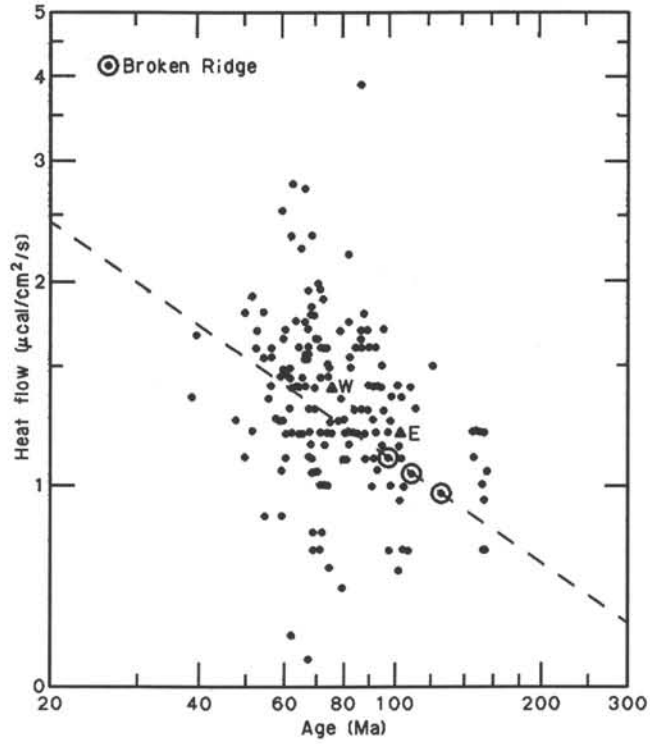

Figure 42. Heat flow vs. age for Indian Ocean crust older than 40 Ma. Results from Leg 121 and Anderson et al. (1977) at Broken Ridge are plotted on the modeled relationship for this crust. Modified from Anderson et al. (1977).